

UC Riverside

UC Riverside Electronic Theses and Dissertations

Title

Boundaries Regulate Environmental Signaling, Cell Wall Mechanics and Growth During Plant Development

Permalink

<https://escholarship.org/uc/item/29b138m8>

Author

Neher, Wesley Robert

Publication Date

2023

Peer reviewed|Thesis/dissertation

UNIVERSITY OF CALIFORNIA
RIVERSIDE

Boundaries Regulate Environmental Signaling, Cell Wall Mechanics and Growth
During Plant Development

A Dissertation submitted in partial satisfaction
of the requirements for the degree of

Doctor of Philosophy

in

Plant Biology

by

Wesley Robert Neher

March 2024

Dissertation Committee:

Prof. Patricia Springer, Co-Chairperson

Prof. Carolyn Rasmussen, Co-Chairperson

Prof. Siobhan Braybrook

Copyright by
Wesley Robert Neher
2024

The Dissertation of Wesley Robert Neher is approved:

Committee Co-Chairperson

Committee Co-Chairperson

University of California, Riverside

Acknowledgements

I would like to thank my major professor, Dr. Patricia Springer, for her consistent support and mentorship over the past six years. You helped me grow as a scientist and I am lucky to have you as a mentor. I am also grateful to my co-PI Dr. Carolyn Rasmussen, and third committee member Dr. Siobhan Braybrook, for their advice, assistance, and collaboration. I always felt I had a strong network of mentors who were rooting for me and invested in my success. I would also like to acknowledge Dr. Anne Sylvester for her advice and correspondence, and her past lab members for their contributions, some of which are incorporated into my second chapter and were essential to getting my work published. Thanks also to current and past members of Springer and Rasmussen labs, my comrades at the bench and in the fields, respectively. I am also appreciative for the two years support I received through the GAANN fellowship, and a quarter of DYP support.

I dedicate this dissertation to my grandfather, Dr. Robert Trostle Neher. You have been a huge role model for me and a significant factor in what drew me towards academia and specifically biology. Our summers at the field station in Montana, were an essential and formative part of my childhood, where I learned to appreciate and respect the natural world. I will always remember the lessons I learned from you. I love you. - Wes

ABSTRACT OF THE DISSERTATION

Boundaries Regulate Environmental Signaling, Cell Wall Mechanics and Growth
During Plant Development

by

Wesley Robert Neher

Doctor of Philosophy, Graduate Program in Botany & Plant Science
University of California, Riverside, March 2024
Prof. Patricia Springer, Co-Chairperson
Prof. Carolyn Rasmussen, Co-Chairperson

Organ boundaries serve several important roles in development, but the mechanisms downstream of boundary-defining factors are not well understood. In Chapter 1 of my dissertation, I show the *Arabidopsis* transcription factor LOB regulates leaf angle via a phototropism-dependent mechanism, reducing phototropic responses at the base of the leaf. LOB and other boundary-defining transcription factors also regulate numerous cell wall genes, implying a biophysical mechanism is an important aspect of boundary function. Given the inherent challenges of measuring cell wall mechanics in the *Arabidopsis* leaf-meristem boundary, I used a different system, the maize ligular region, which is

highly amenable to AFM experiments. In Chapter 2, I characterized mechanical patterns during the development of the ligular region. My findings are consistent with the existence of a cell wall rigidification program in the boundary, which correlates with patterns of growth, cell division, and auxin dynamics. In Chapter 3, I measured epidermal cell geometry and cell wall stiffness over a wide area of the maize leaf. I found that the establishment of the boundary in the maize leaf was linked not just to local changes, but to broader growth and mechanical patterns outside the boundary. This suggests that coordination between the boundary and adjacent leaf zones is involved in the morphogenesis of the maize leaf. My findings further our understanding of how plant boundaries regulate growth.

Table of Contents

Introduction	1
References	21
Chapter 1	
Abstract	29
Introduction	30
Materials and Methods	36
Results	41
Discussion	48
References	53
Figures and Tables	58
Chapter 2	
Abstract.....	71
Introduction.....	72
Materials and Methods.....	79
Results	88
Discussion	100
References.....	107
Figures and Tables.....	114
Chapter 3	
Abstract.....	145
Introduction.....	146

Materials and Methods.....	151
Results.....	155
Discussion.....	161
References	169
Figures and Tables	172
Conclusion.....	185
References	190

List of Tables

Chapter 1

Table 1.1: List of oligonucleotide primers used in this chapter.....	70
--	----

Chapter 2

Table 2.1: Cell division orientation during ligule developmental stages..	140
---	-----

Table 2.2: Pairwise comparison of average IM between epidermal zones via Wilcoxon signed rank test using the <i>W</i> -statistic.....	141
---	-----

Table 2.3: Pairwise comparison of average IM between wall categories via Wilcoxon signed rank test using the <i>W</i> -statistic.....	143
---	-----

Table 2.4: Pairwise comparison of average IM between early and late mechanical stages via Mann-Whitney U-Test.....	144
--	-----

Chapter 3

Table 3.1: Pairwise comparison of average IM between <i>lg1;lg2</i> epidermal zones via Wilcoxon signed rank test using the <i>W</i> -statistic.....	182
--	-----

Table 3.2: Pairwise comparison of average IM between <i>lg1;lg2</i> wall categories via Wilcoxon signed rank test using the <i>W</i> -statistic.....	183
--	-----

Table 3.3: Pairwise comparison of average IM between <i>lg1;lg2</i> early and late mechanical stages via Mann-Whitney U-Test.....	184
---	-----

Introduction:

Boundaries in Development:

During the development of highly organized multicellular organisms, discrete cell fate zones must be specified and maintained in order to form distinct body segments. This is accomplished via the establishment of developmental boundaries that delimit adjacent domains. In animal systems such as *Drosophila*, this is mostly a matter of regulating cell migration and intermixing between neighboring cell populations (Sharrock and Sanson, 2020). In plants, cells are fixed in place relative to their neighbors by the cell wall, and cell fate is determined by positional signals rather than lineage. Therefore, boundaries in plants and animals have a shared function of separating adjacent cell fate zones using different mechanisms. In plants, a boundary is not merely a threshold, but a distinct zone interposed between two others (Wang et al., 2016). This creates a buffer between divergent cell populations, which may help prevent improper patterning by mobile signals and transcription factors. Furthermore, the physical attachment between neighboring plant cells means that cells exert force on their neighbors as they grow, which poses a challenge in establishing multiple distinct growth axes and achieving clean organ separation. By locally restricting cell proliferation and expansion, the plant boundaries help adjacent organs physically separate as they grow (Bell et al., 2012; Hussey, 1971; Lee et al., 2009; Rast and Simon, 2008). While several boundary-defining genes have been identified and

determined to be critical for organ separation, the physical mechanisms by which plant boundaries restrict growth are not fully understood.

Boundary domains are found at the base of all major organs, including leaves, floral organs, branches, flower pedicels, and lateral roots. A boundary zone defines the cleft between the two cotyledons during embryogenesis, and is necessary for the establishment of the SAM (Aida et al., 1999). Additionally, boundaries are involved in leaf serration and ovule development in carpels, as local growth repression between leaf lobes and between developing ovules helps to physically separate areas of greater growth (Bouré et al., 2022; Nahar et al., 2012).

The best-studied plant boundary is the meristem-organ boundary, which forms at the periphery of nascent primordia. New leaves are established by the recruitment of cells from the shoot apical meristem (SAM) into primordia. The mechanisms controlling the initiation of lateral organs are relatively well-understood. Primordia are specified in the peripheral zone of the meristem via polar auxin transport by PIN-FORMED (PIN) auxin efflux transporters, resulting in local auxin maxima at the site of organ initiation. In addition to a local maximum of auxin transcriptional responses (Gallavotti, 2013; Gallavotti et al., 2008; Heisler et al., 2005), other early events associated with leaf initiation include a downregulation of KNOXI genes (Lin et al., 2003, Ori et al., 2000), changes in division plane orientation and cell wall loosening in subepidermal cell layers (Peaucelle et al., 2011), which all precede the bulging out of the leaf primordium.

The boundary is specified very early in leaf development, creating a distinct groove between the meristem and leaf primordium soon after it initiates. The meristem-leaf boundary separates adjacent cell fate zones, maintains a pool of cells that are competent to form axillary meristems, and locally suppresses growth, allowing for the physical separation of the leaf from the stem (Arnaud and Laufs, 2013; Rast and Simon, 2008; Wang et al., 2016).

A number of transcription factors are known to be important for establishing and maintaining the boundary and executing its essential functions. Mutations in these genes typically impair organ separation, resulting in extended areas of contact at the junctions between adjacent organs. Certain factors, such as the MYB transcription factors LOF1 and LOF2 (Lee et al., 2009), and the NAC transcription factors CUC2 and CUC3 (Aida et al., 1999; Cucinotta et al., 2018; Nahar et al., 2012), are essential for determining boundary identity. In null mutants such as *cuc2* and *lof1lof2*, multiple aspects of the boundary are impaired. Particularly, these mutants exhibit impaired organ separation as well as defects in axillary and accessory meristem formation. Not only is growth derepressed in these mutants, but the competence to form new meristems is lost. Other boundary factors are not essential for specifying boundary identity, but are responsible for executing certain boundary-specific functions. For example, the AS2/LBD transcription factor LOB is responsible for locally repressing cell expansion and proliferation via catabolism of brassinosteroid, a growth-promoting hormone (Bell et al., 2012). Loss-of-function mutations in *LOB* result in mild

organ separation phenotypes but have no effect on axillary meristem development or the expression of other boundary-defining factors.

While local growth suppression is a common aspect of boundary function, the responsible mechanisms are not fully understood. In the *Arabidopsis* leaf-meristem boundary, *LOB* upregulates *BAS1*, a gene encoding a BR catabolic enzyme (Bell et al., 2012). By suppressing BR levels, growth in the boundary is repressed. BRs also upregulate *LOB*, forming a feedback loop that maintains the boundary with low BR levels. Many boundary-associated transcription factors such as *CUC2* and *LOB* regulate cell wall-modifying genes, suggesting a biomechanical role for the boundary function (Bell et al., 2012; Bouré et al., 2022). By locally reducing the cell wall's elastic deformability, reducing the irreversible movement of cellulose microfibrils, or otherwise altering cell wall composition, organization, and remodeling activity, the boundary function could change the way the cell wall physically responds to pressure. These possibilities have not been thoroughly explored, but there is growing evidence that boundaries act at least in part through changes in cell wall mechanics (Bouré et al., 2022; Sampathkumar et al., 2019).

The leaf-meristem boundary zone has well-defined roles during the course of development. Early in development, the boundary locally restricts cell expansion and proliferation (Bell et al., 2012; Hussey, 1971; Lee et al., 2009). The boundary also maintains an area that is competent to form axillary meristems (Raman et al., 2008), which is essential for branching, and contributes

to the determination of branch angle (Che et al., 2023; Waite and Dardick, 2018). Lastly, the boundary defines the abscission zone, where a senescent organ detaches from the stem (Liljegren, 2012). Boundary defining factors are expressed steadily in the boundary area throughout development and may play as-yet-unrecognized roles in the axils of mature leaves.

Developmental and Environmental Regulation of Leaf and Branch Angle

Leaf and branch angle are agronomically relevant traits that are regulated by multiple factors. Leaves are the main photosynthetic organs, and their orientation is a key part of a plant's above-ground morphology. The photosynthetic rate is affected by the effective surface area over which a leaf intercepts light. If the leaf intercepts incoming light perpendicular to the path of the photons, the effective surface area is higher, and the light is also less likely to reflect off the surface, resulting in a greater overall absorbance of light (Yates, 1981). More is not always better – excessive light exposure can damage the photosystems and overwhelm the electron transport machinery in the chloroplasts, potentially resulting in oxidative stress and a reduction in total photosynthetic efficiency (Kasahara et al., 2002). Additionally, plants compete with their neighbors for resources, including light. Light that has transmitted through a leaf is generally enriched for green and far-red wavelengths, as these are not absorbed by chlorophyll. This light is therefore of a low quality for further

photosynthesis, and even a high intensity of such transmitted light is likely to be low in photosynthetically active radiation. Plants sense local light quality via phytochromes (Fankhauser, 2001), and light direction via phototropins (Briggs et al., 2001), and generally grow towards high quality red/blue-enriched light and away from low quality far-red/green-enriched light. Low quality light generally indicates shading from neighbors, which a plant will move to escape. Plants optimize their leaf positioning and morphology according to the local microenvironment (Ma and Li, 2019).

Branch angle is also important for sculpting the canopy, and different species have contrasting growth habits, occupying the available canopy space in different ways. At the branch attachment point, the average attachment angle is about 60° upward (Hangarter, 1997; Kawamoto and Morita, 2022; Toyota and Gilroy, 2013). This is mechanically strong, and allows the plant to reach further up, escaping the shade of similar-sized or taller plants and occupying more canopy space, while also projecting out far enough to capture more light for photosynthesis and potentially shade smaller plants, reducing future competition. Branch angle is determined in part by gravitropic mechanisms, resulting in the gravitropic setpoint angle. *TILLER ANGLE CONTROL1 (TAC1)* and *LAZY1* are important genes involved in determining branch angle via gravitropism (Che et al., 2023; Waite and Dardick, 2018).

What is best for a plant to be competitive in nature is not always best in an agricultural setting. Many wild plant species evolved to be competitive or

avoidant/escapist when encountering shade from their neighbors. In the case of high-density agriculture, this can have sub-optimal results, particularly if a few plants outcompete their neighbors, which would result in irregular per-plant yield and possible yield reduction. Generally, more vertical leaf and branch angles are desirable because they allow for increased planting density with less shading competition between neighbors, and often less shading of the lower leaves by the upper leaves (Duncan, 1971; Mantilla-Perez and Salas Fernandez, 2017; Pendleton et al., 1968; Yang et al., 2023). However, if a leaf is too vertically oriented it will not efficiently intercept light, so there must be some optimal angle for a particular species in a particular set of conditions.

Boundaries are important for controlling leaf and branch angle, as the boundary occupies the junction where the organ attaches to the plant body. Mutations affecting the boundary often impair organ separation, resulting in mechanical differences that alter the physical trajectory of the organ (Bell et al., 2012; Lee et al., 2009). Any modulation of light or gravity responses in the boundary could conceivably affect the architecture of the branch point, altering the angle of the organ and its responsiveness to environmental cues.

Phototropin signaling affects plant growth and physiology

Light signaling plays essential roles in plant development and physiology. Light exposure, even at a very low intensity, can promote seed germination in

some species including *Arabidopsis* (Poppe and Schafer, 1997). Seeds may also germinate in the dark under the surface of the soil and must then rapidly escape the soil into the light in order to photosynthesize before their energy reserves run out. Seedlings developing in the dark undergo skotomorphogenesis, which includes the formation of an apical hook at the tip of the hypocotyl, mechanically protecting the cotyledons, with rapid elongation along the length of the hypocotyl growing against gravity (Arsovski et al., 2012; Nemhauser and Chory, 2002). This maximizes the seedling's chances of breaking out of the soil into the light. As soon as light is perceived, de-etiolation occurs, and the plant transitions into a photomorphogenic form (Arsovski et al., 2012; Han et al., 2007). This requires the rapid production of chlorophyll, inhibition of hypocotyl elongation, unfolding of the apical hook and expansion of the cotyledons. Upon light exposure, the red-sensing phytochromes and blue-sensing cryptochromes cooperate to inhibit hypocotyl elongation and promote photomorphogenesis (Más et al., 2000).

Phototropins are blue light receptors that generally act to optimize photosynthesis. They promote increased stomatal aperture in blue light, alongside the cryptochromes (Inada et al., 2004; Mao et al., 2005). Therefore, when the plant is exposed to light of high quality for photosynthesis, the phototropins promote gas exchange, improving the assimilation of CO₂ and minimizing photorespiration. Phototropins also regulate chloroplast movement depending on light intensity (Luesse et al., 2010). In low intensity light, maximizing light capture is favorable. Phototropins promote the chloroplast

accumulation and avoidance responses, optimizing the intracellular positioning of chloroplasts depending on the intensity of blue light. Lastly, phototropins are responsible for directing growth responses to directional blue light (Briggs et al., 2001; Lariguet et al., 2006; Motchoulski and Liscum, 1999). These include negative phototropism in the root, hypocotyl bending, leaf inclination, and blade flattening. Phototropism tends to stimulate a more upright growth habit in *Arabidopsis* seedlings, with leaf blades elevated, uncurled and oriented with the blade surface perpendicular to incoming light (de Carbonnel et al., 2010; Lariguet et al., 2006).

The *Arabidopsis* genome contains two phototropin-encoding genes, *PHOT1* and *PHOT2* (Christie, 2007). The phot1 and phot2 holoproteins lack transmembrane domains and localize to the plasma membrane via an unknown mechanism. The phototropins each contain two LOV domains, which are important for light sensing, as well as a serine/threonine kinase domain, which is involved in transducing a signal (Christie et al., 1999). phot1 is considerably more sensitive than phot2, enabling differential levels of total phot signaling over a wide range of light intensities (de Carbonnel et al., 2010). While phot1 and phot2 usually function redundantly, some of their responses are antagonistic. For example, while both phot1 and phot2 promote chloroplast accumulation responses in dim light, phot2 exclusively mediates the chloroplast avoidance response in bright light, implying phot2 responses must inhibit or override phot1 responses at high levels of phot2 activation (Kasahara et al., 2002; Luesse et al.,

2010). Additionally, some evidence suggests that phot2 signaling suppresses phot1 signaling during the regulation of leaf flattening (de Carbonnel et al., 2010).

The phototropins interact with several other proteins at the plasma membrane. Some of these interactors, the PHYTOCHROME KINASE SUBSTRATE (PKS1, 2, 3 and 4) proteins, as well as the BTB/POZ proteins NON-PHOTOTROPIC HYPOCOTYL3 (NPH3) and ROOT PHOTOTROPISM2 (RPT2), are essential for phototropic responses (de Carbonnel et al., 2010; Inada et al., 2004; Lariguet et al., 2006; Motchoulski and Liscum, 1999). NPH3 is thought to serve as a scaffold via protein-protein interactions, holding together particular combinations of phot and other signaling components. Genetic analysis indicates that particular combinations of phot, PKS, and BTB/POZ proteins mediate distinct downstream responses (de Carbonnel et al., 2010).

Blue light is absorbed by the LOV domains of the phot holoproteins, inducing autophosphorylation, before transducing the signal via its interaction partners (Christie et al., 1999). The downstream signaling events are not fully understood. Phototropic bending is accomplished by affecting the activity of auxin transporters such as PIN (Blakeslee et al., 2004; Ding et al., 2011), which direct the hormone to the side of the organ with less phot signaling activity. Interestingly, both *in vivo* and *in silico* experiments showed the establishment of an auxin gradient is dependent upon H⁺-ATPase activity, and that a pH gradient is a prerequisite to establishing an auxin gradient (Hohm et al., 2014). The redistribution of auxin leads to increased growth on the darker side of the organ,

which causes bending towards the light source. While this has been well demonstrated in hypocotyls, it has not been studied as heavily in leaves.

LOB

The AS2/LBD transcription factor LATERAL ORGAN BOUNDARIES (LOB) is a key regulator of boundary function in *Arabidopsis* (Bell et al., 2012; Husbands et al., 2007). *LOB* is expressed at the base of all major organs, including leaves, floral organs, axillary branches, flower pedicels, and lateral roots (Bell et al., 2012). A mutant phenotype was previously reported in the boundaries of leaves on the inflorescence. In wild-type plants, the main stem, inflorescence leaf, and axillary branch are all well-defined and diverge cleanly from one another at the boundary. In *lob* mutants, there is a mild organ separation phenotype. The cauline leaf and axillary branch exhibit a zone of extended contact due to over-proliferation of cells in the boundary of the *lob* mutant (Bell et al., 2012). A previous microarray experiment revealed numerous direct targets of LOB, Some targets were downregulated while others were upregulated, suggesting LOB's role as a transcriptional regulator is dependent on other factors, such as coactivators and corepressors (Bell et al., 2012). Among the most strongly upregulated genes was *PHYTOCHROME B ACTIVATION-TAGGED SUPPRESSOR 1 (BAS1)*, which encodes a BR-catabolic enzyme. Expressing *BAS1* under the *LOB* promoter in *lob* mutants rescued the

inflorescence boundary phenotype. The improper organ separation can therefore be attributed to the accumulation of BRs due to the lack of BAS1 activity in the boundary. Furthermore, BR's promote *LOB* expression, forming a negative feedback loop in which *LOB* maintains low BR levels in the boundary to restrict growth and facilitate organ separation (Bell et al., 2012).

Although the mutant phenotype in inflorescence boundaries was rescued by *pLOB:BAS1*, other *LOB* targets may also play important roles in the boundary. Intriguingly, three genes encoding important phototropism signaling components, *PHOT1*, *PKS2*, and *NPH3*, were found to be regulated by *LOB*. This raises the possibility that phototropic signaling is altered in the boundary, potentially affecting leaf angle.

LOB's direct targets are also enriched for cell wall modifying genes, many of which are BR-regulated. Therefore, *LOB* may be able to regulate cell wall modification both directly and indirectly via *BAS1*-mediated BR catabolism. While *BAS1* was sufficient to rescue the inflorescence phenotype (Bell et al., 2012), *LOB* could possibly restrict growth in a BR-independent manner by directly regulating cell wall modifying target genes.

Cell wall organization and remodeling

The plant cell wall is an extracellular matrix of polysaccharides and structural proteins that constrains cell expansion, in opposition to turgor. The cell

wall exhibits elastic, viscoelastic, and plastic properties under pressure (Hayot et al., 2012; Peaucelle et al., 2011; Zhang et al., 2019). Elastic strain is instantaneous and reversible. Viscoelastic strain is reversible but slow, owing to the gradual flow of molecules past one another in the cell wall under strain. Plastic strain occurs gradually and is irreversible. During diffuse growth, plastic strain or “creep” will normally only happen by the activity of cell wall modifying enzymes, which interfere with the cross-linkages between cell wall polysaccharides and allow them to irreversibly drift apart from one another (Arsuffi and Braybrook, 2018; Link and Cosgrove, 1998). A cell wall segment that is compressed will not shrink in length, but may bend, buckle or crumple. While elastic and plastic properties often have been found to correlate with one another, they are not synonymous (Bou Daher et al., 2018; Bouré et al., 2022; Peaucelle et al., 2011; Sampathkumar et al., 2019). A cell wall could become more elastic without expanding, and a change in expansion rate will not necessarily result in a corresponding change in its elastic properties. However, changes in the elastic properties of the cell wall may be mechanistically important and could reflect a change in the composition or structure of the wall, which may also affect the growth rate.

The plant cell wall is composed of cellulose microfibrils, cross-linking glycans often called hemicellulose, pectic polysaccharides, and glycoproteins, which are all interconnected in a complex, dynamic, and anisotropic network (Höfte and Voxeur, 2017). Cellulose is the most important structural component,

conferring strength and rigidity to the wall. Cellulose is made up of long, unbranched β -1,4-linked glucan polymers synthesized by cellulose synthase complexes in the cell membrane, which bundle together to form partially crystalline microfibrils (Foster et al., 1996; VanderHart and Atalla, 1984). Microfibrils are often depicted as cylindrical rods, but they have distinct hydrophilic and hydrophobic faces, which may facilitate bundling between microfibrils and interactions with other polysaccharides (Cosgrove, 2014). Microfibrils are also thought to be interconnected by cross-linking glycans, represented chiefly by xyloglucan in most eudicot cell walls. The current “biomechanical hotspot” model for cellulose-XG interactions proposes that only a small fraction of XG in the wall interacts with cellulose directly in tight junctions, where XG acts to adhere two neighboring microfibrils together (Cosgrove, 2014). The third, often most abundant polysaccharide component of the cell wall is pectin, which is made up of a diverse, highly branched, and relatively soluble network of polysaccharides that forms a gel-like matrix surrounding and interconnected with the cellulose network. Lastly, glycoproteins fill structural, mechanical, and enzymatic roles, contributing to the assembly, expansion, and biochemical remodeling of the cell wall. Despite numerous studies, the organization of cell wall polymers, and the functions of individual components, continue to pose a formidable challenge to researchers due to the complexity of the wall, high diversity between tissues and between species, redundancy of

function of cell wall genes, and intense feedback and compensation in response to perturbation of the wall.

Expansins are thought to promote expansion in acidic conditions in a non-enzymatic manner by interfering in cellulose-hemicellulose interactions, allowing crosslinked cellulose microfibrils to creep apart (Link and Cosgrove, 1998). XTH enzymes can similarly promote expansion by cutting and/or grafting the XG crosslinks (Rose et al., 2002). The role of the pectin matrix in regulating expansion is more difficult to predict. Pectic polysaccharides may be soluble, or may form rigid cross-linkages, depending upon the activity of pectin methylesterases (PMEs) (Gupta et al., 2015). Changes in PME activity can alter the apparent elasticity of the cell wall, although it is unclear whether these effects are direct or indirect (Peaucelle et al., 2011; Wolf et al., 2014). It is generally accepted that demethylesterified pectin can form more rigid cross-linkages by ionic interactions with Ca^{2+} (Cao et al., 2020). However, demethylesterified pectin is also a more suitable substrate for degradation by polygalacturonase (Levesque-Tremblay et al., 2015). PME activity also releases acid, potentially promoting expansin activity and cell expansion according to the acid growth hypothesis. Lastly, changes in the pectin matrix could affect cell wall pore size, thus determining the accessibility of other components and the diffusibility of cell wall modifying proteins (Goldberg et al., 2001). More work must be done to address these possibilities in order to understand how PME activity affects cell wall expansibility.

It should be noted that cell wall composition in higher plants is highly variable – there is no one way to build a plant cell wall. The organization discussed thus far is the “type I” primary cell wall organization typical of eudicots and noncommelinid monocots. Notably, grasses and other commelinid monocots have a drastically different polysaccharide profile, commonly referred to as “type II” cell walls (Carpita, 1996; Carpita and Gibeaut, 1993). Whereas pectins are the most abundant polysaccharide by weight in many dicot cell walls, in grasses they are much less abundant (5-10%), as is xyloglucan. Instead grasses make use of more mixed-link glucans, xylans, arabinoxylans and glucuronoarabinoxylans as cross-linking components (Kozlova et al., 2014; McCann and Carpita, 2008). Phenylpropanoids are also present in the type II primary cell wall, which form cross-linkages when the cells mature and stop expanding (de Oliveira et al., 2015; Hatfield et al., 1999). Despite the reduced reliance on XG and pectins, gene families that act on these polysaccharides, such as α -expansins, XTHs, and PMEs are still well-represented in the genome and transcriptome, albeit at lower numbers (Yokoyama and Nishitani, 2004). It is unclear if they function in the same ways as in type I cell walls, and what their relative importance is. It will be challenging to develop a model for cell wall organization and cell expansion that recognizes the underlying commonalities between diverse cell wall types without making improper generalizations.

Cell wall modifying genes have pH optima, and regulation of extracellular pH is thought to regulate cell expansion rates (Cosgrove, 1998; Moustacas et al.,

1991). Classical extensometry experiments showed that acidic pH increases the extension rate of a cell wall segment under tension (Métraux et al., 1980). This occurs primarily due to expansins, which facilitate slippage between cellulose microfibrils. While low pH has traditionally been associated with increased growth, each cell wall modifying enzyme has a pH optimum (Arsuffi and Braybrook, 2018). The effect of a change in pH on enzyme activity would depend on the profile of enzymes in a section of apoplast, and their respective pH optima.

Atomic force microscopy

Atomic force microscopy (AFM) is the best technique currently available for measuring the mechanical characteristics of the cell wall. AFM uses a cantilever to indent a surface such that the depth of indentation, and the force required to achieve that indentation, can be calculated, providing a stiffness value in Newtons per meter. Indentation curves can be processed using a Hertzian contact model, which uses the vertical indentation data to calculate the elastic stiffness of the surface while also taking the shape of the indenting tip into account, giving a value known as the indentation modulus (IM). IM is defined as the ratio between the pressure applied to a surface, the resulting relative change in surface area. It can be thought of as a measurement of the complex elastic

stiffness or, conversely, the deformability of a surface, with higher values indicating higher stiffness.

Several nanoindentation and AFM force spectroscopy experiments have demonstrated that pectin modification affects cell expansion and the apparent elastic properties of the cell wall (Bou Daher et al., 2018; Braybrook and Peaucelle, 2013; Peaucelle et al., 2011). In this application of AFM, live tissue is plasmolyzed to eliminate turgor pressure as a variable, and the IM is measured. However, interpretation of these experiments has not been straightforward. For example, it is generally expected that PME activity should promote rigidification of a pectin network due to increased Ca^{2+} -pectate cross-linkage, as described above. However, inducible overexpression of a PME in the L1 layer of the *Arabidopsis* meristem resulted instead in a dramatic reduction in the apparent stiffness of the cell wall (Peaucelle et al., 2011). Similarly, local overexpression or exogenous application of PMEs induced a local decrease in cell wall stiffness, leading to primordium initiation and outgrowth. Conversely, overexpression of a PME inhibitor (PMEI) in L1 resulted in apparent rigidification of meristem cells and inhibited lateral organ formation. Unintuitively, the more rigid meristems also appeared to have an increased average cell size, suggesting that the more rigid cell walls may have actually been more extensible. This demonstrates that the apparent elasticity of a cell, as measured by AFM, cannot be considered synonymous with or predictive of cell expansibility and growth, though they may often correlate.

AFM can be difficult in samples with a high curvature and dramatic topographical features. The probe must be able to physically access the surface, and this can be difficult in many boundary areas, which tend to be small and form clefts between adjacent organs. Additionally, AFM probes the surface directly, and mechanical differences could occur in deeper cell layers. Using a larger tip perturbs a broader and deeper area of the tissue, which may allow measurement of deeper cell layers (Peaucelle et al., 2011), but relevant mechanical differences could be difficult to interpret or be missed entirely. The ideal boundary zone for measurement with AFM should be relatively large, flat, and physically accessible, with boundary-defining factors strongly expressed in the epidermal layer. Studying such a system would provide stronger support for cell wall rigidification being an important component of the boundary function.

Organ boundaries serve several important roles in development, but the mechanisms downstream of boundary-defining factors are not well understood. In Chapter 1 of this dissertation, I show the *Arabidopsis* transcription factor LOB regulates leaf angle via a phototropism-dependent mechanism, reducing phototropic responses at the base of the leaf. LOB and other boundary-defining transcription factors also regulate the expression of numerous cell wall genes, implying a biophysical mechanism is an important aspect of boundary function. Given the inherent challenges of measuring cell wall mechanics in the *Arabidopsis* leaf-meristem boundary, I used a different system, the maize ligular region, which is highly amenable to AFM experiments. In Chapter 2, I

characterized mechanical patterns during the development of the ligular region. My findings are consistent with the existence of a cell wall rigidification program in the boundary, which correlates with patterns of growth, cell division, and auxin dynamics. In Chapter 3, I measured epidermal cell geometry and cell wall stiffness over a wide area of the maize leaf. I found that the establishment of the boundary in the maize leaf was linked not just to local changes, but to broader growth and mechanical patterns outside the boundary. This suggests that coordination between the boundary and adjacent leaf zones is involved in the morphogenesis of the maize leaf. My findings further our understanding of how plant boundaries regulate growth and cell wall mechanics, and lay the groundwork for future experimentation exploring how cell and tissue-level mechanics interact to control plant morphogenesis.

References:

- Aida, M., Ishida, T. and Tasaka, M.** (1999). Shoot apical meristem and cotyledon formation during Arabidopsis embryogenesis: interaction among the CUP-SHAPED COTYLEDON and SHOOT MERISTEMLESS genes. *Development* **126**, 1563–1570.
- Arnaud, N. and Laufs, P.** (2013). Plant development: brassinosteroids go out of bounds. *Curr. Biol.* **23**, R152–R154.
- Arsovski, A. A., Galstyan, A., Guseman, J. M. and Nemhauser, J. L.** (2012). Photomorphogenesis. *Arabidopsis Book* **10**, e0147.
- Arsuffi, G. and Braybrook, S. A.** (2018). Acid growth: an ongoing trip. *Journal of Experimental Botany* **69**, 137–146.
- Bell, E. M., Lin, W., Husbands, A. Y., Yu, L., Jaganatha, V., Jablonska, B., Mangeon, A., Neff, M. M., Girke, T. and Springer, P. S.** (2012). *Arabidopsis* LATERAL ORGAN BOUNDARIES negatively regulates brassinosteroid accumulation to limit growth in organ boundaries. *Proc. Natl. Acad. Sci. U.S.A.* **109**, 21146–21151.
- Blakeslee, J. J., Bandyopadhyay, A., Peer, W. A., Makam, S. N. and Murphy, A. S.** (2004). Relocalization of the PIN1 Auxin Efflux Facilitator Plays a Role in Phototropic Responses. *Plant Physiology* **134**, 28–31.
- Bou Daher, F., Chen, Y., Bozorg, B., Clough, J., Jönsson, H. and Braybrook, S. A.** (2018). Anisotropic growth is achieved through the additive mechanical effect of material anisotropy and elastic asymmetry. *eLife* **7**, e38161.
- Bouré, N., Peaucelle, A., Goussot, M., Adroher, B., Soubigou-Taconnat, L., Borrega, N., Biot, E., Tariq, Z., Martin-Magniette, M.-L., Pautot, V., et al.** (2022). A cell wall-associated gene network shapes leaf boundary domains. *Development* **149**, dev200359.
- Braybrook, S. A. and Peaucelle, A.** (2013). Mechano-Chemical Aspects of Organ Formation in Arabidopsis thaliana: The Relationship between Auxin and Pectin. *PLOS ONE* **8**, e57813.
- Briggs, W. R., Beck, C. F., Cashmore, A. R., Christie, J. M., Hughes, J., Jarillo, J. A., Kagawa, T., Kanegae, H., Liscum, E., Nagatani, A., et al.** (2001). The Phototropin Family of Photoreceptors. *Plant Cell* **13**, 993–997.

- Cao, L., Lu, W., Mata, A., Nishinari, K. and Fang, Y.** (2020). Egg-box model-based gelation of alginate and pectin: A review. *Carbohydrate Polymers* **242**, 116389.
- Carpita, N. C.** (1996). Structure and Biogenesis of the Cell Walls of Grasses. *Annual Review of Plant Physiology and Plant Molecular Biology* **47**, 445–476.
- Carpita, N. C. and Gibeaut, D. M.** (1993). Structural models of primary cell walls in flowering plants: consistency of molecular structure with the physical properties of the walls during growth. *The Plant Journal* **3**, 1–30.
- Che, X., Splitt, B. L., Eckholm, M. T., Miller, N. D. and Spalding, E. P.** (2023). BRXL4-LAZY1 interaction at the plasma membrane controls Arabidopsis branch angle and gravitropism. *The Plant Journal* **113**, 211–224.
- Christie, J. M.** (2007). Phototropin Blue-Light Receptors. *Annu. Rev. Plant Biol.* **58**, 21–45.
- Christie, J. M., Salomon, M., Nozue, K., Wada, M. and Briggs, W. R.** (1999). LOV (light, oxygen, or voltage) domains of the blue-light photoreceptor phototropin (nph1): Binding sites for the chromophore flavin mononucleotide. *Proc. Natl. Acad. Sci. U.S.A.* **96**, 8779–8783.
- Cosgrove, D. J.** (1998). Cell Wall Loosening by Expansins1. *Plant Physiology* **118**, 333–339.
- Cosgrove, D. J.** (2014). Re-constructing our models of cellulose and primary cell wall assembly. *Current Opinion in Plant Biology* **22**, 122–131.
- Cucinotta, M., Manrique, S., Cuesta, C., Benkova, E., Novak, O. and Colombo, L.** (2018). CUP-SHAPED COTYLEDON1 (CUC1) and CUC2 regulate cytokinin homeostasis to determine ovule number in Arabidopsis. *J. Exp. Bot.* **69**, 5169–5176.
- de Carbonnel, M., Davis, P., Roelfsema, M. R. G., Inoue, S., Schepens, I., Lariguet, P., Geisler, M., Shimazaki, K., Hangarter, R. and Fankhauser, C.** (2010). The Arabidopsis PHYTOCHROME KINASE SUBSTRATE2 Protein Is a Phototropin Signaling Element That Regulates Leaf Flattening and Leaf Positioning. *Plant Physiol.* **152**, 1391–1405.

- de Oliveira, D. M., Finger-Teixeira, A., Rodrigues Mota, T., Salvador, V. H., Moreira-Vilar, F. C., Correa Molinari, H. B., Craig Mitchell, R. A., Marchiosi, R., Ferrarese-Filho, O. and Dantas dos Santos, W.** (2015). Ferulic acid: a key component in grass lignocellulose recalcitrance to hydrolysis. *Plant Biotechnology Journal* **13**, 1224–1232.
- Ding, Z., Galván-Ampudia, C. S., Demarsy, E., Łangowski, Ł., Kleine-Vehn, J., Fan, Y., Morita, M. T., Tasaka, M., Fankhauser, C., Offringa, R., et al.** (2011). Light-mediated polarization of the PIN3 auxin transporter for the phototropic response in Arabidopsis. *Nat Cell Biol* **13**, 447–452.
- Duncan, W. G.** (1971). Leaf Angles, Leaf Area, and Canopy Photosynthesis¹. *Crop Sci.* **11**, cropsoci1971.0011183X001100040006x.
- Fankhauser, C.** (2001). The Phytochromes, a Family of Red/Far-red Absorbing Photoreceptors *. *J. Biol. Chem.* **276**, 11453–11456.
- Foster, T. J., Ablett, S., McCann, M. C. and Gidley, M. J.** (1996). Mobility-resolved ¹³C-NMR spectroscopy of primary plant cell walls. *Biopolymers* **39**, 51–66.
- Gallavotti, A.** (2013). The role of auxin in shaping shoot architecture. *J. Exp. Bot.* **64**, 2593–2608.
- Gallavotti, A., Barazesh, S., Malcomber, S., Hall, D., Jackson, D., Schmidt, R. J. and McSteen, P.** (2008). Sparse inflorescence¹ encodes a monocot-specific YUCCA-like gene required for vegetative and reproductive development in maize. *Proc. Natl. Acad. Sci. U. S. A.* **105**, 15196–15201.
- Goldberg, R., Pierron, M., Bordenave, M., Breton, C., Morvan, C. and Penhoat, C. H. du** (2001). Control of Mung Bean Pectinmethylesterase Isoform Activities: INFLUENCE OF pH AND CARBOXYL GROUP DISTRIBUTION ALONG THE PECTIC CHAINS *. *Journal of Biological Chemistry* **276**, 8841–8847.
- Gupta, R., Kohli, P. and Kalia, M.** (2015). Bioprocessing & Biotechniques Pectin Methylesterases: A Review. **5**,.
- Han, Y.-J., Song, P.-S. and Kim, J.** (2007). Phytochrome-mediated photomorphogenesis in plants. *J. Plant Biol.* **50**, 230–240.
- Hangarter, R. P.** (1997). Gravity, light and plant form. *Plant Cell Environ.* **20**, 796–800.

- Hatfield, R. D., Ralph, J. and Grabber, J. H.** (1999). Cell wall cross-linking by ferulates and diferulates in grasses. *Journal of the Science of Food and Agriculture* **79**, 403–407.
- Hayot, C. M., Forouzesh, E., Goel, A., Avramova, Z. and Turner, J. A.** (2012). Viscoelastic properties of cell walls of single living plant cells determined by dynamic nanoindentation. *Journal of Experimental Botany* **63**, 2525–2540.
- Heisler, M. G., Ohno, C., Das, P., Sieber, P., Reddy, G. V., Long, J. A. and Meyerowitz, E. M.** (2005). Patterns of auxin transport and gene expression during primordium development revealed by live imaging of the *Arabidopsis* inflorescence meristem. *Curr. Biol.* **15**, 1899–1911.
- Höfte, H. and Voxeur, A.** (2017). Plant cell walls. *Current Biology* **27**, R865–R870.
- Hohm, T., Demarsy, E., Quan, C., Allenbach Petrolati, L., Preuten, T., Vernoux, T., Bergmann, S. and Fankhauser, C.** (2014). Plasma membrane H⁺-ATPase regulation is required for auxin gradient formation preceding phototropic growth. *Molecular Systems Biology* **10**, 751.
- Husbands, A., Bell, E. M., Shuai, B., Smith, H. M. S. and Springer, P. S.** (2007). LATERAL ORGAN BOUNDARIES defines a new family of DNA-binding transcription factors and can interact with specific bHLH proteins. *Nucleic Acids Res.* **35**, 6663–6671.
- Hussey, G.** (1971). Cell division and expansion and resultant tissue tensions in the shoot apex during the formation of a leaf primordium in the tomato. *J. Exp. Bot.* **22**, 702–714.
- Inada, S., Ohgishi, M., Mayama, T., Okada, K. and Sakai, T.** (2004). RPT2 Is a Signal Transducer Involved in Phototropic Response and Stomatal Opening by Association with Phototropin 1 in *Arabidopsis thaliana*. *Plant Cell* **16**, 887–896.
- Kasahara, M., Kagawa, T., Oikawa, K., Suetsugu, N., Miyao, M. and Wada, M.** (2002). Chloroplast avoidance movement reduces photodamage in plants. *Nature* **420**, 829–832.
- Kawamoto, N. and Morita, M. T.** (2022). Gravity sensing and responses in the coordination of the shoot gravitropic setpoint angle. *New Phytologist* **236**, 1637–1654.

- Kozlova, L. V., Ageeva, M. V., Ibragimova, N. N. and Gorshkova, T. A.** (2014). Arrangement of mixed-linkage glucan and glucuronoarabinoxylan in the cell walls of growing maize roots. *Annals of Botany* **114**, 1135–1145.
- Lariguet, P., Schepens, I., Hodgson, D., Pedmale, U. V., Trevisan, M., Kami, C., de Carbonnel, M., Alonso, J. M., Ecker, J. R., Liscum, E., et al.** (2006). PHYTOCHROME KINASE SUBSTRATE 1 is a phototropin 1 binding protein required for phototropism. *Proc. Natl. Acad. Sci. U.S.A.* **103**, 10134–10139.
- Lee, D.-K., Geisler, M. and Springer, P. S.** (2009). *LATERAL ORGAN FUSION1* and *LATERAL ORGAN FUSION2* function in lateral organ separation and axillary meristem formation in *Arabidopsis*. *Development* **136**, 2423–2432.
- Levesque-Tremblay, G., Pelloux, J., Braybrook, S. A. and Müller, K.** (2015). Tuning of pectin methylesterification: consequences for cell wall biomechanics and development. *Planta* **242**, 791–811.
- Liljegren, S. J.** (2012). Organ abscission: exit strategies require signals and moving traffic. *Current Opinion in Plant Biology* **15**, 670–676.
- Lin, W., Shuai, B. and Springer, P. S.** (2003). The Arabidopsis *LATERAL ORGAN BOUNDARIES*–domain gene *ASYMMETRIC LEAVES2* functions in the repression of *KNOX* gene expression and in adaxial-abaxial patterning. *Plant Cell* **15**, 2241–2252.
- Link, B. M. and Cosgrove, D. J.** (1998). Acid-Growth Response and α -Expansins in Suspension Cultures of Bright Yellow 2 Tobacco1. *Plant Physiology* **118**, 907–916.
- Luesse, D. R., DeBlasio, S. L. and Hangarter, R. P.** (2010). Integration of phot1, phot2, and PhyB signalling in light-induced chloroplast movements. *J. Exp. Bot.* **61**, 4387–4397.
- Ma, L. and Li, G.** (2019). Auxin-Dependent Cell Elongation During the Shade Avoidance Response. *Frontiers in Plant Science* **10**,.
- Mantilla-Perez, M. B. and Salas Fernandez, M. G.** (2017). Differential manipulation of leaf angle throughout the canopy: current status and prospects. *J. Exp. Bot.* **68**, 5699–5717.
- Mao, J., Zhang, Y.-C., Sang, Y., Li, Q.-H. and Yang, H.-Q.** (2005). A role for Arabidopsis cryptochromes and COP1 in the regulation of stomatal opening. *Proc. Natl. Acad. Sci. U.S.A.* **102**, 12270–12275.

- Más, P., Devlin, P. F., Panda, S. and Kay, S. A.** (2000). Functional interaction of phytochrome B and cryptochrome 2. *Nature* **408**, 207–211.
- McCann, M. C. and Carpita, N. C.** (2008). Designing the deconstruction of plant cell walls. *Current Opinion in Plant Biology* **11**, 314–320.
- Medford, J., Behringer, F., Callos, J. and Feldmann, K.** (1992). Normal and abnormal development in the Arabidopsis vegetative shoot apex. *Plant Cell* **4**, 631–643.
- Métraux, J.-P., Richmond, P. A. and Taiz, L.** (1980). Control of Cell Elongation in Nitella by Endogenous Cell Wall pH Gradients: MULTIAXIAL EXTENSIBILITY AND GROWTH STUDIES 1. *Plant Physiology* **65**, 204–210.
- Motchoulski, A. and Liscum, E.** (1999). Arabidopsis NPH3: A NPH1 Photoreceptor-Interacting Protein Essential for Phototropism. *Science* **286**, 961–964.
- Moustacas, A. M., Nari, J., Borel, M., Noat, G. and Ricard, J.** (1991). Pectin methylesterase, metal ions and plant cell-wall extension. The role of metal ions in plant cell-wall extension. *Biochemical Journal* **279**, 351–354.
- Nahar, M. A.-U., Ishida, T., Smyth, D. R., Tasaka, M. and Aida, M.** (2012). Interactions of CUP-SHAPED COTYLEDON and SPATULA genes control carpel margin development in Arabidopsis thaliana. *Plant Cell Physiol.* **53**, 1134–1143.
- Nemhauser, J. and Chory, J.** (2002). Photomorphogenesis. *Arabidopsis Book* **1**, e0054.
- Ori, N., Eshed, Y., Chuck, G., Bowman, J. L. and Hake, S.** (2000). Mechanisms that control knox gene expression in the Arabidopsis shoot. *Development* **127**, 5523–5532.
- Peaucelle, A., Braybrook, S. A., Le Guillou, L., Bron, E., Kuhlemeier, C. and Höfte, H.** (2011). Pectin-induced changes in cell wall mechanics underlie organ initiation in Arabidopsis. *Curr. Biol.* **21**, 1720–1726.
- Pendleton, J. W., Smith, G. E., Winter, S. R. and Johnston, T. J.** (1968). Field Investigations of the Relationships of Leaf Angle in Corn (*Zea mays* L.) to Grain Yield and Apparent Photosynthesis¹. *Agron. J.* **60**, 422–424.
- Poppe, C. and Schafer, E.** (1997). Seed Germination of Arabidopsis thaliana phyA/phyB Double Mutants Is under Phytochrome Control. *Plant Physiology* **114**, 1487–1492.

- Raman, S., Greb, T., Peaucelle, A., Blein, T., Laufs, P. and Theres, K.** (2008). Interplay of miR164, CUP-SHAPED COTYLEDON genes and LATERAL SUPPRESSOR controls axillary meristem formation in *Arabidopsis thaliana*. *The Plant Journal* **55**, 65–76.
- Rast, M. I. and Simon, R.** (2008). The meristem-to-organ boundary: more than an extremity of anything. *Curr. Opin. Genet. Dev.* **18**, 287–294.
- Rose, J. K. C., Braam, J., Fry, S. C. and Nishitani, K.** (2002). The XTH Family of Enzymes Involved in Xyloglucan Endotransglucosylation and Endohydrolysis: Current Perspectives and a New Unifying Nomenclature. *Plant and Cell Physiology* **43**, 1421–1435.
- Sampathkumar, A., Peaucelle, A., Fujita, M., Schuster, C., Persson, S., Wasteneys, G. O. and Meyerowitz, E. M.** (2019). Primary wall cellulose synthase regulates shoot apical meristem mechanics and growth. *Development* **146**, dev179036.
- Sharrock, T. E. and Sanson, B.** (2020). Cell sorting and morphogenesis in early *Drosophila* embryos. *Seminars in Cell & Developmental Biology* **107**, 147–160.
- Toyota, M. and Gilroy, S.** (2013). Gravitropism and mechanical signaling in plants. *Am. J. Bot.* **100**, 111–125.
- VanderHart, D. L. and Atalla, R. H.** (1984). Studies of microstructure in native celluloses using solid-state carbon-13 NMR. *Macromolecules* **17**, 1465–1472.
- Vaughan, J. G.** (1955). The morphology and growth of the vegetative and reproductive apices of *Arabidopsis thaliana* (L.) Heynh., *Capsella bursa-pastoris* (L.) Medic. and *Anagallis arvensis* L. *Bot. J. Linn. Soc.* **55**, 279–301.
- Waite, J. M. and Dardick, C.** (2018). TILLER ANGLE CONTROL 1 modulates plant architecture in response to photosynthetic signals. *J. Exp. Bot.* **69**, 4935–4944.
- Wang, Q., Hasson, A., Rossmann, S. and Theres, K.** (2016). Divide et impera: boundaries shape the plant body and initiate new meristems. *New Phytologist* **209**, 485–498.

- Wolf, S., van der Does, D., Ladwig, F., Sticht, C., Kolbeck, A., Schürholz, A.-K., Augustin, S., Keinath, N., Rausch, T., Greiner, S., et al. (2014).** A receptor-like protein mediates the response to pectin modification by activating brassinosteroid signaling. *Proc. Natl. Acad. Sci. U.S.A.* **111**, 15261–15266.
- Yang, X., Li, R., Jablonski, A., Stovall, A., Kim, J., Yi, K., Ma, Y., Beverly, D., Phillips, R., Novick, K., et al. (2023).** Leaf angle as a leaf and canopy trait: Rejuvenating its role in ecology with new technology. *Ecology Letters* **26**, 1005–1020.
- Yates, D. J. (1981).** Effect of the Angle of Incidence of Light on the Net Photosynthesis Rates of Sorghum alnum Leaves. *Functional Plant Biol.* **8**, 335–346.
- Yokoyama, R. and Nishitani, K. (2004).** Genomic Basis for Cell-Wall Diversity in Plants. A Comparative Approach to Gene Families in Rice and Arabidopsis. *Plant and Cell Physiology* **45**, 1111–1121.
- Zhang, T., Tang, H., Vavylonis, D. and Cosgrove, D. J. (2019).** Disentangling loosening from softening: insights into primary cell wall structure. *The Plant Journal* **100**, 1101–1117.

Chapter 1

The AS2/LBD transcription factor LOB regulates leaf angle in the *Arabidopsis* rosette via a phot1-dependent mechanism.

Abstract:

Leaf angle is a critical trait for optimal light capture. Phototropism affects leaf positioning in response to blue light illumination. Here, we report that the transcription factor LATERAL ORGAN BOUNDARIES (LOB) affects leaf angle via a phototropism-dependent mechanism. Misexpression of LOB under control of the 35S promoter in *Arabidopsis* seedlings resulted in repression of three genes involved in phototropism, *PHOT1*, *PKS2*, and *NPH3*, and reduced hypocotyl phototropism. LOB was confirmed to physically bind to consensus sequences in *PHOT1* and *PKS2* both in yeast and *in planta*. *lob* mutants had more horizontally oriented leaves, but leaf angle was more responsive to low intensity blue light, suggesting derepression of phototropic signaling in the boundary domain. Overall, LOB regulates seedling architecture by generating a more vertical attachment angle at the base of the petiole, while reducing the responsiveness of the boundary region to blue light.

Introduction:

Plant physiology, growth, and development are informed by environmental cues such as temperature, gravity, touch, light intensity, light quality, light direction, and photoperiod (Guo et al., 2018; Hangarter, 1997; Toyota and Gilroy, 2013). Plants must optimize their use of resources available in their microenvironment, especially light. Several protein families sense light conditions and initiate signals to modulate plant architecture and physiology. Phytochromes are most sensitive to red light, with the type II phytochromes sensing the red/far red ratio (Fankhauser, 2001). Blue and UV-A light sensors include phototropins, cryptochromes, and Zeitlupe proteins (Banerjee and Batschauer, 2005). Phototropins regulate stomatal opening, chloroplast positioning, and growth responses to blue light such as hypocotyl bending, leaf positioning, and blade flattening (Christie, 2007). Cryptochromes are involved in several blue light-responsive processes, often working together with phototropins, such as in the regulation of stomatal opening (Mao et al., 2005), or with phytochromes, as in the repression of hypocotyl elongation during photomorphogenesis (Más et al., 2000). Zeitlupe proteins primarily regulate the circadian clock (Kim et al., 2007; Somers et al., 2000). The deployment of photoreceptor families with varying sensitivity and photolability, tunable downstream responses, and crosstalk between signaling pathways give plants sensitive yet robust means of responding to dynamic light conditions.

Phototropin proteins are so named due to their control of directional light responses (Christie et al., 1999). While phototropins localize to the cytosol, Golgi apparatus, chloroplast periphery, and plasma membrane, they do not have transmembrane domains (Jaedicke et al., 2012). They have a N-terminal region containing the light-sensitive LOV1 and LOV2 domains, and a C-terminal Ser/Thr kinase domain (Christie et al., 1999). The C-terminal domain also contains a diproline motif which is necessary for membrane localization, although the mechanism responsible for plasma membrane localization is still not fully understood (Hirano et al., 2022). The Arabidopsis genome contains two phototropin genes, *PHOTOTROPIN1* (*PHOT1*) and *PHOTOTROPIN2* (*PHOT2*) (Christie, 2007). *phot1* is considerably more sensitive to low intensity blue light ($< 0.1 \mu\text{Em}^{-2}\text{s}^{-1}$) than *phot2* (over $1 \mu\text{Em}^{-2}\text{s}^{-1}$) (Harada et al., 2003; Takemiya et al., 2005). These proteins redundantly promote stomatal opening in response to blue light, along with the cryptochromes (Inada et al., 2004; Kinoshita et al., 2001; Mao et al., 2005). Both *phot1* and *phot2* promote chloroplast accumulation in response to blue light, while *phot2* promotes the chloroplast avoidance response at high intensities of blue light (Luesse et al., 2010). The chloroplast accumulation/avoidance signaling of *phot2* is temperature-sensitive, with low temperatures promoting the avoidance response (Fujii et al., 2017; Kodama et al., 2008). Both phototropins redundantly regulate hypocotyl bending, blade flattening, and leaf inclination (de Carbonnel et al., 2010). They have been shown to physically interact with the PHYTOCHROME KINASE SUBSTRATE (PKS)

family, which has four members in Arabidopsis, *PKS1/2/3/4*, as well as the BTB/POZ proteins NON-PHOTOTROPIC HYPOCOTYL 3 (*NPH3*) and ROOT PHOTOTROPISM 2 (*RPT2*) (Inada et al., 2004; Lariguet and Dunand, 2005; Lariguet et al., 2006; Motchoulski and Liscum, 1999). These phot-interacting proteins are essential for phototropin responses, with *NPH3* and *RPT2* being responsible for transduction of the signal, possibly by regulating the activity of transcription factors in the nucleus (Lin, 2002; Sakai et al., 2000). *PKS2* is more important for controlling leaf inclination than other *PKS* genes (de Carbonnel et al., 2010). There may be combinations of *phot1/2*, *PKS1/2/3/4*, and *NPH3/RPT2* that are specific for certain responses, either due to their expression patterns or differences in downstream effects.

Leaf and branch angle are agronomically important traits in the plant shoot. The number and angle of branches and the orientation of leaves affect the efficiency of photosynthetic light capture, as well as the amount of competition between neighboring plants (Digby and Firn, 2002; Duncan, 1971; Pendleton et al., 1968; Waite and Dardick, 2018). These traits are controlled by several mechanisms, including organ boundary formation, gravitropism, and phototropism. Branch angle is determined primarily by gravitropism. Genes such as *TAC1*, *LAZY1*, and *BRXL4* act within gravity-sensing cells to determine the angle at which branches grow out from the main stem, contributing to the architecture of the canopy (Kawamoto and Morita, 2022; Waite and Dardick, 2018). Leaf angle is determined by several factors and is actively regulated in

response to light conditions. If a leaf is shaded, phytochrome signaling can induce the shade avoidance response (Ma and Li, 2019). Stems and petioles elongate, and leaf angle tends to become more vertical, which increases the chances that the plant will escape the shade. Phototropism is also known to promote more vertical leaf angles in response to blue light (de Carbonnel et al., 2010). Thus, environmental responses interact with intrinsic developmental processes to determine the orientation of leaves and branches. Generally, more vertical leaf and branch orientation allow for increased planting density, which can improve yield.

Boundary domains are zones of restricted growth that separate adjacent organs or organ subunits (Aida and Tasaka, 2006; Rast and Simon, 2008). The AS2/LBD transcription factor LATERAL ORGAN BOUNDARIES (LOB) is partially responsible for growth suppression in boundaries (Bell et al., 2012). *LOB* is expressed at meristem-leaf boundaries, at the base of floral organs and pedicels, and at the flanks of initiating lateral roots (Bell et al., 2012; Shuai et al., 2002). *LOB* has been previously shown to bind to a consensus motif to transcriptionally up- and down-regulate numerous target genes, notably upregulating the brassinosteroid (BR) catabolism gene *PHYB* ACTIVATION TAGGED SUPPRESSOR 1 (*BAS1*) (Bell et al., 2012; Husbands et al., 2007). Null mutations in *lob* resulted in an extended zone of contact between the cauline leaf and axillary stem, and this phenotype was rescued by expressing *BAS1* under control of the *LOB* promoter (Bell et al., 2012). Additionally, *LOB* regulates many

cell wall-modifying genes, many of which have been previously identified as downstream targets of BR signaling. Therefore, LOB cell wall target genes may be regulated directly by LOB itself, and/or indirectly via BAS1-mediated suppression of BR signaling.

Boundary domains are important determinants of plant architecture due to their position at junctions between organs. The boundary function itself helps facilitate organ separation, but furthermore, boundaries are often associated with the development of specialized structures which control the orientation of organs. For example, in legumes, a specialized motor organ called the pulvinus actively controls leaf positioning. *Petiolule-like pulvinus (PLP)*, the *Medicago* ortholog of *LOB*, specifies pulvinus development at boundaries, and affects pulvinus functionality via a *BAS1*-dependent mechanism (Kong et al., 2021). In the maize inflorescence, the LBD transcription factor *ramosa2* is expressed in the bract axil, and affects tassel branch angle (Bortiri et al., 2006). Tassel branch angle is also affected by the development of a structure called the pulvinus, which is distinct from the legume pulvinus and forms at the base of the tassel branches (Bai et al., 2012). Furthermore, leaf angle in grasses is affected by the development of structures at the blade-sheath boundary. Referred to as the auricle in maize, and as the lamina joint in rice, these hinge-like structures control the angle at which the blade projects from the culm. Therefore, the co-opting of boundary-associated factors to regulate organ positioning may have evolved independently in multiple plant lineages. In some cases, as in the legume pulvinus, boundary-

associated organ positioning is affected by multiple inputs such as phytohormones and environmental signals. Due to their position, boundaries are ideally situated to regulate organ positioning, potentially integrating intrinsic and extrinsic cues from multiple organs.

In this study, we show that LOB directly regulates the phototropism genes *PHOT1*, *PKS2*, and *NPH3*. LOB misexpression in *Arabidopsis* seedlings repressed phototropic signaling genes and specifically reduced phototropic hypocotyl bending. *lob-3* mutants had more horizontally oriented leaves under both white light and red light, a phenotype which was not rescued by BAS1. However, the leaf attachment angle was hyperresponsive to low intensity blue light in *lob-3* mutants, suggesting a derepression of phototropism genes in the *LOB* expression domain made the leaf attachment angle more responsive to blue light. Overall, our data suggests that LOB affects *Arabidopsis* seedling architecture, promoting more vertically oriented leaves overall while reducing the responsiveness of the boundary to blue light.

Materials and Methods:

Plant materials and growth conditions:

lob-3, *pLOB:LOB-GR*, *pLOB:BAS1*, *35S:LOB-GR*, and *phot1* (SALK 088841) Are all in the Col-0 background. *lob:DsE* is in the *Ler* background. For plants grown on agar plates, seeds were sterilized with 95% EtOH for 5 minutes, and 5 minutes in 30% bleach, and rinsed repeatedly with sterile water. They were then plated with a regular spacing of about one square centimeter per seed on Murashige and Skoog media with 1% sucrose, pH 5.7, and stratified in the dark at 4°C for 48 hours, then moved to a growth chamber at 100 $\mu\text{Em}^{-2}\text{s}^{-1}$ white light at 22°C on a 16 hour light / 8 hour dark cycle. For seedlings grown on soil, seeds were similarly sterilized and sown on Sunshine Mix soil with 10 μM Marathon and illuminated with 100 $\mu\text{Em}^{-2}\text{s}^{-1}$ white light at 22°C, 16hL/8hD. Light intensity was measured with a Li-COR LI-250A light meter.

Generation of double mutants and transformation:

For the *lob-3 phot1* experiment, a *phot1* T-DNA heterozygous mutant line (SALK 088841) was obtained from SALK and genotyped to confirm the presence of the T-DNA. Homozygous *phot1* mutant plants were identified among progeny of the original line. The homozygous lines were tested via a hypocotyl bending assay and were unresponsive to low-intensity blue light from the side, confirming that *phot1* function is eliminated in this line. Homozygous *lob-3* single mutants

were crossed with *phot1* homozygotes, and double mutants were identified by genotyping the F2 generation. Single mutants and wild-type lines were also identified in the F2 and F3 generations for comparison against the double mutant.

For transformations, *Arabidopsis* plants were grown under standard conditions as previously described. Binary vectors were transformed into GV3101 *Agrobacterium* using standard procedures, and *Arabidopsis* were transformed via the floral dip method, as previously described (Clough and Bent, 1998). Transformants were selected either by BASTA spray (Finale, AgrEvo) on soil or growth on MS media supplemented with 50 μM phosphinothricin (Sigma).

Leaf angle experiments:

Plants were grown in white light conditions as described above for about 12 days, until reaching stage 1.04 (Boyes et al., 2001). They were then transferred to a growth chamber with either continuous 50 $\mu\text{Em}^{-2}\text{s}^{-1}$ red light or continuous 50 $\mu\text{Em}^{-2}\text{s}^{-1}$ red and 0.1 $\mu\text{Em}^{-2}\text{s}^{-1}$ blue light at 22°C for 24 hours. Plants were then removed from the soil or agar plate and laid flat on their side for imaging. Images were collected using a Leica MZ12 Stereoscope and a SPOT RT3 camera at 16-25X total magnification. Cotyledons were removed using forceps. Care was taken to lay the seedlings flat and specifically get images of the base of the petiole of the first pair of true leaves. At least 25 plants were

imaged per treatment per genotype per trial. Leaf angle was determined in FIJI by taking the angle between the two petioles at the point of attachment and dividing by two to give the average leaf attachment angle of the first two true leaves per plant. This results in an angle measurement that is relative to the vertical axis, with smaller angles indicating more vertically-oriented leaves.

For experiments with DEX-inducible lines, plates were prepared with 10 μM DEX, and mock plates were prepared with an equivalent volume of ethanol added. For DEX-induction in soil experiments, plants were given mock and 10 μM DEX-supplemented water.

Hypocotyl bending experiments:

Plates were either supplemented with 10 nM DEX or a mock treatment with an equivalent volume of ethanol. For phototropic experiments, seedlings were grown on vertical square plates in the dark for 3 days before unilateral blue light exposure from the side at an intensity of $0.1 \mu\text{Em}^{-2}\text{s}^{-1}$ for 24 hours. For gravitropic experiments, plants were also grown for 3 days on vertical square plates in the dark and then re-oriented 90 degrees and left for another 24 hours. The hypocotyl bending angle was measured in FIJI between the vector at the base of the hypocotyl and the vector at the apical end of the hypocotyl.

Transcript analysis:

Total RNA was isolated using TRIzol reagent (MRC Inc.). RT-PCR was conducted as previously described. EF1 α was used as the reference gene because of its high and stable expression levels. Primers used are shown in Table 1.1. qRT-PCR was performed using EvaGreen dye on a Bio-Rad CFX Connect thermocycler and analyzed with Bio-Rad CFX Maestro software. Relative transcript levels were calculated using the Pfaffl method (Pfaffl et al., 2004). Significance was calculated via student's t-test.

Chromatin immunoprecipitation:

13-day old *35S:LOB-GR* seedlings were induced by flooding with either 15 μ M DEX or mock treatment. Induction was confirmed by transcript analysis of downstream target *BAS1*. CHIP was carried out as previously described using an anti-LOB or anti-GST polyclonal antibody (Saleh et al., 2008). Relative binding was calculated by comparing DEX-treated to mock-treated samples. All data were normalized to control gene *ACT2*. Primers for binding are listed in Table 1.1.

Yeast-1-hybrid:

A 700 bp region including the putative LOB binding site I of *PHOT1*, a 3-kb region of the *NPH3* gene including the promoter and putative LOB binding sites I & II, and the 1.1 kb region including the putative binding site upstream of *PKS2* were PCR amplified with B1R and B4 Gateway adapters. Using the BP reaction, these fragments were cloned into the pDONR-P4-P1R entry vector (Invitrogen). Then, using the LR Clonase reaction, these fragments were inserted upstream of the HIS auxotrophic selectable marker using the MW #2 vector (Deplancke et al., 2004). *PHOT1*-pMW#2, *PKS2*-pMW#2, and *NPH3*-pMW#2 were transformed into yeast as previously described (Deplancke et al., 2006). The LOB-AD and Empty-AD plasmid were transformed with a lithium acetate protocol (Clontech).

Results:

LOB* misexpression downregulates the phototropism genes *PHOT1*, *PKS2*, and *NPH3

An experiment designed to identify genes regulated by *LOB*, using an inducible misexpression system, identified *PHOT1*, *PKS2*, and *NPH3* as putative downstream targets of *LOB* regulation (Bell et al., 2012). To verify this observation, we quantified transcript levels of phototropism genes using qRT-PCR (Fig. 1.1). Plants expressing *35S:LOB-GR* treated with dexamethasone (DEX) showed an approximately 50% reduction in transcript levels of *PHOT1*, *PKS2*, and *NPH3* compared to mock-treated plants. Furthermore, *35S:LOB-GR* plants treated with both DEX and the translational inhibitor cycloheximide (CHX) showed a 50% reduction in *PHOT1*, *PKS2* and *NPH3* transcript levels compared to plant treated with CHX alone, suggesting that *LOB* directly represses the transcription of these phototropism-related genes. These results are consistent with *PHOT1*, *PKS2* and *NPH3* being direct targets of *LOB* transcriptional regulation.

LOB* directly binds to the genomic regions of *PKS2* and *PHOT1

PHOT1, *PKS2*, and *NPH3* were down-regulated in response to *LOB* misexpression (Fig. 1.1). Analysis of the genomic sequences for these genes revealed the presence of canonical *LOB* binding motifs in exonic regions of

PHOT1 and *NPH3* and in the promoter region of *PKS2* (Fig. 1.2A). *PHOT1* contains two LOB binding sites: one in the first exon containing two LOB consensus motifs separated by 5 bps, and one in the fourth exon. *PKS2* has one binding site containing two LOB binding motifs separated by 23 bps, located in exon of a neighboring gene approximately 600 bps upstream of the *PKS2* transcriptional start site. *NPH3* has five LOB binding motifs: one each in the first, second, and fifth exon, and two in the fourth exon. We tested whether LOB physically interacts with the regions containing these binding motifs using a yeast-1-hybrid assay. Genomic regions containing the LOB binding motifs for *PHOT1*, *PKS2*, and *NPH3* were used as bait while the prey construct was either the GAL4 activation domain (AD) alone or fused to LOB. Yeast grew under restrictive conditions for *PHOT1*+LOB-AD and *PKS2*+LOB-AD, but not the other combinations. Therefore, LOB binds to the *PKS2* and *PHOT1* genomic regions in yeast, but not to *NPH3* (Fig. 1.2B).

To confirm LOB's binding to these genomic regions *in planta*, we performed a chromatin immunoprecipitation (ChIP) experiment. Anti-LOB antibodies were used to pull down LOB and associated DNA 35S:*LOB-GR* seedlings (Fig. 1.2C). Quantification using qPCR detected significant enrichment in DEX-treated samples compared to mock-treated samples for region I of *PHOT1*, but not region II. As a negative control, ChIP with an anti-GST antibody showed no change in the relative enrichment of the binding site between mock and DEX-treated plants (Fig. 1.2C). We also detected significant enrichment of

the LOB binding site upstream of *PKS2* in DEX-treated plants when using anti-LOB, but not anti-GST. However, no significant enrichment was observed for any of the putative LOB binding sites in *NPH3* (Fig. 1.2C). Taken together, the yeast and ChIP results are consistent with LOB directly binding to the *PHOT1* and *PKS2* genomic regions.

***lob* mutants have more horizontally-oriented leaves under standard growth conditions**

Given that phototropic signaling genes are putative targets of LOB regulation, we examined *lob-3* mutants for defects in blue light responses. Phototropin-mediated blue light responses include changes in leaf positioning, so we examined leaf angle in *lob* mutants. We specifically measured the angle at which the petiole attaches to the stem, which we call the leaf attachment angle (Fig. 1.3A,B). While wild-type Col-0 seedlings grown in white light in 16L/8D photoperiod had an average leaf attachment angle of 35.9° relative to the vertical axis, *lob-3* leaves were significantly more horizontal, with an average leaf attachment angle of 45.4° (Fig. 1.3C). Similarly, the enhancer trap mutant *lob::DsE* in the Landsberg *erecta* genetic background had more horizontal leaf attachment angle than the wild-type control. To confirm that LOB loss-of-function is responsible for the leaf angle phenotype, we used a GR-inducible system to restore LOB activity in its native expression domain (Fig. 1.3D). Seedlings were

grown in white light on agar media containing either 15 μM DEX or a mock treatment. *Ler* plants had an average leaf attachment angle of 38.7° in the mock treatment, and 37.9° in the DEX treatment, showing that the DEX treatment has no significant effect on leaf angle in the absence of the *pLOB:LOB-GR* construct (Fig. 1.3D). In contrast *lob::DsE pLOB:LOB-GR* seedlings grown on DEX medium had significantly more vertical leaf attachment angle of 39.1° compared to mock treated, seedlings, which had an average value of 44.1° . The DEX treatment rescued the leaf attachment angle phenotype, restoring the mutant to wild-type leaf angle. Additionally, inducing expression of *pLOB:LOB-GR* in *Ler* resulted in significantly more vertical leaf attachment angle of 33.5° in the Dex-treated plants versus 37.0° in mock-treated plants, suggesting a dose-dependent effect of LOB on leaf attachment angle (Fig. 1.3D). In summary, *LOB* promotes more vertical leaf attachment angles in both *Col-0* and *Ler* genetic backgrounds.

lob mutants were previously reported to have a defect in organ separation, with fusion of the cauline leaf and axillary branch. This phenotype was rescued by expressing the LOB target gene *BAS1*, which encodes a BR catabolic enzyme, under the *LOB* promoter (Bell et al., 2012). This is consistent with increased BR accumulation in the boundary contributing organ fusion in the *lob-3* mutant. To determine if altered BR response also contributes to the change in leaf attachment angle observed in *lob* mutant seedlings, we examined the impact of *pLOB:BAS1* on leaf attachment angle. In both wild-type and *lob-3* backgrounds, *pLOB:BAS1* resulted in slightly more horizontal leaf attachment

angles, exacerbating the mutant phenotype rather than rescuing it (Fig. 1.4).

Therefore the more horizontal angle in *lob* mutants is likely not attributable to a lack of *BAS1* expression in the boundary.

***lob* mutants are hyperresponsive to low-intensity blue light at the base of the petiole**

Phototropic signaling informs directional changes to plant growth in response to directional light cues, including leaf inclination in response to blue light exposure (de Carbonnel et al., 2010, Inoue et al., 2008). Having observed consistent differences in leaf attachment angle in *lob-3* mutants grown in white light, we next asked whether this feature was responsive to blue light illumination. Plants were grown in long days (16L/8D) under white light until stage 1.04 (Boyes et al., 2001), then were exposed to 24h of either 50 $\mu\text{Em}^{-2}\text{s}^{-1}$ red light or red with a low intensity 0.1 $\mu\text{Em}^{-2}\text{s}^{-1}$ of blue light. This intensity of blue light stimulates phot1 signaling, but not phot2 (de Carbonnel et al., 2010). Following the red light treatment, wild-type seedlings had an average leaf attachment angle of 36.9°, and *lob-3* was more horizontal, averaging 46.8° (Fig. 1.5A). After the red+blue treatment, wild-type plants were not significantly different, averaging 38.8°. However, *lob-3* leaves were significantly more vertical than the red-only treatment, averaging 40.6° (Fig. 1.5A). We note that previous studies have observed significant leaf inclination in wild-type seedlings response to the

addition of blue light for 5 days, while in our conditions we observed no significant change in leaf attachment angle in the wild type. We believe this discrepancy is due to our shorter 24h treatment and our focus on the leaf attachment angle at the base of the petiole. While the majority of the leaf did show phototropic responses, there was little change in leaf attachment angle between red and red+blue treatments in wild-type. *lob-3* leaves, meanwhile, were generally more horizontal but were significantly more vertical when low-intensity blue light was present. These findings are consistent with phototropism genes being derepressed in the *lob-3* mutant boundary, resulting in hyperresponsiveness to blue light illumination at the base of the petiole. To investigate whether this phenotype was dependent on *phot1* signaling, we crossed *lob-3* with a *phot1* T-DNA mutant (SALK 088841). The T-DNA mutant was confirmed to have the *phot1* mutant phenotype, exhibiting a lack of hypocotyl bending in response to directional blue light exposure. The *lob-3;phot1* double mutant did not show any difference in leaf attachment angle between red (46.1°) and red/blue treatments (45.0°), suggesting that the increased blue light responsiveness in *lob-3* is attributable to *phot1* signaling (Fig. 1.5B). *pLOB:BAS1* did not affect the blue light hyperresponsiveness in the *lob-3* background, indicating that this phenotype is also not BR-dependent (Fig. 1.4B).

***LOB* misexpression reduced phototropic responses in etiolated seedlings**

To further explore whether *LOB* represses blue light signaling, we examined the effect of ectopic *LOB* activity in etiolated *35S:LOB-GR* seedlings grown on either mock or DEX containing medium. High DEX concentrations (100 nM – 15 μ M) strongly inhibited hypocotyl elongation in *35S:LOB-GR*, consistent with previous reports of *LOB* repressing growth. We therefore used a lower 10 nM concentration which only slightly inhibited hypocotyl growth, allowing us to measure phototropic responses. Upon directional blue light exposure, wild-type seedlings grown on both mock and DEX media responded equally, bending towards the light source. Mock-treated Col-0 seedlings had an average hypocotyl bending angle of 49.2°, while DEX-treated Col-0 had an average of 50.9° (Fig. 1.6A). In contrast, mock treated *35S:LOB-GR* seedlings had a similar response as wild-type with an average bending angle of 52.9°, while DEX-treated seedlings had significantly reduced hypocotyl bending angles, averaging 31.5° (Fig. 1.6A).

Considering that *LOB* misexpression reduced hypocotyl elongation, particularly at higher levels of induction, we needed to determine whether the reduction in phototropic hypocotyl bending was specific to phototropism or due to a more general growth inhibition. We examined another environmental condition that results in tropic growth - gravity. 24 hours after gravistimulation, wild type Col-0 plants had hypocotyl bending angles of 57.5° and 57.3° in mock and DEX-treated plants, respectively (Fig. 1.6B). Similarly, *35S:LOB-GR* plants had

bending angles of 55.1° and 55.7° in mock and DEX treatments, respectively. There was no significant difference in gravitropic bending upon DEX induction in either genotype (Fig. 1.6B). This suggests that the reduction in phototropic hypocotyl bending in *35S:LOB-GR* seedlings grown on DEX is a specific consequence of LOB repressing phototropic signaling, and not due to a more general repression of growth. Taken together, these experiments show that LOB misexpression suppresses phototropic signaling in the hypocotyl.

Discussion:

In this study, we found that the boundary function transcription factor LOB suppresses phototropism at the base of the petiole. Transcript levels of *PHOT1*, *PKS2*, and *NPH3* were all significantly reduced in response to *LOB* misexpression. This repression occurred in the presence of a translational inhibitor, suggesting LOB directly suppresses transcription of these genes. Repression of these three genes in the boundary domain is consistent with data from previous experiments (Tian et al., 2014; Yadav et al., 2014) ChIP-qPCR and Y1H experiments confirmed direct binding of LOB to canonical target sequences in the genomic regions of *PHOT1* and *PKS2*. We could not confirm LOB binding to the genomic sequence of *NPH3*, possibly because the LOB-DNA interaction is weak or transient, or that LOB binding *NPH3* is dependent upon a cofactor that is only present in the boundary region.

Misexpression of LOB also resulted in reduced hypocotyl phototropism. Because LOB has previously been shown to repress growth, we used a low concentration of DEX to induce *35S:LOB-GR*, which did not appreciably suppress hypocotyl elongation. We found that this level of induction partially repressed phototropism, whereas gravitropic responses were unaffected. These observations are consistent with LOB repressing phototropic signaling.

The repression of phototropism-related gene expression implies that LOB attenuates phototropic responses in the boundary domain. Phototropic responses include increased stomatal aperture, chloroplast accumulation and avoidance, hypocotyl bending, leaf inclination, and blade flattening. In particular, the three phototropism-related genes identified as *LOB* targets by our microarray experiment have been shown to work together in leaf positioning responses to blue light illumination (de Carbonnel et al., 2010). Consistent with this, we found that *lob-3* mutants displayed increased phototropic responsiveness at the leaf attachment point. Generally, *lob-3* mutants had more horizontally-oriented leaves than the wild type. Wild-type seedlings did not exhibit significant differences in leaf attachment angle between white, red, and red + blue treatments, although the petiole and blade exhibited stereotypical blue light responses. *lob-3* mutants had significantly more vertical leaves in the white and red + blue treatments than the red treatment, demonstrating that the leaf attachment angle was responsive to the presence of blue wavelengths. This is consistent with *LOB* regulating leaf angle via repression of phototropism genes in the boundary.

Previous experiments found significant changes in leaf angle in wild type plants following a 5 day blue light treatment of soil-grown seedlings, but leaf inclination in response to shorter term treatments have not been reported. The wild type boundary may locally suppress phototropic signaling, but still participate in the response to long-term blue light exposure. The hyperresponsiveness of *lob-3* to blue light was found to be PHOT1-dependent, because double mutants for *lob-3;phot1* did not exhibit a difference in leaf attachment angle between red and red/blue treatments. LOB also regulates the phot1 interaction partners *NPH3* and *PKS2*, which also participate in phot2-mediated blue light responses. *PHOT2* was not found to be a LOB target, but phot2 signaling could still be affected by LOB due to repression of phot2 cofactors. While only phot1 is sensitive enough to detect low-intensity blue light, both phot1 and phot2 are activated at higher intensities, and both are implicated in leaf inclination responses to blue light. In this experiment, we focused exclusively on phot1 signaling because *PHOT1* is a direct LOB target. We used low-intensity blue light to specifically activate phot1 without activating phot2. Additional experiments are necessary to assess any potential impact on phot2 signaling.

The previously reported phenotype for *lob-3* was impaired separation between leaves and axillary branches (Bell et al., 2012), which was attributed to increased BR signaling. The expression of the LOB target *BAS1* under the *LOB* promoter in the *lob-3* mutant was sufficient to rescue the organ fusion phenotype. This led to a model in which LOB induces *BAS1* expression, resulting in

increased BR catabolism and reduced growth in the boundary domain (Arnaud and Laufs, 2013; Bell et al., 2012; Gendron et al., 2012). In this study, we found that *pLOB:BAS1* did not rescue the *lob-3* leaf attachment angle phenotypes under any light conditions, suggesting that these phenotypes are not BR-dependent.

Light conditions are well known to affect plant architecture (Legris, 2023). Plants tend to modify their leaf positioning in order to optimize photosynthesis by bending towards high-quality light and escaping shade. Phytochrome signaling controls shade avoidance in response to a low red:far red ratio (Pierik & de Wit, 2013; Ma & Li, 2019). Local application of far-red-enriched light to a single leaf results in the inclination of that leaf via hyponastic growth and elongation of the petiole. Far-red enriched light at the tip of a leaf is sufficient to trigger changes in auxin transport in the petiole, stimulating hyponasty (Küpers et al. 2023). This increases the likelihood that a leaf can avoid, escape, and/or overgrow nearby competitors in a canopy. Blue light also stimulates leaf inclination via phototropin signaling (Inoue et al., 2008, de Carbonnel et al., 2010). While the direction of incident light is critical for informing the directionality of the tropic response, it is not fully understood how phototropic responses may differ in different parts of the plant, or how local application of blue light affects the whole leaf. For example, upon blue light exposure, the petiole generally straightens, by growing more on the bottom side, and the blade similarly uncurls, but the angle at the petiole-blade junction increases, which would be consistent with increased growth on the top

side. There is evidence that different combinations of phot, PKS, and NPH3/RPT2 proteins control distinct phototropic responses (de Carbonnel et al., 2010; Legris et al., 2021). Differential regulation of phototropic signaling components in different domains may be important for optimal phototropic responses.

The reason for LOB's repression of phototropic signaling is not immediately clear. On one hand, the boundary would seem to be a convenient "hinge point" from which multiple signals could be integrated and large changes in leaf positioning could be regulated, similar to the activity of the pulvinus at the base of a pea leaf. On the other hand, one possible explanation is that the boundary is a disadvantageous location for blue light signaling to occur. Cells in the boundaries are likely to be shaded by younger leaves in the rosette, and the net direction of incoming blue light in the boundary is likely not reflective of the conditions experienced by the rest of the leaf. The boundary is not responsible for conducting much photosynthesis, so it may be more advantageous to suppress phototropic signaling there while allowing the rest of the leaf to sense and direct the response to blue light, in order to achieve the optimal architecture. While *Arabidopsis* lacks any specialized structure for controlling leaf angle such as the pulvinus, LOB can affect leaf and branch angle via multiple mechanisms. There may be a conserved role for the boundary function in the regulation of leaf angle.

References:

- Aida, M. and Tasaka, M.** (2006). Genetic control of shoot organ boundaries. *Curr. Opin. Plant Biol.* **9**, 72–77.
- Arnaud, N. and Laufs, P.** (2013). Plant development: brassinosteroids go out of bounds. *Curr. Biol.* **23**, R152–R154.
- Bai, M.-Y., Shang, J.-X., Oh, E., Fan, M., Bai, Y., Zentella, R., Sun, T. and Wang, Z.-Y.** (2012). Brassinosteroid, gibberellin and phytochrome impinge on a common transcription module in Arabidopsis. *Nat. Cell Biol.* **14**, 810–817.
- Banerjee, R. and Batschauer, A.** (2005). Plant blue-light receptors. *Planta* **220**, 498–502.
- Bell, E. M., Lin, W., Husbands, A. Y., Yu, L., Jaganatha, V., Jablonska, B., Mangeon, A., Neff, M. M., Girke, T. and Springer, P. S.** (2012). *Arabidopsis* LATERAL ORGAN BOUNDARIES negatively regulates brassinosteroid accumulation to limit growth in organ boundaries. *Proc. Natl. Acad. Sci. U.S.A.* **109**, 21146–21151.
- Bortiri, E., Chuck, G., Vollbrecht, E., Rocheford, T., Martienssen, R. and Hake, S.** (2006). *ramosa2* Encodes a LATERAL ORGAN BOUNDARY Domain Protein That Determines the Fate of Stem Cells in Branch Meristems of Maize. *The Plant Cell* **18**, 574–585.
- Boyes, D. C., Zayed, A. M., Ascenzi, R., McCaskill, A. J., Hoffman, N. E., Davis, K. R. and Görlach, J.** (2001). Growth Stage–Based Phenotypic Analysis of Arabidopsis: A Model for High Throughput Functional Genomics in Plants. *The Plant Cell* **13**, 1499–1510.
- Christie, J. M.** (2007). Phototropin Blue-Light Receptors. *Annu. Rev. Plant Biol.* **58**, 21–45.
- Christie, J. M., Salomon, M., Nozue, K., Wada, M. and Briggs, W. R.** (1999). LOV (light, oxygen, or voltage) domains of the blue-light photoreceptor phototropin (*nph1*): Binding sites for the chromophore flavin mononucleotide. *Proc. Natl. Acad. Sci. U.S.A.* **96**, 8779–8783.
- Clough, S. J. and Bent, A. F.** (1998). Floral dip: a simplified method for *Agrobacterium* -mediated transformation of *Arabidopsis thaliana*. *Plant J.* **16**, 735–743.

- de Carbonnel, M., Davis, P., Roelfsema, M. R. G., Inoue, S., Schepens, I., Lariguet, P., Geisler, M., Shimazaki, K., Hangarter, R. and Fankhauser, C.** (2010). The Arabidopsis PHYTOCHROME KINASE SUBSTRATE2 Protein Is a Phototropin Signaling Element That Regulates Leaf Flattening and Leaf Positioning. *Plant Physiol.* **152**, 1391–1405.
- Deplancke, B., Dupuy, D., Vidal, M. and Walhout, A. J. M.** (2004). A Gateway-Compatible Yeast One-Hybrid System. *Genome Res.* **14**, 2093–2101.
- Deplancke, B., Vermeirssen, V., Arda, H., Martinez, N. and Walhout, A.** (2006). Gateway-Compatible Yeast One-Hybrid Screens. *Cold Spring Harb. Protoc.* **2006**,.
- Digby, J. and Firn, R. D.** (2002). Light modulation of the gravitropic set-point angle (GSA). *J. Exp. Bot.* **53**, 377–381.
- Duncan, W. G.** (1971). Leaf Angles, Leaf Area, and Canopy Photosynthesis1. *Crop Sci.* **11**, cropsci1971.0011183X001100040006x.
- Fankhauser, C.** (2001). The Phytochromes, a Family of Red/Far-red Absorbing Photoreceptors *. *J. Biol. Chem.* **276**, 11453–11456.
- Fujii, Y., Tanaka, H., Konno, N., Ogasawara, Y., Hamashima, N., Tamura, S., Hasegawa, S., Hayasaki, Y., Okajima, K. and Kodama, Y.** (2017). Phototropin perceives temperature based on the lifetime of its photoactivated state. *Proceedings of the National Academy of Sciences* **114**, 9206–9211.
- Gendron, J. M., Liu, J.-S., Fan, M., Bai, M.-Y., Wenkel, S., Springer, P. S., Barton, M. K. and Wang, Z.-Y.** (2012). Brassinosteroids regulate organ boundary formation in the shoot apical meristem of *Arabidopsis*. *Proc. Natl. Acad. Sci. U.S.A.* **109**, 21152–21157.
- Guo, X., Liu, D. and Chong, K.** (2018). Cold signaling in plants: Insights into mechanisms and regulation. *J. Integr. Plant Biol.* **60**, 745–756.
- Hangarter, R. P.** (1997). Gravity, light and plant form. *Plant Cell Environ.* **20**, 796–800.
- Harada, A., Sakai, T. and Okada, K.** (2003). phot1 and phot2 mediate blue light-induced transient increases in cytosolic Ca²⁺ differently in *Arabidopsis* leaves. *Proc. Natl. Acad. Sci. U.S.A.* **100**, 8583–8588.

- Hirano, S., Sasaki, K., Osaki, Y., Tahara, K., Takahashi, H., Takemiya, A. and Kodama, Y.** (2022). The localization of phototropin to the plasma membrane defines a cold-sensing compartment in *Marchantia polymorpha*. *PNAS Nexus* **1**, pgac030.
- Husbands, A., Bell, E. M., Shuai, B., Smith, H. M. S. and Springer, P. S.** (2007). LATERAL ORGAN BOUNDARIES defines a new family of DNA-binding transcription factors and can interact with specific bHLH proteins. *Nucleic Acids Res.* **35**, 6663–6671.
- Inada, S., Ohgishi, M., Mayama, T., Okada, K. and Sakai, T.** (2004). RPT2 Is a Signal Transducer Involved in Phototropic Response and Stomatal Opening by Association with Phototropin 1 in *Arabidopsis thaliana*. *Plant Cell* **16**, 887–896.
- Jaedicke, K., Lichtenthäler, A. L., Meyberg, R., Zeidler, M. and Hughes, J.** (2012). A phytochrome–phototropin light signaling complex at the plasma membrane. *Proc. Natl. Acad. Sci. U.S.A.* **109**, 12231–12236.
- Kawamoto, N. and Morita, M. T.** (2022). Gravity sensing and responses in the coordination of the shoot gravitropic setpoint angle. *New Phytologist* **236**, 1637–1654.
- Kim, W.-Y., Fujiwara, S., Suh, S.-S., Kim, J., Kim, Y., Han, L., David, K., Putterill, J., Nam, H. G. and Somers, D. E.** (2007). ZEITLUPE is a circadian photoreceptor stabilized by GIGANTEA in blue light. *Nature* **449**, 356–360.
- Kinoshita, T., Doi, M., Suetsugu, N., Kagawa, T., Wada, M. and Shimazaki, K.** (2001). phot1 and phot2 mediate blue light regulation of stomatal opening. *Nature* **414**, 656–660.
- Kodama, Y., Tsuboi, H., Kagawa, T. and Wada, M.** (2008). Low temperature-induced chloroplast relocation mediated by a blue light receptor, phototropin 2, in fern gametophytes. *J Plant Res* **121**, 441–448.
- Kong, Y., Meng, Z., Wang, H., Wang, Y., Zhang, Y., Hong, L., Liu, R., Wang, M., Zhang, J., Han, L., et al.** (2021). Brassinosteroid homeostasis is critical for the functionality of the *Medicago truncatula* pulvinus. *Plant Physiology* **185**, 1745–1763.
- Lariguet, P. and Dunand, C.** (2005). Plant Photoreceptors: Phylogenetic Overview. *J. Mol. Evol.* **61**, 559–569.

- Lariguet, P., Schepens, I., Hodgson, D., Pedmale, U. V., Trevisan, M., Kami, C., de Carbonnel, M., Alonso, J. M., Ecker, J. R., Liscum, E., et al.** (2006). PHYTOCHROME KINASE SUBSTRATE 1 is a phototropin 1 binding protein required for phototropism. *Proc. Natl. Acad. Sci. U.S.A.* **103**, 10134–10139.
- Lin, C.** (2002). Blue Light Receptors and Signal Transduction. *Plant Cell* **14**, S207–S225.
- Luesse, D. R., DeBlasio, S. L. and Hangarter, R. P.** (2010). Integration of phot1, phot2, and PhyB signalling in light-induced chloroplast movements. *J. Exp. Bot.* **61**, 4387–4397.
- Ma, L. and Li, G.** (2019). Auxin-Dependent Cell Elongation During the Shade Avoidance Response. *Frontiers in Plant Science* **10**,.
- Mao, J., Zhang, Y.-C., Sang, Y., Li, Q.-H. and Yang, H.-Q.** (2005). A role for Arabidopsis cryptochromes and COP1 in the regulation of stomatal opening. *Proc. Natl. Acad. Sci. U.S.A.* **102**, 12270–12275.
- Más, P., Devlin, P. F., Panda, S. and Kay, S. A.** (2000). Functional interaction of phytochrome B and cryptochrome 2. *Nature* **408**, 207–211.
- Motchoulski, A. and Liscum, E.** (1999). *Arabidopsis* NPH3: A NPH1 Photoreceptor-Interacting Protein Essential for Phototropism. *Science* **286**, 961–964.
- Pendleton, J. W., Smith, G. E., Winter, S. R. and Johnston, T. J.** (1968). Field Investigations of the Relationships of Leaf Angle in Corn (*Zea mays* L.) to Grain Yield and Apparent Photosynthesis¹. *Agron. J.* **60**, 422–424.
- Rast, M. I. and Simon, R.** (2008). The meristem-to-organ boundary: more than an extremity of anything. *Curr. Opin. Genet. Dev.* **18**, 287–294.
- Sakai, T., Wada, T., Ishiguro, S. and Okada, K.** (2000). RPT2: A Signal Transducer of the Phototropic Response in Arabidopsis. *Plant Cell* **12**, 225–236.
- Saleh, A., Alvarez-Venegas, R. and Avramova, Z.** (2008). An efficient chromatin immunoprecipitation (ChIP) protocol for studying histone modifications in Arabidopsis plants. *Nat. Protoc.* **3**, 1018–1025.
- Shuai, B., Reynaga-Peña, C. G. and Springer, P. S.** (2002). The Lateral Organ Boundaries Gene Defines a Novel, Plant-Specific Gene Family. *Plant Physiol.* **129**, 747–761.

- Somers, D. E., Schultz, T. F., Milnamow, M. and Kay, S. A.** (2000). ZEITLUPE Encodes a Novel Clock-Associated PAS Protein from Arabidopsis. *Cell* **101**, 319–329.
- Sun, Y., Fan, X.-Y., Cao, D.-M., Tang, W., He, K., Zhu, J.-Y., He, J.-X., Bai, M.-Y., Zhu, S., Oh, E., et al.** (2010). Integration of brassinosteroid signal transduction with the transcription network for plant growth regulation in Arabidopsis. *Dev. Cell* **19**, 765–777.
- Takemiya, A., Inoue, S., Doi, M., Kinoshita, T. and Shimazaki, K.** (2005). Phototropins Promote Plant Growth in Response to Blue Light in Low Light Environments. *Plant Cell* **17**, 1120–1127.
- Toyota, M. and Gilroy, S.** (2013). Gravitropism and mechanical signaling in plants. *Am. J. Bot.* **100**, 111–125.
- Waite, J. M. and Dardick, C.** (2018). TILLER ANGLE CONTROL 1 modulates plant architecture in response to photosynthetic signals. *J. Exp. Bot.* **69**, 4935–4944.

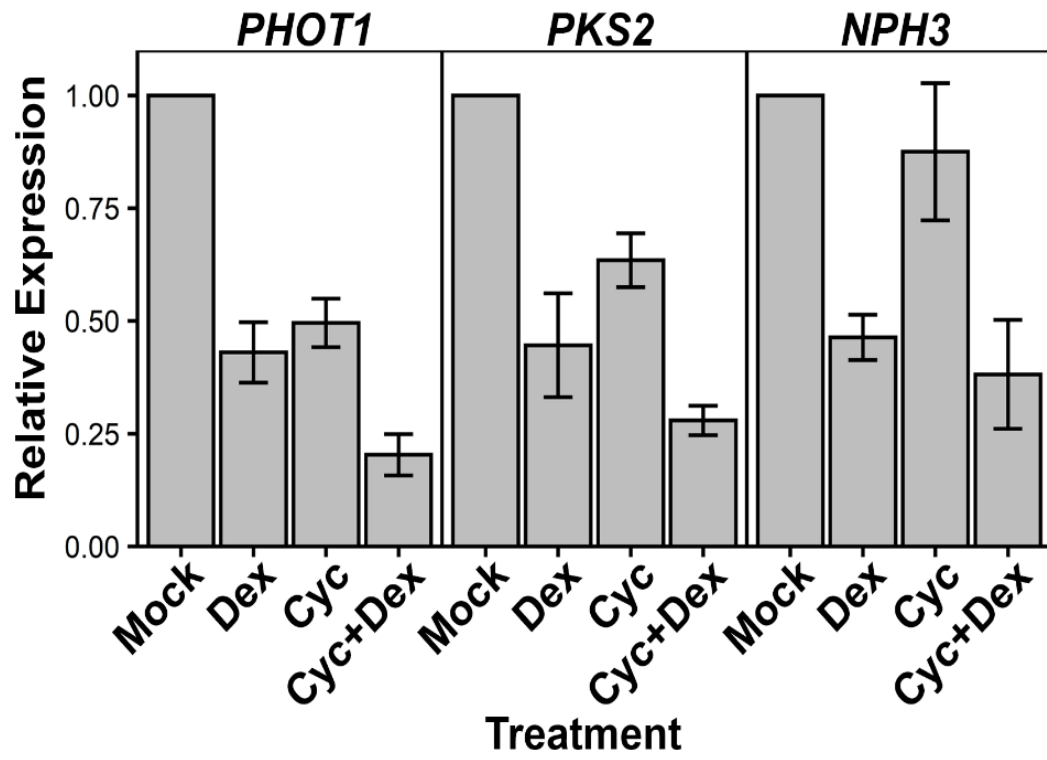


Figure 1.1: LOB misexpression directly represses *PHOT1*, *PKS2*, and *NPH3* transcript levels in *Arabidopsis* seedlings

Transcript levels of *PHOT1*, *PKS2*, and *NPH3* in 9 day-old *Arabidopsis* seedlings grown on agar expressing *35S:LOB-GR* after 4 hour treatment with either mock, 5 μ M Dex, 10 μ M CHX, or 5 μ M Dex + 10 μ M CHX. *EF1 α* was used as the reference gene.

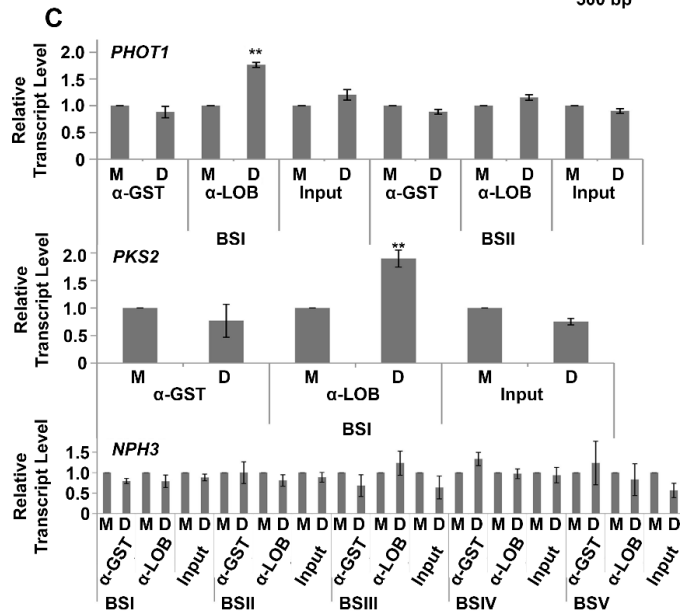
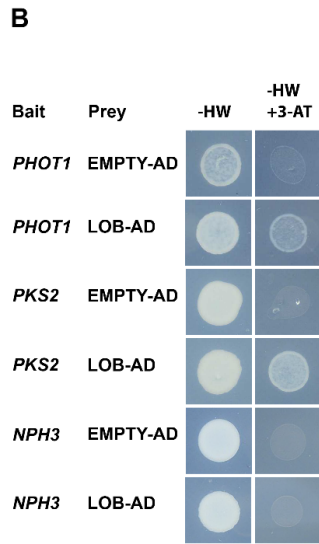
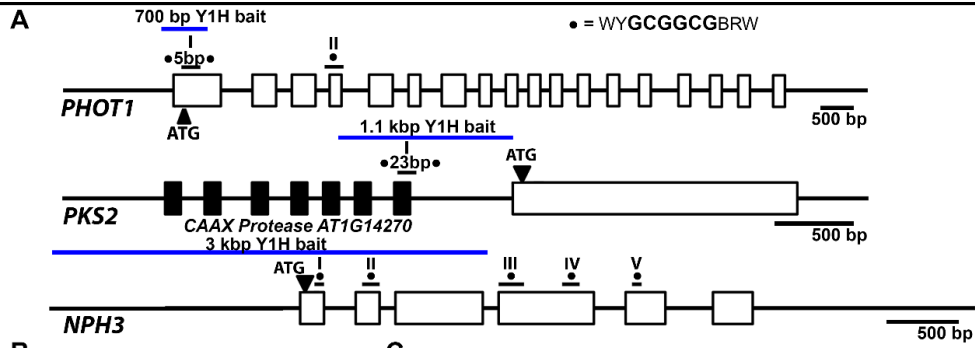


Figure 1.2: LOB binds to the genomic sequences of *PHOT1* and *PKS2*

(A) Schematic showing the genomic regions of *PHOT1*, *PKS2* and *NPH3*. Regions containing LOB binding motifs targeted by ChIP-qPCR are indicated with small black bars. Dots indicate the number of LOB consensus binding motifs in each target area, and the distance between them. Blue bars indicate the region used as bait for the Y1H experiment. Scale bars are 500bp. (B) Yeast-1-hybrid experiment. Yeast transformed with the indicated bait and prey constructs were grown on selection media with or without 3-AT. The optimal concentration of 3-AT was determined independently for each line. 30, 20, and 15 mM 3-AT was used for *PHOT1*, *PKS2*, and *NPH3* bait lines, respectively. (C) ChIP-qPCR experiment to determine LOB binding *in planta*. Relative enrichment of putative LOB binding sites from three biological replicates using either α -LOB or α -GST after flooding with either 15 μ M Dex or mock treatment. *ACT2* was used as the reference gene.

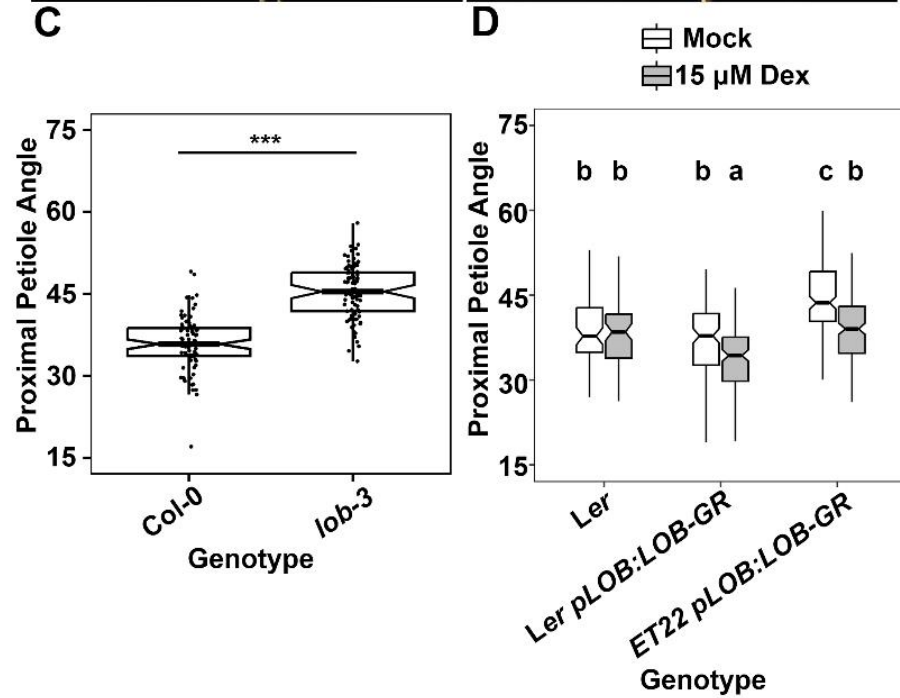
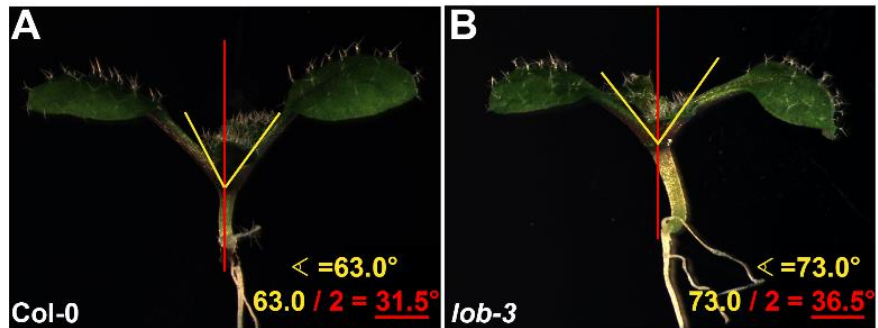


Figure 1.3: LOB promotes vertical leaf attachment angle

(A) Leaf attachment angle in stage 1.04 Col-0 and *lob-3* mutant seedlings, grown in long days in white light on MS agar plates. Box plots show pooled data from three experimental replicates. *** indicates $p < 0.01$ as determined by student's t-test. (B) leaf attachment angle in 9 day-old *Ler*, *pLOB:LOB-GR* and *ET22 pLOB:LOB-GR* grown in long days in white light on MS agar plates, mock or with 15 μ M Dex.

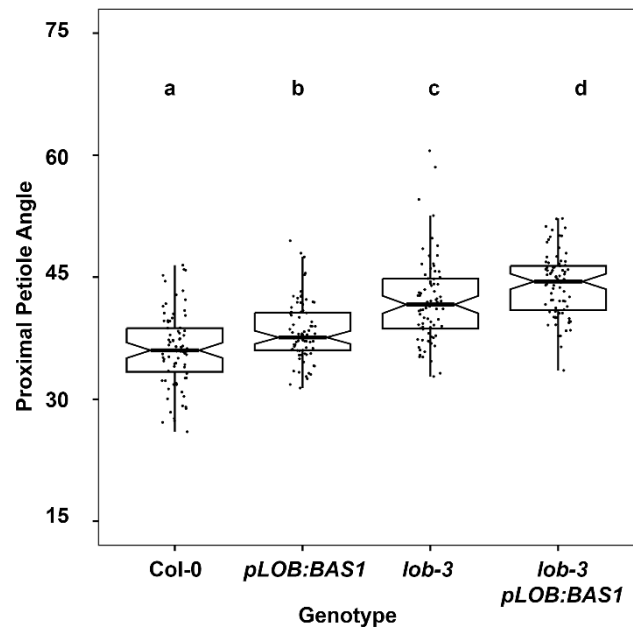





Figure 1.4: *pLOB:BAS1* does not rescue the *lob-3* leaf angle phenotype

(A) Leaf attachment angle in stage 1.04 seedlings grown in long days in white light on MS agar plates. Box plots show pooled data from three experimental replicates. Letters indicate statistical significance, $p < 0.05$ as determined by student's t-test. (B) Leaf inclination phenotype in response to blue light is also not rescued by *pLOB:BAS1*

A  100 $\mu\text{Em}^2\text{s}^{-1}$ White
 50 $\mu\text{Em}^2\text{s}^{-1}$ Red
 50 $\mu\text{Em}^2\text{s}^{-1}$ Red + 0.1 $\mu\text{Em}^2\text{s}^{-1}$ Blue

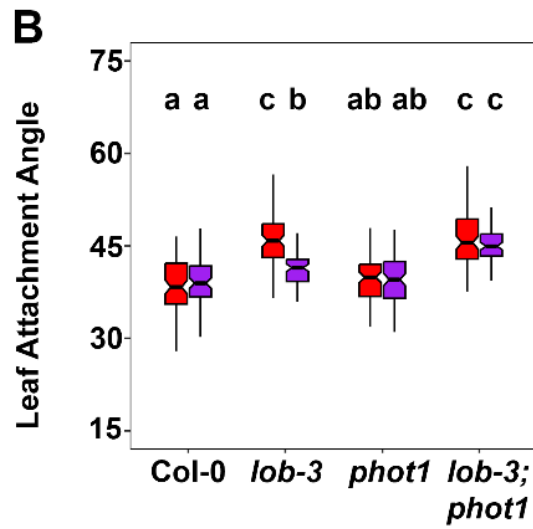
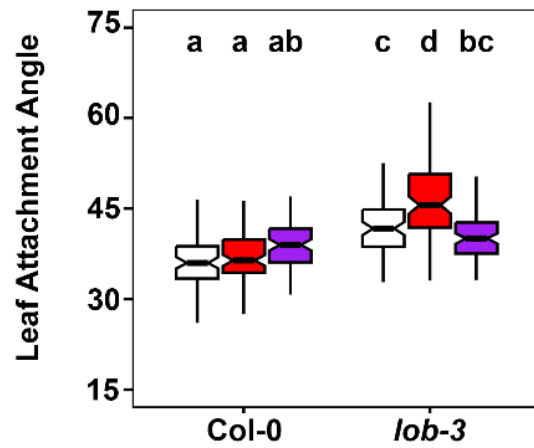


Figure 1.5: *lob-3* mutants hyper-respond to low-intensity blue light in a *PHOT1*-dependent manner

(A) Leaf attachment angle of Col-0 and *lob-3* seedlings grown in standard conditions until stage 1.04, then illuminated with either 50 $\mu\text{Em}^{-2}\text{s}^{-1}$ red light or 50 $\mu\text{Em}^{-2}\text{s}^{-1}$ red + 0.1 $\mu\text{Em}^{-2}\text{s}^{-1}$ blue light continuously for 24 hours. (B) As above using wild-type, *lob-3*, *phot1*, and *lob-3;phot1* F3 seedlings coming out of a cross between *lob-3* and *phot1* homozygous lines.

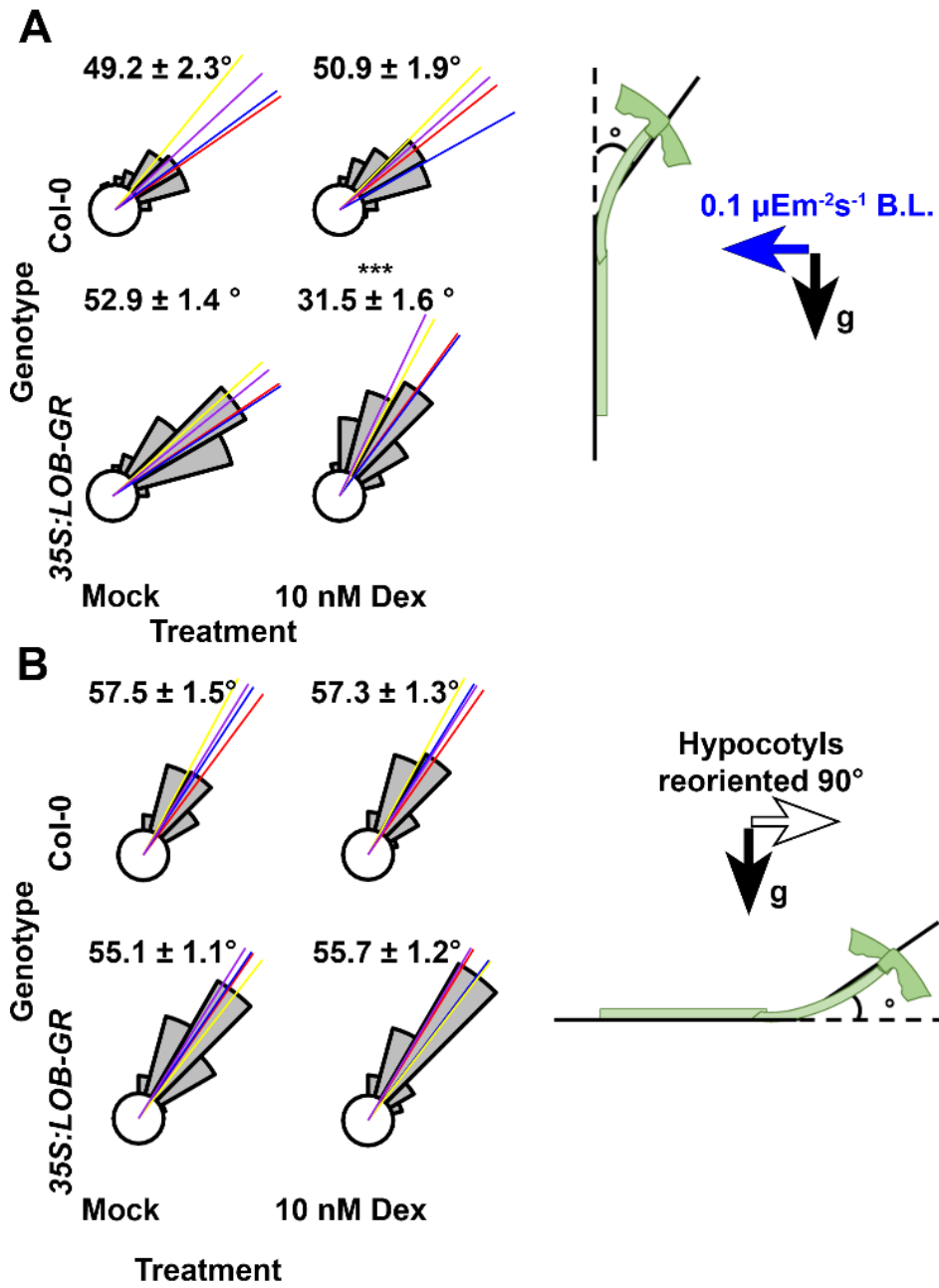


Figure 1.6: Ectopic LOB activity represses phototropic bending in the hypocotyl

(A) Phototropism experiment in etiolated hypocotyls. Radial histograms show the distribution of hypocotyl bending responses in 3 day-old Col-0 and *35S:LOB-GR* seedlings grown on vertical mock or 10 nM Dex MS agar plates wrapped in foil, exposed to $0.1 \mu\text{Em}^{-2}\text{s}^{-1}$ blue light from the right. Histogram created with pooled data from four experimental replicates. Colored lines indicate the mean bending angle for each experimental replicate. (B) As above, testing gravitropic responses instead. Seedlings were grown in the dark for 3 days, then rotated 90° and left for another 24 hours.

Table 1.1 – List of oligonucleotide primers used in this chapter

Primer name	Purpose	Sequence (5' -> 3')	T _m (°C)
phot1RP	Genotype for T-DNA	TCATCCAAAGATTCGCTCTTC	52.6
phot1LP	Genotype for T-DNA	TCGAACATTTCTTGGCAAATTC	50.4
LOB-RKF	Genotype for T-DNA	CCACACACAGTCCATGCATTA	55.3
LOB-RKR	Genotype for T-DNA	GCGTCGTCATCAAACCTATA	52.6
LBa1	Genotype for T-DNA	TGGTTCACGTAGTGGCCATGC	73.0
qPHOT1b-F	qPCR	CACTGATCCTAGGCTTCCCG	52.7
qPHOT1b-R	qPCR	GTGGTTAGATCAGTCTCTGGACC	56.4
qPKS2-F	qPCR	AGCCAGAGTTTGTGCTTCAG	55.7
qPKS2-R	qPCR	GCAGCCAAGAGTAGCGAGAA	57.2
qNPH3b-F	qPCR	TCCCTGTGTAAGCCCATCTAA	56.1
qNPH3b-R	qPCR	AGACTCCATCTTGGTCTGAAG	55.4
qACT2-F	qPCR reference gene	GCACCCAGTTCTACTCACAG	55.2
qACT2-R	qPCR reference gene	CAACATACATGGCAGGGAC	53.5
qUBC9-F	qPCR reference gene	GATAGCCCTTATTCTGGAGGAG	54.1
qUBC9-R	qPCR reference gene	TTGGATGGAACACCTTCGT	54.0
qEF1a-F	qPCR reference gene	TTGAGATGCACCACGAGTCT	56.0
qEF1a-R	qPCR reference gene	CTGGGAGGTGAAGTTAGCA	56.0
pPHOT1 Y1H attB1R	Cloning promoter for Y1H	GGGGACTGCTTTTTTGTACAAA CTTGACCAGAGTTCCTCACGCCTA	67.9
pPHOT1 Y1H attB4	Cloning promoter for Y1H	GGGGACAACCTTTGTATAGAAAAGT TGTCAAACCATCCATCTACCACA	65.0
pPKS2 Y1H attB1R	Cloning promoter for Y1H	GGGGACTGCTTTTTTGTACAAAC TTGAGCTATGTCGTGTGGGTTCC	67.5
pPKS2 Y1H attB4	Cloning promoter for Y1H	GGGGACAACCTTTGTATAGAAA GTTTCAGTTTCTCAACGTCGATTCC	64.4
pNPH3 Y1H attB1R	Cloning promoter for Y1H	GGGGACTGCTTTTTTGTACAACTTG TGCAGTGATTACACGAACGA	66.7
pNPH3 Y1H attB4	Cloning promoter for Y1H	GGGGACAACCTTTGTATAGAAAAG TTGGTTCCTACGAGCGAGAAGA	65.7
PHOT1 BSI FP	ChIP qPCR	ACCTCATGGATGGCTCTGAA	55.9
PHOT1 BSI RP	ChIP qPCR	GTGGCTTTCCCGTCTTTGT	55.7
PHOT1 BSII FP	ChIP qPCR	ATCGCAGAGAAACTCGCAA	54.8
PHOT1 BSII RP	ChIP qPCR	CCAGCACTTGCATACATAATCG	54.1
PKS2 BSI FP	ChIP qPCR	AGGCCGATCTCCATTTCTTC	54.6
PKS2 BSI RP	ChIP qPCR	TCGTGTTTATCTCAATCTTCGTCTC	54.6
NPH3 BSI FP	ChIP qPCR	TGATGTGGGAATCTGAGAGC	54.3
NPH3 BSI RP	ChIP qPCR	ACCAAGATTGGCCTCTAAGC	54.4
NPH3 BSII FP	ChIP qPCR	TGCCTATGATTAGGTTTGTGTC	53.4
NPH3 BSII RP	ChIP qPCR	CCATAAACTTTCTCTAGTTCAGCTT	54.8
NPH3 BSIII FP	ChIP qPCR	CAGCATAATCCCTCCACAGAA	54.4
NPH3 BSIII RP	ChIP qPCR	GTTCGAATTGCATCCCTACG	53.8
NPH3 BSIV FP	ChIP qPCR	TGGCTAAAGCATTGCTGATCT	56.0
NPH3 BSIV RP	ChIP qPCR	AGCATGAGAGGAAACGGCTA	54.7
NPH3 BSV FP	ChIP qPCR	TGTACGATGTTGATCTTGTTCAGAG	54.8
NPH3 BSV RP	ChIP qPCR	AAGCCTCGCCACTCTCATT	56.8

Chapter 2

The maize preligule band is subdivided into distinct domains with contrasting cellular properties prior to ligule outgrowth

Abstract

The maize ligule is an epidermis-derived fringe which arises from the preligule band (PLB) at a boundary between the blade and sheath. A hinge-like auricle also develops immediately distal to the ligule and contributes to blade angle. Here, we characterize the stages of PLB and early ligule development in terms of topography, cell area, division orientation, cell wall rigidity, and auxin response dynamics. Differential thickening of epidermal cells and localized periclinal divisions contributed to the formation of a ridge within the PLB, which ultimately produces the ligule fringe. Patterns in cell wall rigidity were consistent with the subdivision of the PLB into two regions along a distinct line positioned at the nascent ridge. The proximal region produces the ligule, while the distal region contributes to one epidermal face of the auricles. Whereas the auxin transporter PIN1 accumulated in the PLB, observed differential auxin transcriptional response did not underlie the partitioning of the PLB. Our data demonstrate that two zones with contrasting cellular properties, the preligule and preauricle, are specified within the ligular region prior to ligule outgrowth.

Introduction

Organogenesis in plants is dependent on positionally determined cell patterning and regulation of cell division and expansion. Morphogenesis and differentiation ultimately give rise to diverse leaf shapes with distinct domains, such as petiolate leaves in many eudicots and sheathing leaves in grasses (Moon and Hake, 2011). It is known that leaf morphogenesis involves the establishment of genetically defined developmental boundaries and accompanying shifts in cell, tissue and organ polarity. An emerging leaf acquires organ polarity in three dimensions relative to the plant axis, including proximodistal (apical to basal), mediolateral, and adaxial to abaxial (inner to outer leaf side). Change in the rate and direction of cell division and expansion in these three polar dimensions are key components of organogenesis and contribute to sculpting leaf shape (Echevin et al., 2019). How cell division and cell expansion contribute to establishing boundaries remains an open question and is critical to understand how leaf domains develop.

Boundary domains are often established prior to morphogenesis and contain distinct cells with altered signaling and cell wall properties. A well-studied boundary in plants is at the shoot apical meristem (SAM) where a leaf emerges and acquires new organ polarity. At the SAM-leaf boundary, cell growth is repressed thereby facilitating the separation and emergence of the incipient leaf from the meristem (Hussey, 1971; Kwiatkowska and Dumais, 2003). The boundary is maintained at the base of the leaf throughout development and can

be recapitulated at other locations as leaf domains differentiate (Bouré et al., 2022; Johnston et al., 2014; Nahar et al., 2012; Xiao et al., 2022).

Mutations in genes encoding boundary-defining transcription factors such as *CUP-SHAPED COTYLEDON2 (CUC2)*, *CUP-SHAPED COTYLEDON3 (CUC3)*, *LATERAL ORGAN BOUNDARIES (LOB)*, and *LATERAL ORGAN FUSION1 (LOF1)* lead to improper organ separation due in part to derepression of cell division and expansion within the boundary domain (Bell et al., 2012; Gendron et al., 2012; Hibara et al., 2006; Lee et al., 2009). While mutant studies highlight the importance of boundary-defining transcription factors, the mechanisms regulating cell growth in boundaries are not fully understood. *LOB* regulates brassinosteroid (BR) catabolism in boundary domains as one mechanism of limiting growth (Arnaud and Laufs, 2013). Cell wall-modifying genes are enriched among the transcriptional targets of BRs, and BR signaling is known to affect cell wall composition and structure, suggesting that cell wall biophysical properties are a component of boundary function (Bai et al., 2012; Graeff et al., 2021; Sun et al., 2010). Consistent with this, cell wall-related gene ontology terms are also significantly enriched among the transcriptional targets of *LOB*, while *CUC2* represses many genes associated with cell wall loosening (Bell et al., 2012; Bouré et al., 2022; Cucinotta et al., 2018). Other experiments show that cell wall-related genes are enriched among highly translated transcripts in the boundary (Tian et al., 2014). Additionally, cells in boundary domains have more rigid cell walls, as measured with atomic force microscopy (AFM) (Bouré et

al., 2022; Sampathkumar et al., 2019). Changes in cell wall composition or remodeling activity could contribute to the decreased rate of cell expansion in boundary domains, but more experiments are needed to determine how the boundary function modulates growth. While the SAM-leaf primordium boundary has been relatively well-studied, less is known about how other developmental boundaries are specified in plants and contribute to organogenesis.

A challenge to analyzing the SAM-leaf boundary is its physical inaccessibility. The maize leaf provides a unique opportunity to study an accessible boundary at the ligular region, which plays an important role in the proximodistal patterning of the leaf. The two largest domains of grass leaves are the proximal sheath and the distal blade separated by the ligular region (Fig. 2.1), where several specialized structures develop. At the blade-sheath junction, a thin epidermis-derived structure called the ligule emerges at the boundary between blade and sheath and covers the gap between consecutive ensheathing leaves. Also at the blade-sheath junction, two wedge-shaped structures called auricles develop on both sides of the midrib. Auricles are thought to facilitate the outward bending of the blade to optimize photosynthetic light capture (Emerson, 1912). The ligule is derived from a distinct region of the adaxial epidermis called the preligule band (PLB), a narrow, linear boundary domain between the preblade and presheath of the leaf primordium (Becraft et al., 1990; Sylvester et al., 1990). Due to physical proximity and the genetic links between the PLB, ligule and auricle, the adaxial epidermal portion of the pre-auricle is also hypothesized to be

derived from the PLB and/or from blade tissue adjacent to the upper boundary of the PLB. These hypotheses have not yet been resolved.

Transcription factors in maize that contribute to the development of the ligular region have been identified, including *LIGULELESS1* (LG1) and *LIGULELESS2* (LG2), which specify ligule and auricle development in a partially redundant manner (Becraft et al., 1990; Walsh et al., 1998). Single mutants *lg1-R* and *lg2-R* affect the position of the blade-sheath boundary and alter the pattern of ligule and auricle development, while the *lg1-R; lg2-R* double mutant has an indistinct blade-sheath boundary and lacks both ligule and auricle (Foster et al., 2004; Harper and Freeling, 1996). Mutations in *LIGULELESS* genes result in more vertical leaf angles because the auricles do not develop properly (Emerson, 1912). Rice *lg1* and *lg2* mutants display phenotypes similar to those in maize, suggesting functional conservation in grasses, despite differences in ligular region structures (Lee et al., 2007; Wang et al., 2021).

The ligule is a clear example of how cell division and expansion contribute to establishment of a boundary. Changes in division rate and orientation occur during the earliest stage of ligule morphogenesis (Becraft et al., 1990; Sharman, 1942; Sylvester et al., 1990). Cells divide more frequently in the adaxial epidermis in the PLB based on the emergence of new cross-walls (Freeling, 1992; Sylvester et al., 1990), and *LG1* transcript accumulates at this site of increased division (Johnston et al., 2014; Moreno et al., 1997). Several rounds of epidermal anticlinal divisions (perpendicular to the surface), along with

decreased cell expansion, reduce cell surface area (Becraft et al., 1990; Sylvester et al., 1990). The PLB becomes visible as a narrow band of small cells aligned laterally across the adaxial epidermis at the boundary between the blade and sheath domains. After several rounds of anticlinal divisions, periclinal divisions (parallel to the surface) are observed in both the PLB and the underlying ground tissue, and a ridge forms within the PLB ([Sylvester et al., 1990](#)). The auricle differentiates between the ridge and the blade while the ligule develops as a fringe of cells growing up and out from the PLB ridge (Freeling, 1992; Sylvester et al., 1990).

The proximodistal transcriptomic profile of the ligular region has been analyzed with high spatial resolution by laser-capture microdissection followed by RNA-seq in wild-type B73 and *lg1-R* mutants ([Johnston et al., 2014](#)), demonstrating that genes involved in leaf initiation and patterning at the SAM are redeployed later during ligule development. Notably, transcript levels of *KNOTTED1-LIKE HOMEBOX1 (KNOXI)* class and other boundary-associated genes such as *CUP-SHAPED COTYLEDON2-like (CUC2-like)* are significantly higher in the PLB ([Johnston et al., 2014](#)). *In situ* hybridization showed *CUC2-like* transcripts were detected throughout the PLB early in development, but later became restricted to the distal zone of the PLB, where a cleft will form as the ligule grows out. Xiao et al. (2022) further supported the link between *liguleless2* and boundary-associated gene expression in the context of bract suppression in the inflorescence. These patterns of gene expression support the idea that the

PLB functions as a boundary domain. While the SAM-leaf boundary is characterized by a low mitotic rate (Hussey, 1971), the PLB displays increased cell division relative to neighboring regions ([Becraft et al., 1990](#); [Sylvester et al., 1990](#)). Reduced cell size is a shared feature between the PLB and SAM-leaf boundary (Becraft et al., 1990; Hussey, 1971).

PIN-FORMED (PIN) auxin efflux genes and several other auxin-responsive genes are upregulated in the PLB, suggesting a role for auxin in ligule development (Johnston et al., 2014; Moon et al., 2013). Polar auxin transport and high auxin transcriptional responses are associated with the initiation and development of many structures during plant development, including leaves, branches, lateral roots, root hairs, and vasculature (Barazesh and McSteen, 2008; Bennett et al., 2014; Du and Scheres, 2018; Hajný et al., 2022; Jones et al., 2009; Leyser, 2018; McSteen and Leyser, 2005; Pitts et al., 1998; Scarpella et al., 2010). Transcriptomic experiments indicate that prior to and during ligule development, auxin responses are higher in the blade than in the sheath (Leiboff et al., 2020, Johnston et al., 2014). Auxin dynamics at the blade sheath boundary are thought to be involved in PLB development and ligule outgrowth (Johnston et al., 2014). More recently, polar auxin transport was shown to be necessary for ligule development (Satterlee et al., 2023). One proposed model is that *PIN-like*, *KNOXI*, and *CUC2-like* genes are expressed in the early PLB, but subsequent antagonism by auxin responses restricts the expression of boundary-associated

genes to the cleft, resulting in further refinement of the PLB into subdomains ([Johnston et al., 2014](#)).

Here we document the stages of ligule development and identify changes in cell wall rigidity in different regions. Ligule morphology correlates with sheath length and provides a convenient proxy for estimating ligule developmental stage. During early ligule outgrowth, we compared cell depth, division orientation, and cell wall rigidity along the proximodistal axis. There was a clear divergence in cellular properties between proximal and distal PLB-derived domains prior to ligule outgrowth. Hypothesizing that auxin dynamics may underlie this differentiation, we examined the accumulation of auxin reporters during ligule development. While the auxin transporter PIN1a marked with YFP (Yellow Fluorescent Protein) was observed in the PLB, we did not detect local differences in auxin transcriptional responses prior to ligule outgrowth. Our findings of cell growth patterns and biophysically distinct regions within the PLB may be explained by structural remodeling of cells required for the establishment and physical separation of a new axis associated with ligule outgrowth.

Materials and Methods

Plant Growth and Dissection

Maize plants were grown in two-gallon pots in standard greenhouse conditions (28 °C, 16 hours light, 8 hours dark) for 2-4 weeks at the Laramie Research and Extension Center at the Agriculture Experiment Station at the University of Wyoming or in greenhouses under similar conditions at UC Riverside. Maize plants used for imaging included the inbreds B73, Mo17, and plants containing fluorescent markers developed by the Maize Cell Genomics project (<http://maize.jcvi.org/cellgenomics/index.php>). Maize lines expressing *PIN1a-YFP* and *DR5rev:mRFP* ([Gallavotti et al., 2008](#)), *DR5*, *YFP-TUBULIN*, *CFP-TUBULIN*, or *TAN-YFP* have been previously described ([Mohanty et al., 2009](#)). Transgenic plants were selected by resistance to a solution of 4g/L glufosinate-ammonium (Basta, Bayer Sciences) in 0.5% Tween, applied to the leaf. Plants were genotyped by PCR using primers CYFP LSP1 (5' agcgcgatcacatggtcct) and PIN4110R (5' ttcccgaagctgaagtcgtcc) or DR5-870F (5' tgaagggcgagatcaagatgag) and DR5-1225R (5' ctcaacacatgagcgaaacc).

For dissections, leaves were sequentially removed from the plant and leaf numbers counted from leaf 1 in toward the SAM. The length of the sheath region was measured with calipers, and the ligule growth stage was assessed by either confocal or scanning electron microscopy (all stages), or in a separate set of experiments by atomic force microscopy (AFM) (below 3.5mm sheath length).

The leaves examined ranged from leaf number 4 to 12, depending on plant age and the developmental stage at which the plants were collected. Although the mediolateral position was not strictly controlled, imaging and measurements were collected from the lateral and marginal domains of the leaf primordium, not the central domain (Hay and Hake, 2004).

Imaging and measuring cell size and division arrays using YFP-TUBULIN lines

Adaxial ligule regions of freshly dissected plants were mounted in water in Rose chambers and micrographs were analyzed for cell area and division plane orientation using ImageJ (<http://rsbweb.nih.gov/ij/>). All imaged cells in the ligular region that had visible YFP-labeled preprophase bands, mitotic spindles or phragmoplasts were considered. Angles of preprophase bands, spindles or phragmoplasts were classified as anticlinal transverse, anticlinal longitudinal, periclinal, or oblique relative to the long axis of the leaf, as shown in Fig. 2.4A. 3-5 leaves expressing YFP-Tubulin were imaged per stage. To calculate cell area in each leaf, three boxes each encompassing 20-100 cells were drawn spanning the PLB or over a portion of the elongating ligule in the confocal micrographs, and the number of cells in each box was counted. Areas of the boxes were divided by the number of cells in each box to calculate the average cell area.

At the PLB and late PLB stages, the relative position of actively dividing cells within the PLB was determined using ImageJ. First, the proximal and distal extremities of the ligular region were traced according to differences in cell size and shape (Fig. 2.4A). Then, actively dividing cells, as indicated by the presence of a preprophase band labeled with either YFP-TUBULIN or TAN-YFP, were located within the PLB (Movie S1). Their relative position was calculated by measuring the distance from the proximal end of the PLB to the center of the dividing cell, and then from the proximal end to the distal end of the PLB, and dividing the former value by the latter. This generates values ranging from 0 at the proximal end of the PLB to 1 at the distal end (Fig. 2.4A).

Confocal microscopy

Images were acquired on two spinning disk confocal microscopes. The EM-CCD camera (ImagEM, Hamamatsu) was mounted on an IX71 stand equipped with a spinning-disc confocal head (CSU-X1; Yokogawa). A LMM5 laser launch was used to provide illumination (Spectral Applied research). Laser lines of 488 and 561 nm were used to excite PIN1a-YFP, YFP-TUBULIN, TAN1-YFP and *DR5rev.mRFP* with band pass filters ET525/50M and ET595/50M (Chroma Technology) respectively. Some image acquisition was performed using Metamorph 7.7 software (Molecular Devices). Images were acquired using 20x (0.85 NA) and 40x oil (1.30 NA) Olympus objectives. For additional samples in

the early PLB, PLB, and late PLB stages of ligule development, the dissected ligular region was stained with 10 µg/mL propidium iodide for 10 minutes and mounted in water. Confocal scans were collected using the 40X objective lens through the epidermis with a Z-step of 0.2 µm using a Hamamatsu 9100C EM-CCD camera mounted on a Nikon Ti stand with a spinning disc confocal head (CSU-W1, Yokogawa) and a 40X water (1.1 NA) Nikon water objective. Propidium iodide, TAN1-YFP or YFP-TUBULIN, and/or CFP-TUBULIN were excited at 561nm; 514nm; 445nm and collected at 620/20nm; 540/30nm; 480/40 nm respectively.

Scanning electron microscopy (SEM)

Two-, three- and four-week-old B73 leaf samples were used for SEM to characterize ligule stages. Sheath lengths were measured and the ligular region was excised with a scalpel, mounted with two-sided tape and loaded directly into the sample chamber of the tabletop electron microscope (Hitachi TM-1000), with included software used to acquire images.

Image and statistical analysis

Image analysis was performed using ImageJ (rsbweb.nih.gov/ij/), FIJI (ImageJ), or Metamorph v. 7.7. Data were analyzed in Excel and Access (Microsoft Office) and graphs produced in Graphpad (Prism) and R. For

measuring PIN1a-YFP polarity (Fig. 2.11M), 30 cells at each stage from four different plants were used for analysis. PIN1a-YFP fluorescence intensity measurements were performed by scanning through a Z stack of an entire epidermal cell. The plane with the highest fluorescence intensity value was selected at each side of the randomly selected cell. A one-pixel thick line was drawn across each side of the cell cortex and average intensity values were recorded. Ratios were calculated by dividing the highest average intensity value by the lowest for each analyzed cell in Excel and the error bars are 95% confidence intervals.

For measuring DR5 fluorescence intensity, images were background subtracted using a rolling ball radius of 50 pixels and normalized. A box was drawn between veins to avoid fluorescence of underlying vasculature (see Fig. 2.12F). Average fluorescence intensity was recorded from the boxed area of at least 1000 square pixels from a five μm deep maximum projection. For DR5 expression, three plants were used per stage and standard error bars are shown in Figure 2.12. The average intensity values from areas between vascular bundles of three samples in a single plant were normalized by dividing each value by the lowest average DR5 intensity value. Significance tests comparing the distribution of PIN1a-YFP fluorescence intensity ratios were performed using the non-parametric Kolmogorov-Smirnov (KS) test.

Cell depth was measured for PI-stained leaves dissected from three plants in the early PLB, PLB, and late PLB stages using ImageJ. The image stack was

projected as an orthoslice and the thicknesses of cells were measured at transverse wall segments by counting the number of z-steps between the top and bottom of the wall segment. Statistical differences were assessed via the non-parametric Kruskal-Wallis test, with a Dunn's post-hoc for pairwise comparisons.

For the distribution of anticlinal and periclinal divisions in the ligular region, the sheathward and bladeward extremities of the ligular region were determined by differences in cell size and shape in confocal scans of TAN-YFP plants stained with PI. For the purpose of this analysis only, the sheathward limit of the ligular region was relative position 0, while the bladeward limit was relative position 1. The relative proximodistal position of cells undergoing anticlinal and periclinal divisions was determined. One sample chi-square tests for variance were used to determine whether a certain division type was uniformly distributed or confined to a particular subdomain of the ligular region.

Representative confocal Z-stacks at each stage were analyzed using MorphoGraphX to extract cell area, surface curvature, and cell depth data as described by the MorphoGraphX user manual and previous experiments (Kierzkowski et al., 2012; <http://www.MorphoGraphX.org>). Stacks were processed using a Gaussian blur with a sigma of 0.3 μm . The epidermal surface was found using Edge Detect, with the proper threshold determined for each scan individually, and the surfaces were smoothed using Fill Holes, Erode, Dilate, and Smooth functions as necessary. Meshes of the surfaces were generated using the Marching Cubes function at a cube size of 1 μm , and the Z-stacks were

projected onto the resulting meshes. Cells were seeded manually, then Watershed Segmentation was performed at the default threshold. Cell geometric data was calculated and heatmaps of cell size were projected onto the segmented mesh. Average curvatures of the surfaces were calculated at a neighborhood value of 50 μm and projected onto the segmented surfaces as heatmaps. The edges of the curvature maps were deleted due to errors in the curvature calculations near the edges. Curvature and cell area were plotted together on the same surface by plotting cell area as heatmaps, then plotting tissue curvatures at the center of each cell as linear vectors indicating the direction, sign, and magnitude of maximum curvature. For cell depth, blurred Z-stacks were used for auto-seeded ITK watershed segmentation, at threshold values that were optimized for each sample. The segmentation was corrected manually by comparing to the original Z-stack. Incomplete cells around the edges were deleted, as were many of the underlying cells. Cell meshes of the remaining cells were created using the 3D Marching Cubes function at a cube size of 1 μm . The cell meshes were analyzed in 3D and cell depths were projected as a heatmap.

When analyzing AFM data, the difference in sheath length between the two observed tissue-level mechanical patterns was assessed via a Mann-Whitney U-test. For manual resampling, at least 50 indentations were used per wall category per tissue zone per sample to calculate average IM values. After manual resampling, global variation in IM with respect to wall category and tissue

zone were assessed via Kruskal-Wallis tests. Then pairwise Wilcoxon signed rank tests were performed at significance levels of $p < 0.05$ and $p < 0.01$, using the W -statistic. Variation in IM with respect to developmental stage was assessed via Mann-Whitney U-tests.

Atomic Force Microscopy

Developing ligules were dissected as described above and sheath length was measured using electronic calipers. To eliminate turgor pressure and only consider cell wall mechanical properties, leaves were plasmolyzed prior to being measured. The samples were quickly placed in 0.55M mannitol solution for at least 15 minutes to induce plasmolysis, before being affixed to a microscope slide using double-sided tape. Additional mannitol solution was used to immerse the sample and pre-wet the probe.

AFM was performed using a JPK NanoWizard 4a AFM in force mapping mode, at the California NanoSystems Institute at UCLA. Indentations were performed with a constant maximum force of 500 nN, with extend and retract times of 0.1s, at a spatial resolution of at least one indentation per 2 microns. The probes used were PPP-NCL probes with a 10 nm pyramidal tip, with an average force modulus of 45 N/m. Each tip was calibrated separately to accommodate slight differences.

Data were processed using the JPKSPM software. The raw indentation data were converted into IM (indentation modulus) using the Hertzian contact model as described (Peaucelle et al., 2011). Because the maximum scan area was too small to adequately sample all epidermal regions in a single scan, multiple overlapping scans were measured, processed, and manually reassembled by identifying cell walls in the overlapping areas. To quantify IM along the longitudinal axis of the leaf, regional IM values were averaged using a sliding window approach. For a given leaf, a 25 μm -wide rectangle was drawn, and repositioned along the longitudinal axis until the local maximum for average IM was located in the ligular region. This position was designated relative position 0, and the average IM for that bin was set as 1. Regional averages for IM were then measured along the proximodistal axis in 25 μm -wide bins, with a 12.5 μm step between bins. Position and average IM were normalized to the local maximum at for each leaf measured. Manual resampling of the scans was performed using a custom script in MATLAB (github.com/mathworks). Force maps were projected as a heatmap and at least 50 pixels within each epidermal zone and cell wall category were selected and averaged for each sample. We thoroughly sampled each cell in each tissue region, resampling at least 5 indentations per wall category per cell.

Results

Ligule developmental stages correlate with sheath length

To establish developmental reference stages for ligule morphogenesis, we characterized features such as topography and cell size. Existing literature describes the stages of ligule development relative to plastochron number, a value indicating the relative age of a leaf. Plastochron number is difficult to determine because it requires either sectioning or dissection down to the meristem ([Johnston et al., 2014](#); [Sylvester et al., 1990](#)). For accuracy, we used sheath length as a reliable and convenient proxy for predicting the stage of ligule development (Fig. 2.2A,B). Stages of ligule development were characterized in relation to sheath length in two-, three-, and four-week-old plants (Figs. 2.2, 2.3). Sheath lengths were measured in sequentially dissected leaves and ligule regions were observed by scanning electron microscopy (SEM; Fig. 2.2C-G). Ligule developmental stages were also visualized using confocal microscopy of leaves expressing YFP-TUBULIN (Fig. 2.2H-L). Although the ligule develops continuously and progressively, morphological features of the ligule correlated significantly with sheath length in expanding adult leaves (Fig. 2.2B).

The stages distinguishable by SEM were defined as preligule band (PLB), late PLB, and early, mid, and late fringe. At a median sheath length of 1.2 mm, comparable to late plastochron 6 and early plastochron 7 ([Johnston et al., 2014](#)), the PLB consisted of a band of small cells spanning ~60-100 μm in

proximal/distal length. At this stage, a slight ridge was often visible at the blade-sheath junction, with an inflection point at the PLB (Fig. 2.2C,H). At the late PLB stage, this ridge was very pronounced with the adjacent sheath surface elevated above the blade surface (Fig. 2.2D,I). Median sheath length was 1.9 mm, comparable to late plastochron 7 (Johnston et al., 2014), and cell area reached a minimum at this stage (Table 2.1). Leaves in the early fringe stage had a median sheath length of 3.5 mm, comparable to plastochron 8. Ligule cells were aligned at the leading edge of the ridge, beginning to grow over the more distal PLB-derived cells (Fig. 2.2E,J). Cell area increased throughout the development of the fringe (Table 2.1). Leaves in the mid fringe stage had a median sheath length of 8.7 mm. The ligule appeared “corrugated” and uneven relative to the plane of the leaf (Fig. 2.2F,K). At a median sheath length of 54.1 mm, the ligule was in the late fringe stage defined by elongate hair-like cells at the leading edge of the ligule, which projected over the developing auricle and blade (Fig. 2.2G,L). These observations demonstrate that ligule development correlates with sheath growth (Figs. 2.2B, 2.3). This shows that sheath length can be used to approximate the developmental stage of the ligule.

Changes in cell division orientation and expansion are associated with PLB and fringe growth

Changes in cell division and expansion patterns are characteristic of the PLB. We used a live cell marker for microtubules, YFP-TUBULIN (Mohanty et al., 2009), to assess cell area and division plane orientation at each of the defined ligule stages. We calculated the relative frequencies of different divisions by classifying the orientation of preprophase bands, mitotic spindles and phragmoplasts (Fig. 2.4A).

Visualizing microtubule mitotic structures enabled us to discern an earlier developmental stage than was visible with SEM, which primarily identifies new cross walls as an indicator of a recent cell division (Sylvester et al 1990). This early PLB stage was observed at sheath lengths of 0.3 – 1.1 mm, comparable with early plastochron 6 (Johnston et al., 2014). The predominance of longitudinal anticlinal divisions (>50%) at the blade-sheath junction was the distinguishing feature, the leaf surface was flat in the proximodistal direction, and average cell area was $\sim 159 \mu\text{m}^2$ (Fig. 2.4B, Table 2.1). In the PLB stage, transverse anticlinal divisions were the most frequent and a low frequency of periclinal divisions was observed (Fig. 2.2B). In addition, the average PLB cell area decreased to $\sim 135 \mu\text{m}^2$ (Table 2.1). In the late PLB stage, periclinal divisions were observed most frequently ($\sim 46\%$) and the average cell area was further reduced to $\sim 106 \mu\text{m}^2$. These results show reduced cell sizes in the PLB and shifts in division orientation from anticlinal to periclinal by the late PLB stage.

During the early fringe stage, periclinal divisions were reduced, with ~48% of the divisions oriented in the transverse anticlinal plane. Cell expansion increased so that early fringe cells were ~80% larger than late PLB cells. Mid fringe cells divided mostly in the transverse anticlinal orientation (71%), and cell area increased dramatically. Ligule cells in the late fringe stage no longer divided, but continued expanding, producing larger and more variably sized cells (Fig. 2.4B and Table 2.1). These results show that changes in division plane orientation contribute to early ligule emergence, with cell expansion driving ligule elongation at the late fringe stage.

Representative confocal Z-stacks were processed using the MorphoGraphX software package to better visualize changes in cell area and surface topography (Fig. 2.5; MorphoGraphX.org). The resulting projections showed a reduction in cell area during PLB development, although cell size in the ligular region was not uniform (Fig. 2.5A). Projections of average curvature showed the formation of a sharp ridge by the late PLB stage and revealed that the cells proximal to the ridge were noticeably larger than cells distal to the ridge (Fig. 2.5B).

Differential cell expansion and division orientation within the PLB contribute to the formation of the preligule ridge

During early ligule development, a ridge forms so that the sheath surface is elevated relative to the blade surface. Whereas periclinal divisions are known to contribute to the formation of this ridge, it is not clear whether they occur throughout the whole ligular region or are specific to a subset of cells that form the ligule. The relative positions of periclinal and anticlinal divisions within the ligular region were determined using either YFP-TUBULIN or TANGLED-YFP, a protein that localizes to the division site (Martinez et al., 2017; Walker et al., 2007; Movie S1). The ligular region was defined as the zone of reduced cell area between the blade and sheath (Fig. 2.6A). In the PLB stage, sporadic periclinal divisions were visualized in the proximal 2/3rds of the ligular region but not in the distal 1/3rd (Fig. 2.6B,C). In the late PLB stage, periclinal divisions were exclusively observed in the median 50% of the ligular region, localized to the nascent preligule ridge, but absent from both extremities (Fig. 2.6C). At both stages, anticlinal divisions were broadly distributed over the entire proximodistal length of the ligular region (Fig. 2.6C). Therefore, epidermal periclinal divisions occur in the proximal ligular region, but not in the distal cells that contribute to the auricle.

While periclinal divisions in the PLB and underlying mesophyll cells are known to contribute to the formation of the ridge at the blade-sheath boundary (Sharman, 1941), proximodistal differences in cell thickness (depth) have not

been quantified. To determine whether differential thickening of epidermal cells contributed to the formation of the ridge, we measured cell depth in the epidermis of the sheath, ligular region, and blade during the early, mid, and late stages of PLB development (Fig. 2.6D). In the early PLB stage, cell depth was uniform, averaging 11-12 μm in the sheath, PLB, and blade (Fig. 2.6D). During the PLB stage, the sheath and proximal ligular region cells averaged 16.4 μm deep, while the distal ligular region and blade cells were 13 μm deep (Fig. 2.6D). This relative thickening of the sheath coincided with the formation of the ridge. By the late PLB stage, the rate of periclinal divisions in the PLB increased and the preligule ridge became more pronounced, with cells on the proximal side of the ridge averaging 19.2 μm deep (Fig. 2.6D). Meanwhile, the distal PLB-derived cells were the thinnest in the epidermis, averaging 13.9 μm deep. We used MorphoGraphX to extract cell depth data from representative confocal Z-stacks, which largely agreed with our measurements (Fig. 2.6E-G). Our findings regarding epidermal cell depth are consistent with previously published TEMs of the developing ligule (Sharman, 1941; Sharman, 1942). These data show that differential cell thickening contributes to the changes in epidermal topography during the early stages of ligule development.

Mechanical changes within the epidermis precede ligule outgrowth

Differences in cell size and division orientation indicated that two zones with contrasting cellular behavior are established in the ligular region prior to emergence of the fringe. The elastic properties of the cell wall often correlate with cell expansion and reflect physical differences both between different cell populations and subcellular cell wall domains (Bou Daher et al., 2018; Peaucelle et al., 2011). We sought to identify cell wall mechanical patterns in epidermal cells during development of the ligular region. Atomic force microscopy (AFM) uses a physical probe to measure the topography and various physical characteristics of surfaces. AFM data were used to calculate indentation modulus (IM), which is the complex elastic stiffness of the area being indented. High IM values indicate greater rigidity.

We used AFM to measure the rigidity of cell walls across epidermal regions in B73 leaves from the early PLB stage through the early fringe stage. Periclinal walls had relatively low rigidity, while anticlinal walls had higher rigidity, consistent with previous experiments in plasmolyzed tissue ([Bou Daher et al., 2018](#); [Peaucelle et al., 2011](#); [Sampathkumar et al., 2019](#)). To reveal tissue-scale patterns in rigidity along the proximodistal axis, we analyzed the AFM scans using a sliding window approach (see methods, Fig. 2.7). Generally, the sheath had lower average rigidity than the blade at all stages of development. During early PLB and PLB stages, the central ligular region was the most rigid epidermal zone (Fig. 2.7A,B). During late PLB and early fringe stages, a different

mechanical pattern was observed in the ligular region. A distinct “transition” zone at the proximal end of the ligular region contained cells that were similar in shape to the sheath cells, but smaller and mechanically softer. The center of the ligular region had small cells with the lowest average rigidity. The distal ligular region, meanwhile, remained the most rigid epidermal zone (Fig. 2.7C,D). Similar results were obtained in Mo17 leaves (Fig. 2.8), indicating that these patterns were not unique to the B73 genetic background. Therefore, a change in mechanical properties occurs between the PLB and late PLB stages, with significant softening in the middle of the PLB, while the distal pre-auricle region remains rigid.

To determine when the mechanical changes in the ligular region occur relative to ligule outgrowth, we directly compared topographical features to the rigidity data from the same AFM scans. In PLB stage leaves, a shallow ridge was visible in the ligular region (Fig. 2.9A,B). Late PLB stage leaves had a steeper ridge, but relatively flat blade and sheath regions (Fig. 2.9C,D). The ligule grows out from this ridge, extending over the pre-auricle cells toward the blade. At early stages, the most rigid cells were centrally located in the PLB, but at later stages were located more distally, consistent with the position of the nascent ligule-auricle cleft. A distinct low-rigidity band, located on the crest of the ridge, was observed in the late PLB and early fringe stages (Fig. 2.7D, Fig. 2.9C,D). Cell wall softening in the late PLB stage correlates with the increases in cell area during the early fringe stage.

The sliding window method revealed two distinct mechanical patterns in the epidermis, however this analysis may be biased because anticlinal walls are perceived as more rigid than periclinal walls in plasmolyzed tissue (Peaucelle et al., 2011), and cell size varies between epidermal regions. To avoid potential measurement bias due to cell size differences, we manually resampled rigidity from the AFM scans to compare transverse, longitudinal, and periclinal cell wall segments (Fig. 2.10, Table 2.2). Generally, manual resampling confirmed the trends reported above, producing rigidity profiles that were similar to the sliding window analyses (Figs. 2.7, 12.10A,B, Table 2.2). In addition, considering each wall orientation separately allowed us to assess elastic asymmetry, defined as differences in the rigidity of different wall orientations (Bou Daher et al., 2018; Fig. 2.10C,D, Table 2.3). For example, in early stage leaves the average rigidity of transverse walls was higher than that of longitudinal walls in the blade and sheath, but not in the PLB, indicating reduced elastic asymmetry in the PLB cells (Fig. 2.10C, Table 2.3). The softer longitudinal walls in the blade and sheath are consistent with the primary direction of organ growth. Lastly, this approach enabled us to compare the average rigidity between the early and late stages (Table 2.4), revealing that the sheath anticlinal walls rigidified significantly in the late stage while the cells on the preligule ridge softened. Manual resampling supported the tissue-level patterns in rigidity observed with the sliding window approach and enabled further comparisons between the two mechanical stages and cell wall segments with different orientations.

The pattern of PIN1a-YFP signal changes during ligule development and is ubiquitous in ligule cells

Auxin has roles in many aspects of leaf development, including specification of founder cells (Reinhardt et al., 2003; Scanlon, 2003). Additionally, application of exogenous auxin was sufficient to induce cell wall biochemical and mechanical changes in the SAM (Braybrook and Peaucelle, 2013). Previous work showed PIN auxin-efflux carrier transcripts *PIN1a*, *PIN1c*, *PIN5*, and *SoPIN1/PIN1d/PIN4* accumulate in the PLB, and PIN1a-YFP signal is strong in the PLB and underlying mesophyll (Conklin et al., 2019; Johnston et al., 2014; Moon et al., 2013), suggesting a role for auxin in ligule specification and/or outgrowth ([Johnston et al., 2014](#)). Live cell imaging of PIN1a-YFP was conducted during all stages of ligule development. At the early PLB stage, PIN1a-YFP localized to the plasma membrane of cells over the vasculature in both the epidermis and mesophyll (Fig. 2.11A,B). In the PLB stage, PIN1a-YFP was observed uniformly in the PLB and underlying mesophyll (Fig. 2.11C,D). The PIN1a-YFP-expressing zone consistently narrowed from ~60 μm in the PLB stage to ~45 μm at the late PLB stage, with signal only in the small PLB cells and underlying mesophyll, and not in the cells at the extremities of the ligular region (Fig. 2.11E,F). In the early fringe stage, the PIN1a-YFP-accumulating zone expanded only in the sheathward/proximal direction (Figs. 2.11G, 2.12C). PIN1a-YFP signal was observed in ligule cells at all stages of fringe development (Fig.

2.11G-I). The narrowing of the zone containing PIN1a-YFP signal correlates with the increase in the periclinal division rate in the late PLB stage and precedes the outgrowth of the ligule fringe.

PIN1a-YFP is less polarized in the PLB and ligule fringe compared to the blade

PIN proteins are auxin efflux transporters, and polar localization of PINs can result in directional auxin flow. PIN1 polarization, defined as asymmetric accumulation of the protein between polar domains of the plasma membrane, correlates with the direction of auxin transport (Wisniewska et al., 2006). We examined PIN1a-YFP localization in the developing ligule, as an indication of directional auxin transport. We compared the relative polarity of PIN1a-YFP in developing ligule cells to that of blade epidermal cells (Fig. 2.12K-M). In contrast to the blade, where clear PIN1a-YFP polarity was observed (Fig. 2.12J), PIN1a-YFP localization in PLB and ligule cells appeared relatively nonpolar. Consistent with this observation, the fluorescence intensity ratio of PIN1a-YFP in the blade was 1.71 ± 0.11 showing that the PIN1a-YFP is polarized in the blade, as expected (Fig. 2.12L,M). PIN1a-YFP was primarily localized to the rootward side of blade epidermal cells consistent with basipetal auxin transport in leaf primordia (Sawchuk et al., 2013; Scarpella et al., 2010). In contrast, PIN1a-YFP signal was significantly less polarized in the PLB and the forming ligule (Fig. 2.12K,M), with

mean ratios ranging from 1.21 +/- 0.04 to 1.47 +/-0.09 (Fig. 2.12M). Whereas PIN1a-YFP signal was strong in the PLB and ligule throughout development, its subcellular localization was relatively nonpolar.

Auxin transcriptional responses reported by DR5 are low in the PLB and increase during ligule elongation

DR5 is a synthetic promoter containing auxin response elements, which can be used in combination with reporters to approximate auxin transcriptional responses (Ulmasov et al., 1997). We examined expression of *DR5rev:mRFP* (*DR5*) in plants coexpressing *PIN1a-YFP* (Fig. 2.13), to determine if changes in auxin responses correlated with proximal-distal specification in the PLB. If auxin transcriptional responses were associated with the specification of the ligule founder cells, high *DR5* signal would be expected in the proximal and central regions of the PLB prior to ligule outgrowth, similar to the localization of *PIN1a-YFP*. *DR5* signal was high in the underlying vasculature, which indicated auxin responses in those regions (Fig. 2.13). Special care was taken to measure *DR5* intensity only in epidermal cells located between vascular bundles, thus excluding the strong signal from underlying vasculature (e.g. areas labeled with a V for vasculature in Fig. 2.13). In contrast to strong *PIN1a-YFP* signal (Fig. 2.13 A-E), *DR5* signal was weak throughout the entire PLB, and gradually increased after the ligule fringe formed (F- test, $p < 0.01$, Fig. 2.13F-P). These data suggest

that DR5-related auxin responses do not underlie the specification of the ligule founder cells, although we cannot rule out the possibility that a distinct, DR5-independent subset of auxin responses may occur.

Discussion

A key problem in plant development is understanding how new growth axes are generated distinct from pre-existing growth axes. Establishment of boundaries and boundary-like domains can help facilitate the physical separation of new organs or structures by locally limiting growth, but the mechanisms restricting cell expansion in boundaries are not clear (Bell et al., 2012; Gendron et al., 2012; Lee et al., 2009). In maize, the formation of the ligule is a particularly complex morphogenic process because a thin flap forms entirely from epidermal cells and cleanly diverges from the rest of the epidermis along a well-defined cleft at the ligule-auricle junction.

Here we examine cellular properties during early ligule development. In the early PLB (Fig. 2.13B), PIN1a-YFP localizes throughout the entire PLB, with the strongest signal overlying the vasculature. At this stage, cell division orientation is exclusively anticlinal, epidermal cell depth is uniform, and the topography of the leaf surface is nearly flat in the proximodistal direction. Epidermal cell walls are more rigid in the PLB compared to the blade and sheath. In the PLB stage (Fig. 2.13C), PIN1a-YFP signal becomes stronger and more

uniform throughout the entire ligular region, but the protein remains relatively nonpolar at the subcellular level. During the PLB stage, cells in the sheath epidermis and proximal ligular region increase in depth considerably more than the distal ligular region and blade, and periclinal divisions are observed in the proximal ligular region. These changes contribute to the formation of a ridge that forms immediately proximal to the zone with the most rigid cell walls. During the late PLB stage (Fig. 2.13D), the zone of PIN1a-YFP accumulation narrows, localizing to the nascent ridge. The frequency of periclinal divisions reaches a maximum and the cells on the ridge have softer cell walls. At this stage, the proximal and distal zones of the ligular region differ in epidermal thickness, division plane orientation, cell wall rigidity, and PIN1a-YFP accumulation. In the early fringe stage, the soft cells on the more proximal ridge grow over the top of the more distal rigid cells, forming a well-defined cleft (Fig. 2.13E). The newly separated growth axis of the early ligule fringe then elongates primarily via transverse divisions and cell expansion. Our findings are consistent with the model proposed by Johnston et al. (2014), which was based on transcript-level data, that the PLB is partitioned into subdomains prior to ligule outgrowth, which may predict the distinction between forming ligule and auricle on the adaxial surface. Aside from potential preligule-preauricle specification, there may be additional subdomains that are not currently recognized.

The abrupt shift from anticlinal to periclinal division orientation is a key feature of developmental events in plants. Mechanisms regulating this shift are

not well understood. Previous predictive modeling of cell divisions via soap-film minimization showed the geometry of cells in the late PLB favors periclinal divisions (Martinez et al., 2018). Late PLB cells are small in the epidermal surface, but relatively thick in the depth axis, resulting in a columnar cell shape. Cells tend to divide along the shortest axis, so the Martinez et al. (2018) geometry-based surface minimization model most commonly predicts periclinal divisions in these cells. Our data show that the earliest periclinal divisions in the PLB stage are observed in the proximal and central PLB cells, which have thickened more in the depth axis than the distal cells. Furthermore, the periclinal division rate is highest at the late PLB stage, when cell area at the epidermal surface is the smallest. Differential cell thickening establishes a geometry in the proximal and central PLB cells that favors periclinal division plane orientation.

Our data add to the existing body of nanoindentation and AFM experiments on live plant cells (Bou Daher et al., 2018; Majda et al., 2017; Peaucelle et al., 2011; Routier-Kierzkowska et al., 2012). The dramatic softening of cell walls in the proximal PLB preceding ligule outgrowth is highly reminiscent of AFM experiments in *Arabidopsis*, where biochemical changes and mechanical softening in the cell walls correlate with increased growth ([Peaucelle et al., 2011](#), [Bou Daher et al., 2018](#)). The juxtaposition between rigid and soft epidermal cells along a discrete line is conspicuous, and suggests that differential regulation of cell wall properties within adjacent cell populations mechanically contributes to the sharp cleft at the preligule-preauricle junction, reminiscent of earlier studies

showing that mechanical patterns contribute to abrupt changes in directional growth at the shoot apex (Selker et al., 1992). PLB cells also exhibit reduced elastic asymmetry between transverse and longitudinal wall segments. Elastic asymmetry was shown to correlate with anisotropic expansion in the *Arabidopsis* hypocotyl ([Bou Daher et al., 2018](#)). A shift to isotropic growth is observed during leaf initiation from the SAM peripheral zone (Sassi et al., 2014), so it is possible that a similar trend may occur during early ligule outgrowth. These findings may inform future experiments exploring differences in cell expansion and growth anisotropy during maize leaf development.

We note that the indentation modulus of the cell wall is not a direct indicator of extensibility nor actual cell expansion, which is a plastic, irreversible process (Cosgrove, 2016). The cell wall is heterogeneous and materially anisotropic; each cell exists within the structure of multiple tissue layers, and changes in wall chemistry, heterogeneity and degree of plasticity occur during growth and development. Computational modeling could help explore the mechanics of nanoindentation in live plant tissue, and the biological implications of the elastic properties of the cell wall. Finally, more experiments are necessary to determine the cell wall components, remodeling enzymes, or other properties underlying the observed differences in rigidity between epidermal regions.

The accumulation of PIN-like genes in the PLB has been previously reported, suggesting a role for auxin transport in ligule development ([Johnston et al., 2014](#); [Moon et al., 2013](#)). We observed that the PIN1a-YFP-accumulating

zone narrowed significantly during the late PLB stage, becoming restricted to the small PLB cells in the center of the ligular region. This could be consistent with the focusing of auxin toward a convergence point, as it is during leaf initiation (Conklin et al., 2019). However, PIN1a-YFP accumulation in the PLB and ligule was relatively nonpolar, and no obvious DR5 maximum was observed in the PIN1-accumulating domain. This is puzzling because *PIN1a* is an auxin-responsive gene and other auxin-regulated genes, including *AUXIN RESPONSE FACTORS* (*ARFs*), *SMALL AUXIN UP-REGULATED RNAs* (*SAURs*), and *GRETCHEN HAGEN3* (*GH3*) genes are differentially expressed in the PLB (Johnston et al., 2014). Nonpolar auxin efflux and a lack of DR5 signal are consistent with low auxin transcriptional responses in the PLB, rather than the elevated responses associated with the initiation of many other plant organs. There are 15 *PIN* genes in maize (Yue et al., 2015), several of which are upregulated in the PLB, such as *PIN5*, *PIN1c*, and *SoPIN1/PIN1d* (GRMZM2G171702) (Johnston et al., 2014). Other PIN proteins could localize differently than our PIN1a-YFP construct. For example, AtPIN1 is involved in polar auxin transport in the epidermis of the *Arabidopsis* meristem during leaf initiation, but in maize this role is filled by SoPIN1/PIN1d, which belongs to the SISTER-OF-PIN1 (SoPIN1) clade, while AtPIN1 orthologs ZmPIN1a and ZmPIN1b act in internal tissue layers (Carraro et al., 2006; Li et al., 2019; O'Connor et al., 2014). The expression of *TIR1/AFBs*, *IAAs*, and *ARFs*, and differential affinities for auxin, can affect the sensitivity of auxin signaling in a

given region (Vernoux et al., 2011). While *TIR/AFB* auxin receptor genes are expressed relatively consistently between the blade, ligular and sheath zones, both *ARFs* and *IAs* are differentially expressed in the PLB (Johnston et al., 2014). It is possible that a distinct subset of auxin responses is activated in the PLB without high *DR5* expression. Particularly, *GRMZM2G158359*, a likely ortholog of the transmembrane noncanonical auxin receptor gene *AtTMK1*, is significantly upregulated in the PLB (FDR<0.05, Johnston et al., 2014), suggesting that extracellular auxin could serve a signaling role in the PLB without activating canonical TIR1/AFB-AuxIAA signaling (Cao et al., 2019; Lin et al., 2021; Xu et al., 2014). With so much complexity governing auxin signaling and responses, the role of auxin in the development of the ligular region remains unclear.

Our data support a model in which the boundary between blade and sheath in the maize leaf is progressively refined in the ligular region, producing two subdomains, as previously proposed based on SEM and gene expression data (Sylvester et al., 1990; Johnston et al., 2014). Shifts in topography, cell growth, division orientation, and PIN localization correlate with changes in cell wall biophysical properties in the ligular region. The rigid PLB is partitioned into a soft, proximal incipient ligule, and a rigid, distal zone, which we propose is the early differentiation of auricle cells on the adaxial surface. These events correlate with ligule outgrowth and presage the development of the auricle between the ligule and blade. How this occurs across the three dimensions of the leaf is an

intriguing question, given the auricle hinge becomes anatomically unique in all polarity dimensions. Next steps are to refine molecular and cellular changes in the transverse and mediolateral three-dimensions to fully understand how ligule- and auricle-specific cell growth is coordinated.

References:

- Arnaud, N. and Laufs, P.** (2013). Plant development: brassinosteroids go out of bounds. *Curr. Biol.* **23**, R152–R154.
- Bai, M.-Y., Shang, J.-X., Oh, E., Fan, M., Bai, Y., Zentella, R., Sun, T. and Wang, Z.-Y.** (2012). Brassinosteroid, gibberellin and phytochrome impinge on a common transcription module in Arabidopsis. *Nat. Cell Biol.* **14**, 810–817.
- Barazesh, S. and McSteen, P.** (2008). Hormonal control of grass inflorescence development. *Trends Plant Sci.* **13**, 656–662.
- Becraft, P. W., Bongard-Pierce, D. K., Sylvester, A. W., Poethig, R. S. and Freeling, M.** (1990). The *liguleless-1* gene acts tissue specifically in maize leaf development. *Dev. Biol.* **141**, 220–232.
- Bell, E. M., Lin, W., Husbands, A. Y., Yu, L., Jaganatha, V., Jablonska, B., Mangeon, A., Neff, M. M., Girke, T. and Springer, P. S.** (2012). *Arabidopsis* LATERAL ORGAN BOUNDARIES negatively regulates brassinosteroid accumulation to limit growth in organ boundaries. *Proc. Natl. Acad. Sci. U.S.A.* **109**, 21146–21151.
- Bennett, T., Hines, G. and Leyser, O.** (2014). Canalization: what the flux? *Trends Genet.* **30**, 41–48.
- Bou Daher, F., Chen, Y., Bozorg, B., Clough, J., Jönsson, H. and Braybrook, S. A.** (2018). Anisotropic growth is achieved through the additive mechanical effect of material anisotropy and elastic asymmetry. *eLife* **7**, e38161.
- Bouré, N., Peaucelle, A., Goussot, M., Adroher, B., Soubigou-Taconnat, L., Borrega, N., Biot, E., Tariq, Z., Martin-Magniette, M.-L., Pautot, V., et al.** (2022). A cell wall-associated gene network shapes leaf boundary domains. *Development* **149**, dev200359.
- Braybrook, S. A. and Peaucelle, A.** (2013). Mechano-chemical aspects of organ formation in *Arabidopsis thaliana*: The relationship between auxin and pectin. *PLOS ONE* **8**, e57813.
- Cao, M., Chen, R., Li, P., Yu, Y., Zheng, R., Ge, D., Zheng, W., Wang, X., Gu, Y., Gelová, Z., et al.** (2019). TMK1-mediated auxin signalling regulates differential growth of the apical hook. *Nature* **568**, 240–243.

- Carraro, N., Forestan, C., Canova, S., Traas, J. and Varotto, S.** (2006). *ZmPIN1a* and *ZmPIN1b* encode two novel putative candidates for polar auxin transport and plant architecture determination of maize. *Plant Physiol.* **142**, 254–264.
- Conklin, P. A., Strable, J., Li, S. and Scanlon, M. J.** (2019). On the mechanisms of development in monocot and eudicot leaves. *New Phytol.* **221**, 706–724.
- Cosgrove, D. J.** (2016). Plant cell wall extensibility: connecting plant cell growth with cell wall structure, mechanics, and the action of wall-modifying enzymes. *J. Exp. Bot.* **67**, 463–476.
- Cucinotta, M., Manrique, S., Cuesta, C., Benkova, E., Novak, O. and Colombo, L.** (2018). CUP-SHAPED COTYLEDON1 (CUC1) and CUC2 regulate cytokinin homeostasis to determine ovule number in Arabidopsis. *J. Exp. Bot.* **69**, 5169–5176.
- Du, Y. and Scheres, B.** (2018). Lateral root formation and the multiple roles of auxin. *J. Exp. Bot.* **69**, 155–167.
- Echevin, E., Le Gloanec, C., Skowrońska, N., Routier-Kierzkowska, A.-L., Burian, A. and Kierzkowski, D.** (2019). Growth and biomechanics of shoot organs. *J. Exp. Bot.* **70**, 3573–3585.
- Emerson, R. A.** (1912). The inheritance of the ligule and auricles of corn leaves. *Nebr. Agri. Exp. Stn. Ann. Rep.* **25**, 81–88.
- Foster, T., Hay, A., Johnston, R. and Hake, S.** (2004). The establishment of axial patterning in the maize leaf. *Development* **131**, 3921–3929.
- Freeling, M.** (1992). A conceptual framework for maize leaf development. *Developmental Biology* **153**, 44–58.
- Gallavotti, A., Yang, Y., Schmidt, R. J. and Jackson, D.** (2008). The relationship between auxin transport and maize branching. *Plant Physiol.* **147**, 1913–1923.
- Gendron, J. M., Liu, J.-S., Fan, M., Bai, M.-Y., Wenkel, S., Springer, P. S., Barton, M. K. and Wang, Z.-Y.** (2012). Brassinosteroids regulate organ boundary formation in the shoot apical meristem of *Arabidopsis*. *Proc. Natl. Acad. Sci. U.S.A.* **109**, 21152–21157.
- Graeff, M., Rana, S., Wendrich, J. R., Dorier, J., Eekhout, T., Aliaga Fandino, A. C., Guex, N., Bassel, G. W., De Rybel, B. and Hardtke, C. S.** (2021). A single-cell morpho-transcriptomic map of brassinosteroid action in the Arabidopsis root. *Mol. Plant* **14**, 1985–1999.

- Hay, A., Hake, S.** (2004). The dominant mutant *Wavy auricle in blade1* disrupts patterning in a lateral domain of the maize leaf. *Plant Physiol.* **135**, 300-308.
- Hajný, J., Tan, S. and Friml, J.** (2022). Auxin canalization: From speculative models toward molecular players. *Curr. Opin. Plant Biol.* **65**, 102174.
- Harper, L. and Freeling, M.** (1996). Interactions of *liguleless1* and *liguleless2* function during ligule induction in maize. *Genetics* **144**, 1871–1882.
- Hibara, K., Karim, Md. R., Takada, S., Taoka, K., Furutani, M., Aida, M. and Tasaka, M.** (2006). *Arabidopsis* CUP-SHAPED COTYLEDON3 regulates postembryonic shoot meristem and organ boundary formation. *Plant Cell* **18**, 2946–2957.
- Hussey, G.** (1971). Cell division and expansion and resultant tissue tensions in the shoot apex during the formation of a leaf primordium in the tomato. *J. Exp. Bot.* **22**, 702–714.
- Johnston, R., Wang, M., Sun, Q., Sylvester, A. W., Hake, S. and Scanlon, M. J.** (2014). Transcriptomic analyses indicate that maize ligule development recapitulates gene expression patterns that occur during lateral organ initiation. *Plant Cell* **26**, 4718–4732.
- Jones, A. R., Kramer, E. M., Knox, K., Swarup, R., Bennett, M. J., Lazarus, C. M., Leyser, H. M. O. and Grierson, C. S.** (2009). Auxin transport through non-hair cells sustains root-hair development. *Nat. Cell Biol.* **11**, 78–84.
- Kierzkowski, D., Nakayama, N., Routier-Kierzkowska, A. L., Weber, A., Bayer, E., Schorderet, M., Reinhardt, D., Kuhlemeier, C. & Smith, R. S.** (2012). Elastic domains regulate growth and organogenesis in the plant shoot apical meristem. *Science* **335**, 1096-1099.
- Kwiatkowska, D. and Dumais, J.** (2003). Growth and morphogenesis at the vegetative shoot apex of *Anagallis arvensis* L. *J. Exp. Bot.* **54**, 1585–1595.
- Lee, J., Park, J.-J., Kim, S. L., Yim, J. and An, G.** (2007). Mutations in the rice *liguleless* gene result in a complete loss of the auricle, ligule, and laminar joint. *Plant Mol. Biol.* **65**, 487–499.
- Lee, D.-K., Geisler, M. and Springer, P. S.** (2009). *LATERAL ORGAN FUSION1* and *LATERAL ORGAN FUSION2* function in lateral organ separation and axillary meristem formation in *Arabidopsis*. *Development* **136**, 2423–2432.
- Leiboff, S., Strable, J., Johnston, R., Federici, S., Sylvester, A.W., Scanlon, M.J.** (2020). Network analyses identify a transcriptomic proximodistal prepattern in the maize leaf primordium. *New Phytol.* **230**: 218–227.

- Leyser, O.** (2018). Auxin signaling. *Plant Physiol.* **176**, 465–479.
- Li, Y., Zhu, J., Wu, L., Shao, Y., Wu, Y. and Mao, C.** (2019). Functional divergence of *PIN1* paralogous genes in rice. *Plant Cell Physiol.* **60**, 2720–2732.
- Lin, W., Zhou, X., Tang, W., Takahashi, K., Pan, X., Dai, J., Ren, H., Zhu, X., Pan, S., Zheng, H., et al.** (2021). TMK-based cell-surface auxin signalling activates cell-wall acidification. *Nature* **599**, 278–282.
- Majda, M., Grones, P., Sintorn, I.-M., Vain, T., Milani, P., Krupinski, P., Zagórska-Marek, B., Viotti, C., Jönsson, H., Mellerowicz, E. J., et al.** (2017). Mechanochemical polarization of contiguous cell walls shapes plant pavement cells. *Dev. Cell* **43**, 290–304.
- Martinez, P., Luo, A., Sylvester, A. and Rasmussen, C. G.** (2017). Proper division plane orientation and mitotic progression together allow normal growth of maize. *Proc. Natl. Acad. Sci. U.S.A.* **114**, 2759–2764.
- Martinez, P., Allsman, L. A., Brakke, K. A., Hoyt, C., Hayes, J., Liang, H., Neher, W., Rui, Y., Roberts, A. M., Moradifam, A., et al.** (2018). Predicting division planes of three-dimensional cells by soap-film minimization. *Plant Cell* **30**, 2255–2266.
- McSteen, P. and Leyser, O.** (2005). Shoot branching. *Annu. Rev. Plant Biol.* **56**, 353–374.
- Mohanty, A., Luo, A., DeBlasio, S., Ling, X., Yang, Y., Tuthill, D. E., Williams, K. E., Hill, D., Zadrozny, T., Chan, A., et al.** (2009). Advancing cell biology and functional genomics in maize using fluorescent protein-tagged lines. *Plant Physiol.* **149**, 601–605.
- Moon, J. and Hake, S.** (2011). How a leaf gets its shape. *Curr. Opin. Plant Biol.* **14**, 24–30.
- Moon, J., Candela, H. and Hake, S.** (2013). The *Liguleless narrow* mutation affects proximal-distal signaling and leaf growth. *Development* **140**, 405–412.
- Moreno, M. A., Harper, L. C., Krueger, R. W., Dellaporta, S. L. and Freeling, M.** (1997). *liguleless1* encodes a nuclear-localized protein required for induction of ligules and auricles during maize leaf organogenesis. *Genes Dev.* **11**, 616–628.

- Nahar, M. A.-U., Ishida, T., Smyth, D. R., Tasaka, M. and Aida, M.** (2012). Interactions of *CUP-SHAPED COTYLEDON* and *SPATULA* genes control carpel margin development in *Arabidopsis thaliana*. *Plant Cell Physiol.* **53**, 1134–1143.
- O'Connor, D. L., Runions, A., Sluis, A., Bragg, J., Vogel, J. P., Prusinkiewicz, P. and Hake, S.** (2014). A division in PIN-mediated auxin patterning during organ initiation in grasses. *PLOS Comput. Biol.* **10**, e1003447.
- Peaucelle, A., Braybrook, S. A., Le Guillou, L., Bron, E., Kuhlemeier, C. and Höfte, H.** (2011). Pectin-induced changes in cell wall mechanics underlie organ initiation in *Arabidopsis*. *Curr. Biol.* **21**, 1720–1726.
- Pitts, R. J., Cernac, A. and Estelle, M.** (1998). Auxin and ethylene promote root hair elongation in *Arabidopsis*. *Plant J.* **16**, 553–560.
- Reinhardt, D., Pesce, E.-R., Stieger, P., Mandel, T., Baltensperger, K., Bennett, M., Traas, J., Friml, J. and Kuhlemeier, C.** (2003). Regulation of phyllotaxis by polar auxin transport. *Nature* **426**, 255–260.
- Routier-Kierzkowska, A.-L., Weber, A., Kochova, P., Felekis, D., Nelson, B. J., Kuhlemeier, C. and Smith, R. S.** (2012). Cellular force microscopy for in vivo measurements of plant tissue mechanics. *Plant Physiol.* **158**, 1514–1522.
- Sampathkumar, A., Peaucelle, A., Fujita, M., Schuster, C., Persson, S., Wasteneys, G. O. and Meyerowitz, E. M.** (2019). Primary wall cellulose synthase regulates shoot apical meristem mechanics and growth. *Development* **146**, dev179036.
- Sassi, M., Ali, O., Boudon, F., Cloarec, G., Abad, U., Cellier, C., Chen, X., Gilles, B., Milani, P., Friml, J., et al.** (2014). An auxin-mediated shift toward growth isotropy promotes organ formation at the shoot meristem in *Arabidopsis*. *Curr. Biol.* **24**, 2335–2342.
- Satterlee, J. W., Evans, J. A., Conlon, B.R. Conklin, P., Martinez-Gomez, J., Yen, J. R., Wu, H., Sylvester, A. W., Specht, C.D., Cheng, J., Johnston, R., Coen, E., Scanlon, M.J.** (2023). A *Wox3*-patterning module organizes planar growth in grass leaves and ligules. *Nature Plants* **9**: 720-732.
- Sawchuk, M. G., Edgar, A. and Scarpella, E.** (2013). Patterning of leaf vein networks by convergent auxin transport pathways. *PLoS Genet.* **9**, e1003294.

- Scanlon, M. J.** (2003). The polar auxin transport inhibitor N-1-naphthylphthalamic acid disrupts leaf initiation, KNOX protein regulation, and formation of leaf margins in maize. *Plant Physiol.* **133**, 597–605.
- Scarpella, E., Barkoulas, M. and Tsiantis, M.** (2010). Control of leaf and vein development by auxin. *Cold Spring Harb. Perspect. Biol.* **2**, a001511.
- Selker, J. M. L., Steucek, G. L. and Green, P. B.** (1992). Biophysical mechanisms for morphogenetic progressions at the shoot apex. *Dev. Biol.* **153**, 29–43.
- Sharman, B. C.** (1941). Development of the ligule in *Zea mays* L. *Nature* **147**, 641–641.
- Sharman, B. C.** (1942). Developmental anatomy of the shoot of *Zea mays* L. *Ann. Bot.* **6**, 245–282.
- Sun, Y., Fan, X.-Y., Cao, D.-M., Tang, W., He, K., Zhu, J.-Y., He, J.-X., Bai, M.-Y., Zhu, S., Oh, E., et al.** (2010). Integration of brassinosteroid signal transduction with the transcription network for plant growth regulation in *Arabidopsis*. *Dev. Cell* **19**, 765–777.
- Sylvester, A. W., Cande, W. Z. and Freeling, M.** (1990). Division and differentiation during normal and *liguleless-1* maize leaf development. *Development* **110**, 985–1000.
- Tian, C., Zhang, X., He, J., Yu, H., Wang, Y., Shi, B., Han, Y., Wang, G., Feng, X., Zhang, C., et al.** (2014). An organ boundary-enriched gene regulatory network uncovers regulatory hierarchies underlying axillary meristem initiation. *Mol. Syst. Biol.* **10**, 755.
- Ulmasov, T., Murfett, J., Hagen, G. and Guilfoyle, T. J.** (1997). Aux/IAA proteins repress expression of reporter genes containing natural and highly active synthetic auxin response elements. *Plant Cell* **9**, 1963–1971.
- Vernoux, T., Brunoud, G., Farcot, E., Morin, V., Van den Daele, H., Legrand, J., Oliva, M., Das, P., Larrieu, A., Wells, D., et al.** (2011). The auxin signalling network translates dynamic input into robust patterning at the shoot apex. *Mol. Syst. Biol.* **7**, 508.
- Walker, K. L., Müller, S., Moss, D., Ehrhardt, D. W. and Smith, L. G.** (2007). *Arabidopsis* TANGLED identifies the division plane throughout mitosis and cytokinesis. *Curr. Biol.* **17**, 1827–1836.
- Walsh, J., Waters, C. A. and Freeling, M.** (1998). The maize gene *liguleless2* encodes a basic leucine zipper protein involved in the establishment of the leaf blade–sheath boundary. *Genes Dev.* **12**, 208–218.

- Wang, R., Liu, C., Chen, Z., Sun, S. and Wang, X.** (2021). *Oryza sativa* *LIGULELESS* 2s determine lamina joint positioning and differentiation by inhibiting auxin signaling. *New Phytol.* **229**, 1832–1839.
- Wisniewska, J., Xu, J., Seifertová, D., Brewer, P. B., Ruzicka, K., Blilou, I., Rouquié, D., Benková, E., Scheres, B. and Friml, J.** (2006). Polar PIN localization directs auxin flow in plants. *Science* **312**, 883.
- Xiao, Y., Guo, J., Dong, Z., Richardson, A., Patterson, E., Mangrum, S., Bybee, S., Bertolini, E., Bartlett, M., Chuck, G., et al.** (2022). Boundary domain genes were recruited to suppress bract growth and promote branching in maize. *Science Advances* **8**, eabm6835.
- Xu, T., Dai, N., Chen, J., Nagawa, S., Cao, M., Li, H., Zhou, Z., Chen, X., De Rycke, R., Rakusová, H., et al.** (2014). Cell surface ABP1-TMK auxin-sensing complex activates ROP GTPase signaling. *Science* **343**, 1025–1028.
- Yue, R., Tie, S., Sun, T., Zhang, L., Yang, Y., Qi, J., Yan, S., Han, X., Wang, H. and Shen, C.** (2015). Genome-wide identification and expression profiling analysis of *ZmPIN*, *ZmPILS*, *ZmLAX* and *ZmABCB* auxin transporter gene families in maize (*Zea mays* L.) under various abiotic stresses. *PLOS ONE* **10**, e0118751.

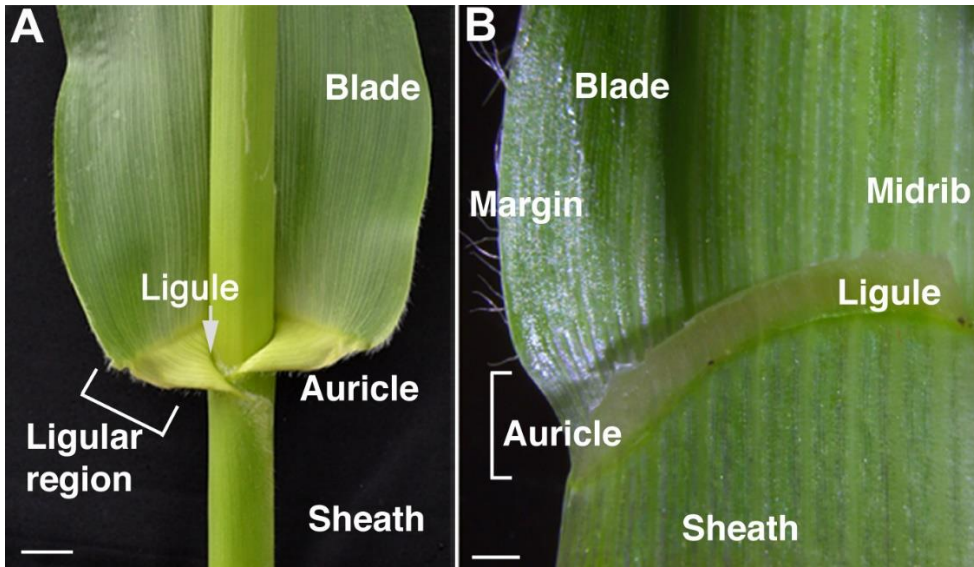


Figure 2.1: Maize leaf structure

The maize leaf is composed of a distal blade and proximal sheath separated at the ligular region (bracket), consisting of a ligule and auricle. Scale bar = 2 cm.

(B) The leaf is cut at the midrib to expose the adaxial view of the ligular region.

Scale bar = 1 mm.

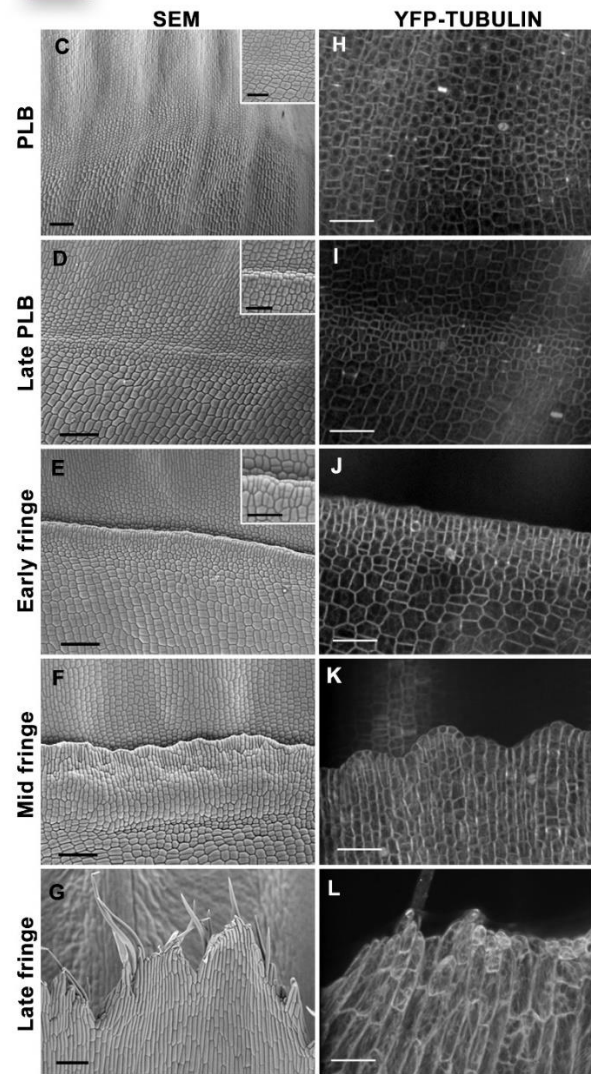
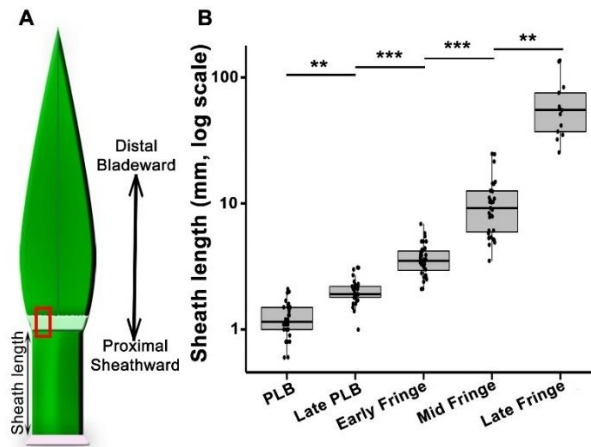


Figure 2.2: Stages of ligule development correlate with sheath length.

(A) Cartoon outlining maize leaf domains and proximodistal axis (B) Box-whisker plot showing sheath height correlates with ligule stage. Statistical significance assessed via Kruskal-Wallis test with Dunn's post-hoc and Benjamini-Hochberg p-value adjustment for multiple comparisons. ** indicates $p < 0.05$, *** indicates $p < 0.01$. (C-G) Scanning electron micrographs show stages of ligule development in four-week old plants. Scale bar = 100 μm . Higher magnification insets in (C-E) show small cells in the preligule band, scale bar = 50 μm . (H-L) Ligule stages visualized via confocal microscopy using YFP-TUBULIN marker. Mid and late fringe micrographs are maximum projections of Z stacks three to five μm in depth. Scale bar = 50 μm

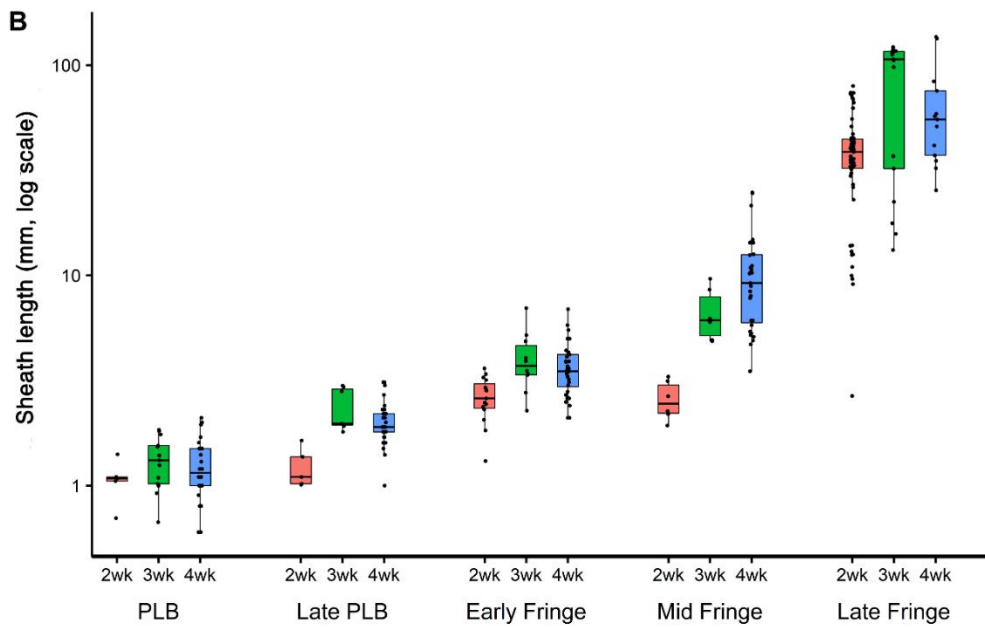
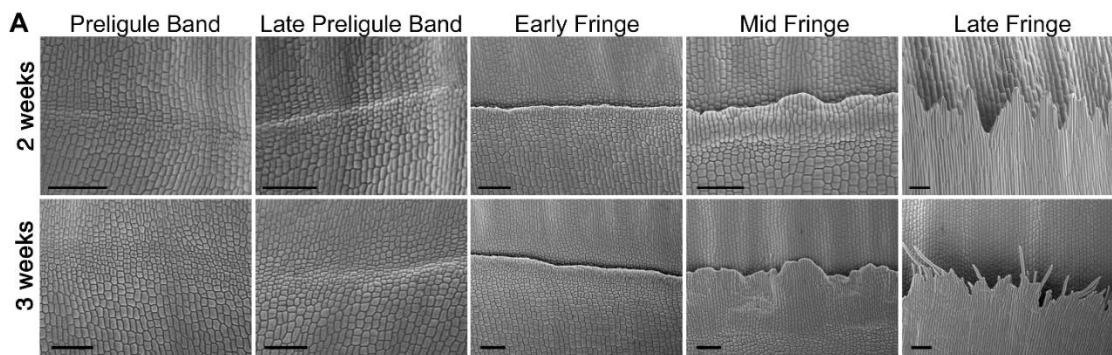


Figure 2.3: Stages of ligule development relative to sheath height in 2-, 3-, and 4-week-old plants

Scanning electron micrographs of sequentially dissected leaves of 2- and 3-week-old maize plants. (B) Stages of ligule development in 2-, 3-, and 4-week-old maize plants relative to sheath length. Scale bar = 100 μm .

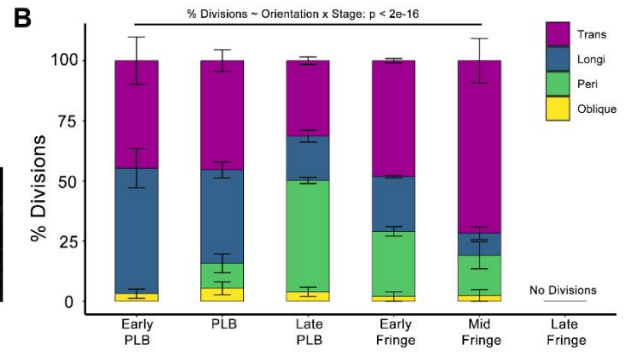
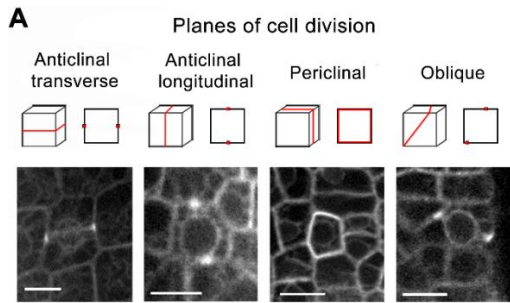


Figure 2.4: Dynamic changes in division plane orientation during ligule development

(A) Cartoons show different division plane orientations as seen in 3D and in a single Z-slice, along with examples of preprophase bands in cells expressing YFP-TUBULIN. Scale bars = 15 μm . (B) The percentage of dividing cells that exhibit each division orientation at each stage of ligule development. Error bars indicate standard error. $n=3-5$ leaves per stage, 11-46 mitotic cells per leaf. Significance determined via ANOVA.

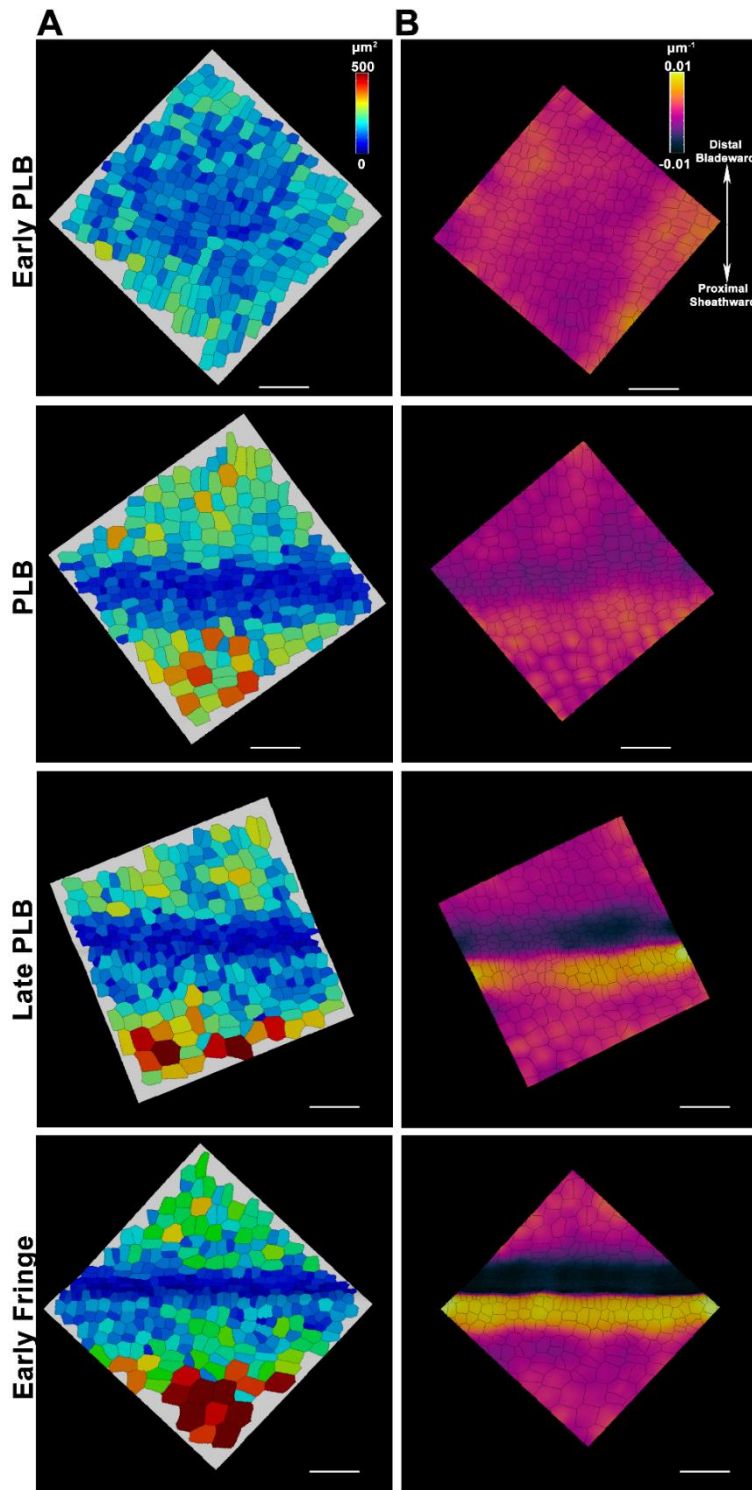


Figure 2.5: Changes in cell area and surface topography during early ligule development

Representative Z-stacks from the ligular region were processed using MorphoGraphX. (A) Heatmaps showing spatiotemporal differences in cell area in the ligular region. (B) Same surfaces as in (A), with heatmaps of average curvature of the surface at a neighborhood of 50 μm . Scale bars = 50 μm .

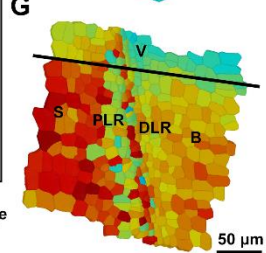
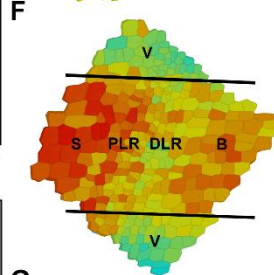
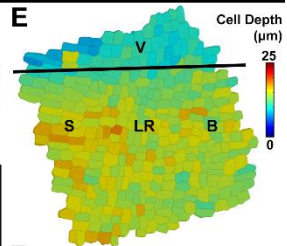
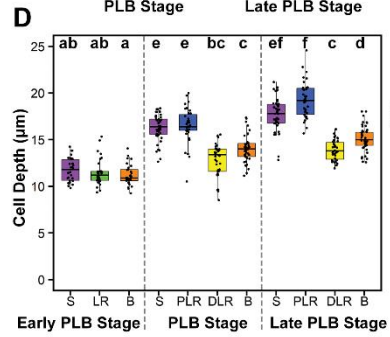
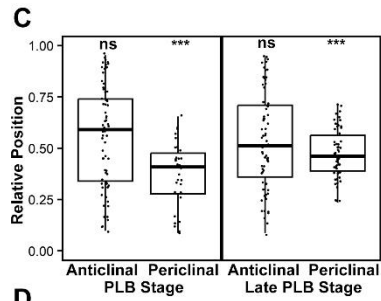
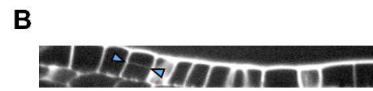
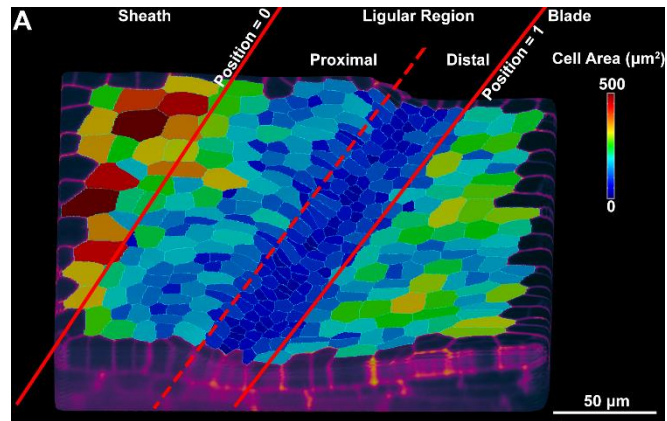


Figure 2.6: Differential cell thickening and periclinal divisions contribute to formation of the preligule ridge

(A) MorphoGraphX projection outlining the zones of the ligular region. Position 0 is the proximal extremity of the ligular region while 1 is the distal extremity. (B) An orthoslice highlighting a periclinal division in the proximal ligular region. (C) Relative position of periclinal divisions within the ligular region was determined from confocal micrographs of plants expressing either CFP-Tubulin or TAN-YFP. Distribution was analyzed via one-sample chi-squared tests for variance. ns=not significant $p>0.05$, *** $p<0.01$ (D) Cell depth was measured from confocal z-stacks at anticlinal faces of cells that had not yet undergone periclinal divisions, in the ligular region of the maize leaf adaxial epidermis. (n=3 leaves per stage, 10-15 cells per region per leaf) Significance was determined via Kruskal-Wallis test with Dunn's post-hoc, adjusting p-values via the Benjamini-Hochberg method for multiple comparisons, at an alpha of 0.05. Letter rankings indicate comparisons between all stages and epidermal zones. (E-G) 3D MorphoGraphX heatmaps of cell depth during early ligule development. The original scans for (E) and (G) are the same as those used for the corresponding stage in Figure 2.5. S=Sheath, LR=Ligular Region, PLR=Proximal Ligular Region, DLR=Distal Ligular Region, B=Blade

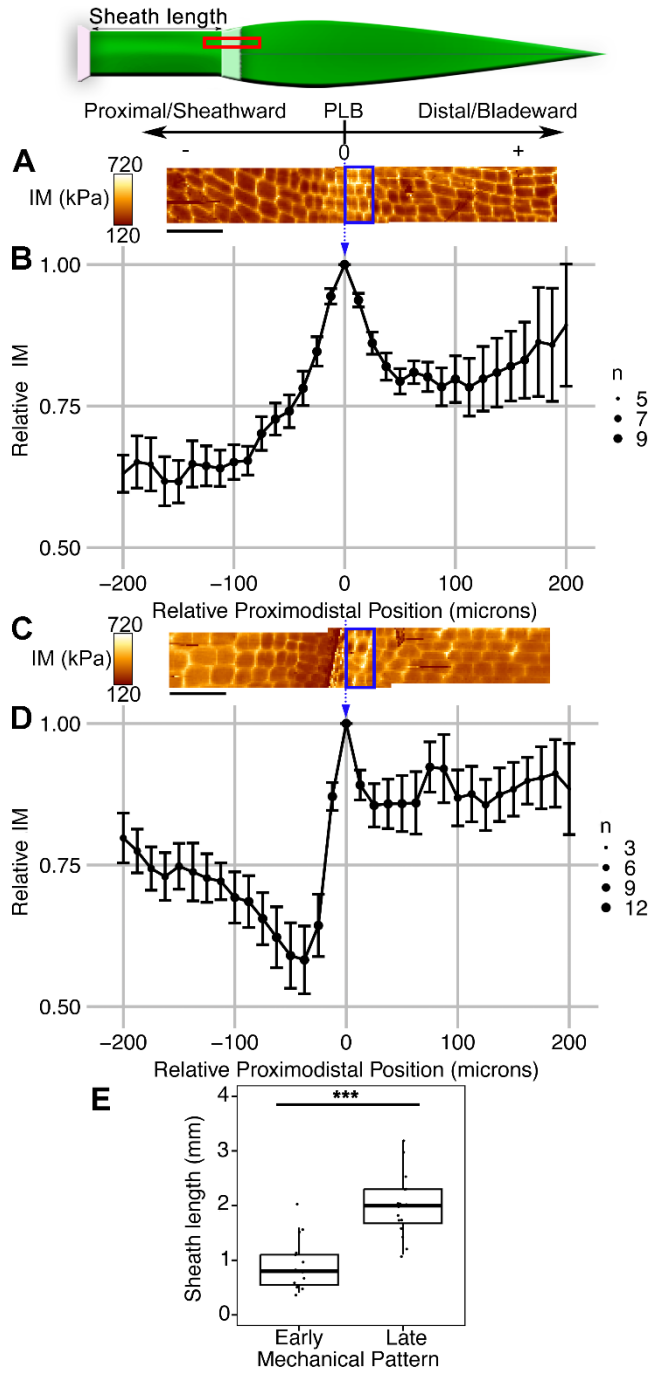


Figure 2.7: AFM analysis of ligular region reveals two distinct mechanical phases during ligule development

Cartoon at top shows orientation of leaf and region of interest for AFM scans and sliding window analysis, with the local maximum in IM for each leaf set as position 0. (A) Representative scans of leaf in the PLB stage reveals a local maximum in IM within the PLB. Two overlapping 50 x 200 μm scans are shown. Blue box indicates the position of the window for the measurement at relative position 0. Red lines indicate limits of the ligular region. (B) Sliding window analysis averaging all B73 samples exhibiting the early pattern (Early PLB and PLB stages; n=9). (C) Representative scans of leaf in the early fringe stage (D) Sliding window analysis averaging all B73 samples exhibiting the late pattern (Late PLB and Early Fringe stages, n=13). (A,C) are to scale relative to (B,D) Scale bars = 50 μm . Size of dot (n) indicates coverage at that relative position. Error bars = S.E. (E) Sheath lengths of leaves with the early and late mechanical patterns. *** indicates $p < 0.01$, calculated via Mann-Whitney U-test.

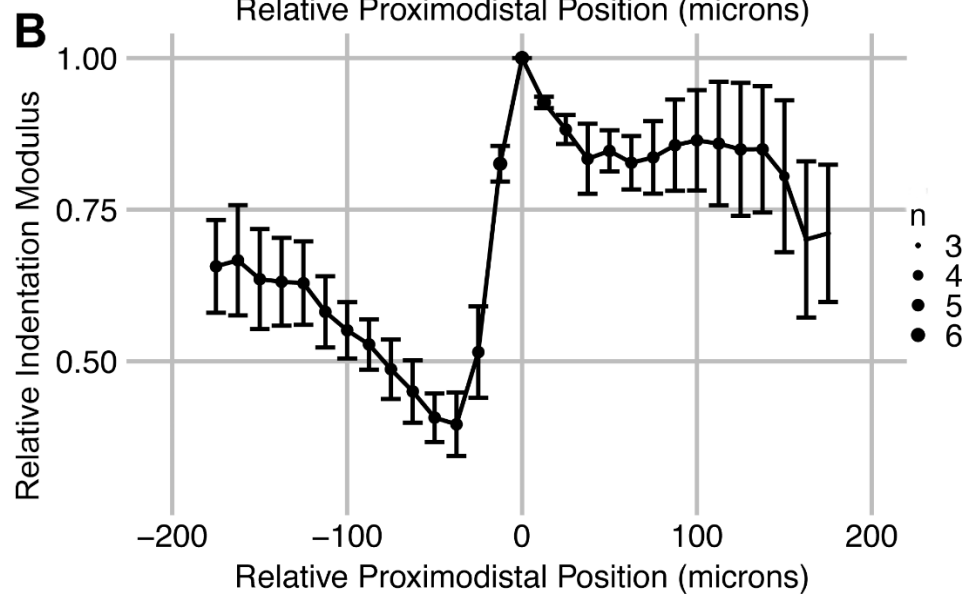
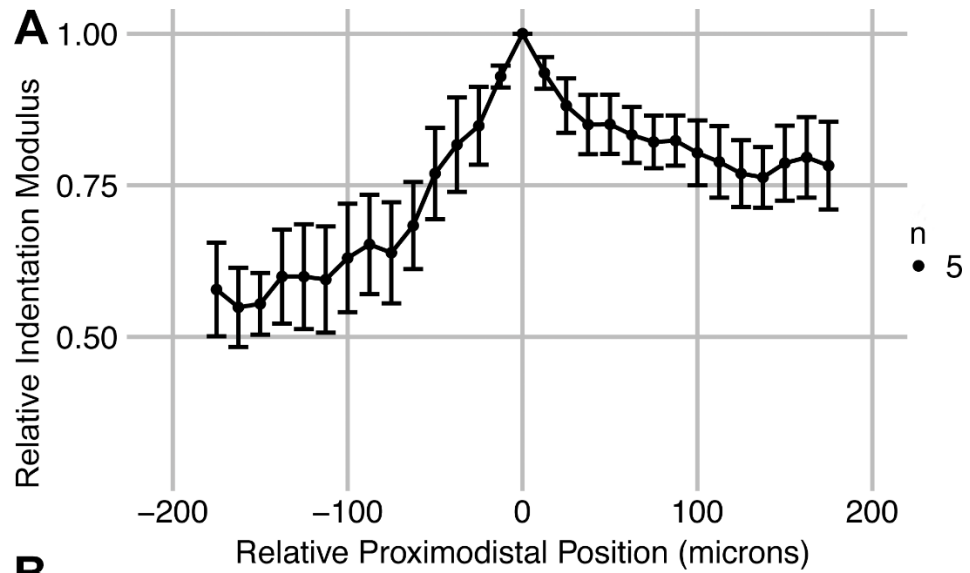


Figure 2.8: AFM force mapping sliding window analysis of Mo17 leaves

Sliding window regional averages in IM. Data normalized to the local maximum in the PLB, set as position=0, relative IM=1. Top panel is the average of all Mo17 plants (n=5) exhibiting the early mechanical pattern. Bottom panel is the average of all Mo17 plants (n=6) exhibiting the late mechanical pattern. Error bars indicate standard error.

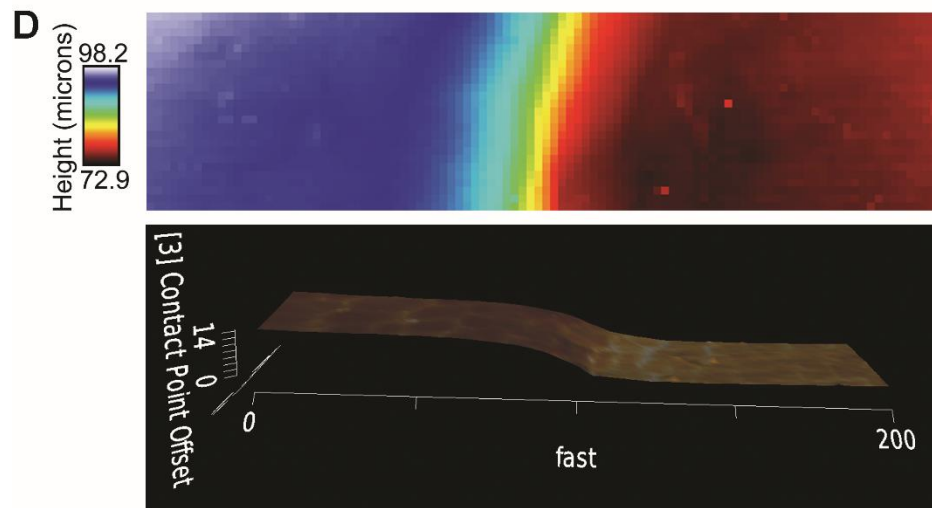
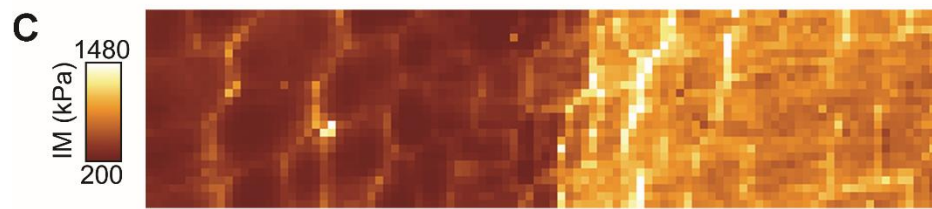
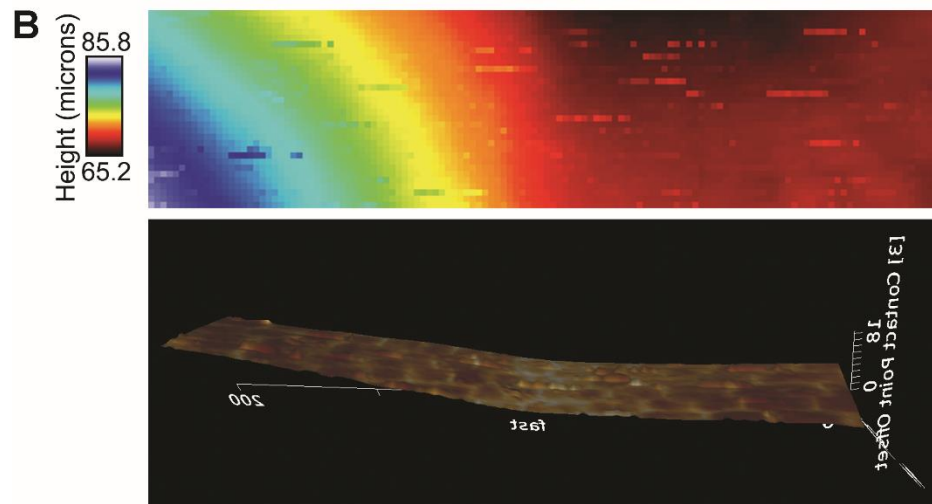
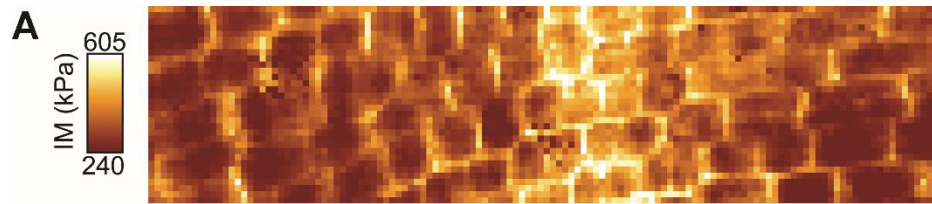


Figure 2.9: Mechanical transition within PLB relative to topography

(A) AFM scan of a leaf in the PLB stage, sheath length 0.6mm. Resolution is 1.6 μm per pixel. (B) Topography of the same sample as (A). This height map was first normalized along the mediolateral axis to highlight topography in the proximodistal direction. Height portrayed via both heatmap and 3D projection (C) AFM scan of a leaf in the late PLB stage, sheath length 2.0mm. Resolution is 2.0 μm per pixel. (D) Topography of the same sample as (C). Scale bars = 50 μm .

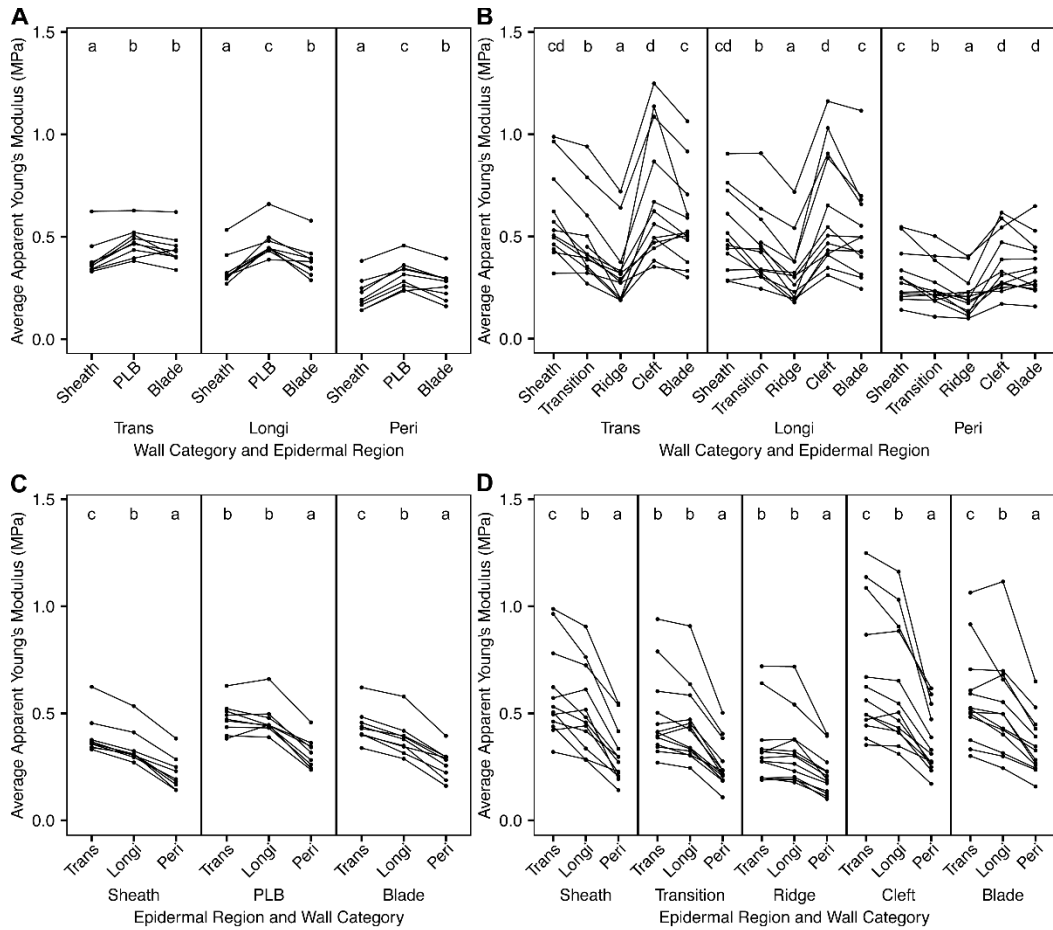


Figure 2.10: Manual resampling reveals regional and subcellular patterns in IM

IM was resampled for each wall category in each epidermal region of each sample. Samplings from different wall categories or tissue zones in the same leaf are connected with lines. Each dot indicates the average IM of at least 50 indentations from a particular wall category in a particular epidermal zone in one leaf. (A) All early-stage B73 samples, grouped by epidermal zone. (B) All late-stage B73 samples, grouped by epidermal zone. (C,D) Same data but instead grouped by wall category. Statistical analysis was performed independently for each panel and subpanel. Statistical significance was determined via Kruskal-Wallis test followed by pairwise Wilcoxon signed rank tests using the *W*-value at an alpha of $p < 0.05$.

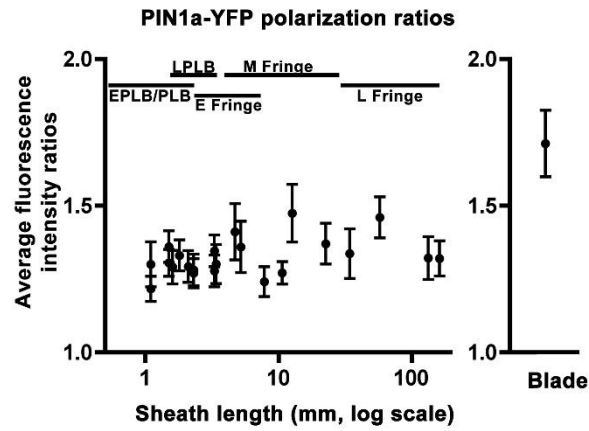
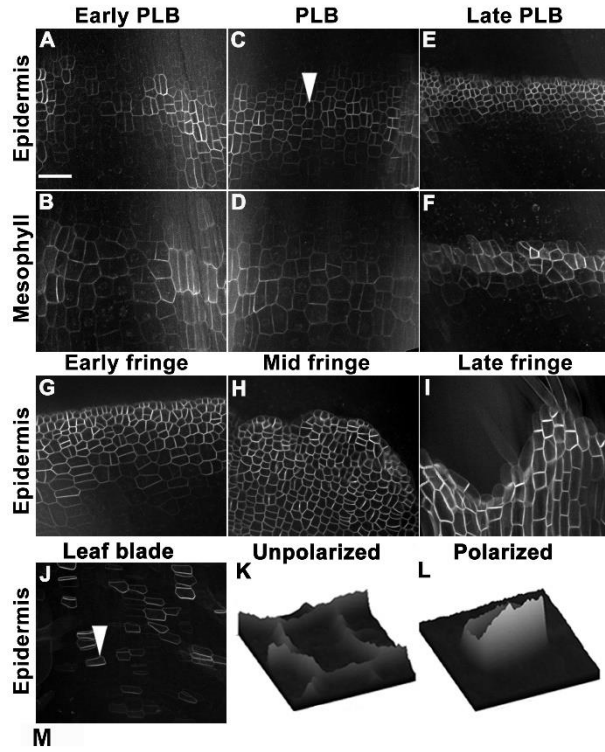


Figure 2.11: PIN1a-YFP localization in the PLB and ligule.

Panels (A,C,E) are single Z plane images of epidermal cells in early PLB, PLB and late PLB respectively; (B,D,F) are corresponding single Z planes of the next cell layer in the subtending mesophyll. PIN1a-YFP was observed in the early fringe (G), mid fringe (H) and late fringe (I). In (J) PIN1-YFP signal was peripheral in blade cells above the ligule fringe. (K,L) Relative fluorescence intensity surface plots are displayed for the cell by arrowheads in (C), showing a PLB cell with low polarity, and in (J), showing a blade cell with increased polarity. (M) PIN1a-YFP polarization ratios compared at ligule stages and in the blade, as calculated from 30 or more cells from four different plants. Error bars are 95% confidence intervals. Blade cells were significantly more polarized than PLB or fringe cells (p value ≤ 0.01 using the Kolmogorow-Smirnov test). Scale bar = 50 μm .

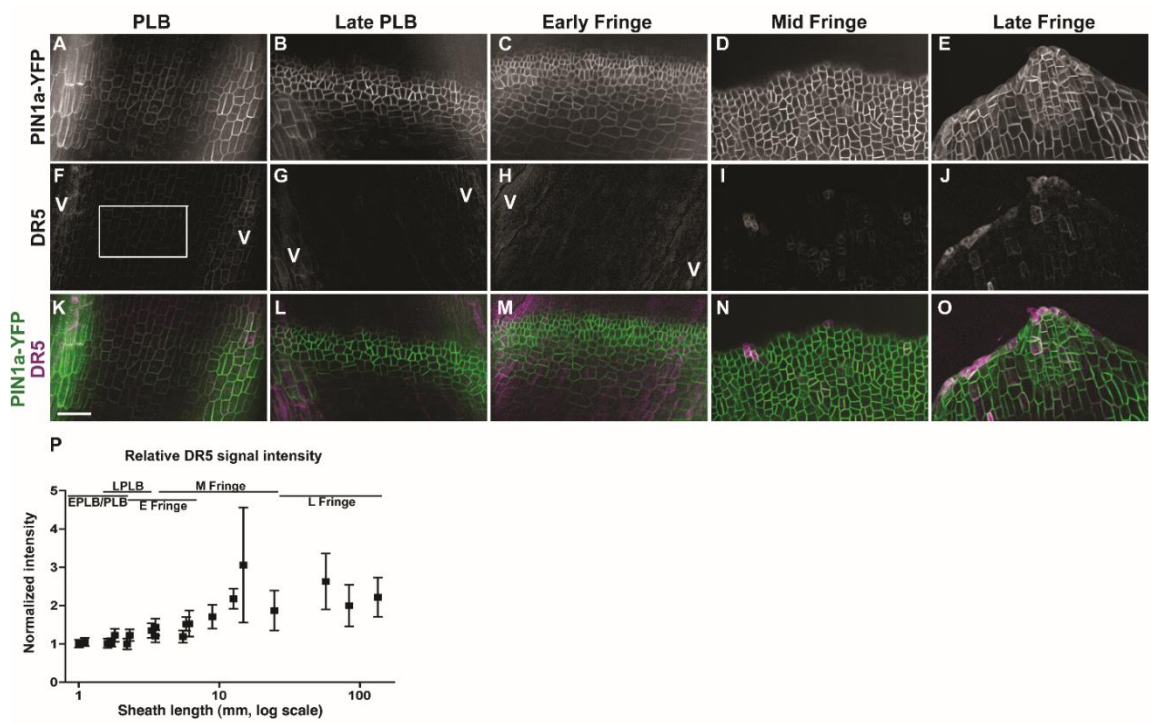


Figure 2.12: PIN1a-YFP and DR5rev:mRFP_{er} (DR5) localization during ligule development.

PIN1a-YFP accumulation is shown in the top panels (A-E); DR5 in the middle panel (F-J) with merged PIN1a-YFP (green) and DR5 (magenta) in the bottom panel (K-O). Normalized DR5 fluorescence intensity values are shown (P). Each point is the average of three or more measurements per sample. DR5 intensity values increased significantly and were more variable during later ligule stages (F-test, $p < 0.01$). Error bars show standard error. Scale bar = 50 μm .

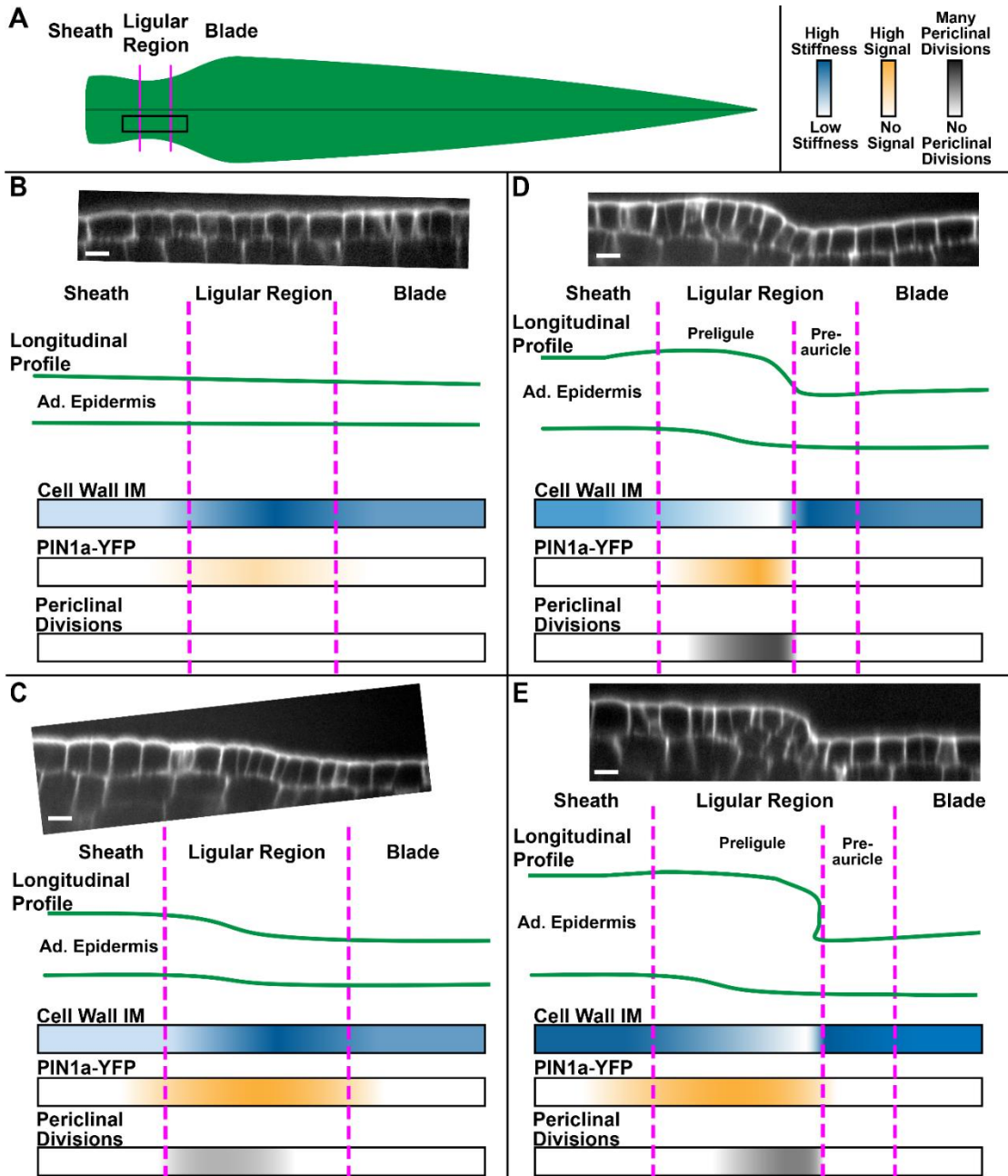


Figure 2.13: Summary of patterns observed during early ligule development

(A) Cartoon of maize leaf primordium and proximodistal zones. Black box indicates the area studied. (B-D) Patterns in epidermal topography are shown using representative confocal micrograph projections and cartoons.

Proximodistal patterns in cell wall IM, PIN1a-YFP signal, and the position/frequency of periclinal divisions are shown using color gradients. (B) Early PLB stage, (C) PLB Stage, (D) Late PLB Stage, (E) Early Fringe Stage.

Scale bars=15 μ m.

Table 2.1: Cell division orientation during ligule developmental stages

Statistical differences for cell division % were determined by MANOVA testing for an effect of developmental stage and division orientation on % divisions, followed by one-way ANOVAs testing for differences with respect to stage and orientation separately. Latin letters indicate significant differences in the % of different division orientations in each stage, while Greek letters indicate significant differences for one division type between stages.

Developmental stage	n Individual leaves measured per stage	Sheath length range in mm	Cell size (μm^2 +/- S.E.)	Total mitotic cells observed	Anticlinal longitudinal division (% +/- S.E.)	Anticlinal transverse divisions (% +/- S.E.)	Periclinal divisions (% +/- S.E.)	Oblique divisions (% +/- S.E.)
Early Preligule band	4	0.8 - 1.3	158 +/- 9 n=414	77	52 +/- 9% b γ	49 +/- 8% b $\alpha\beta$	0% a α	3 +/- 2% a α
Preligule band	3	1.5 - 2.1	134 +/- 9 n=315	59	38 +/- 3% b $\beta\gamma$	45 +/- 5% b $\alpha\beta$	10 +/- 4% a $\alpha\beta$	5 +/- 3% a α
Late Preligule band	5	1.8 - 3.1	105 +/- 6 n=759	132	18 +/- 2% b $\alpha\beta$	31 +/- 2% c α	46 +/- 1% d δ	4 +/- 2% a α
Early fringe	3	2.5 - 4.4	186 +/- 16 n=304	62	22 +/- 1% b $\alpha\beta$	48 +/- 1% c $\alpha\beta$	27 +/- 2% b γ	2 +/- 2% a α
Mid fringe	3	5.4 - 12.5	450 +/- 145 n=539	45	9 +/- 5% a α	71 +/- 9% b β	16 +/- 5% a $\beta\gamma$	2 +/- 2% a α
Late fringe	3	35.1 - 57.5	1511 +/- 147 n=246	0	n/a	n/a	n/a	n/a

Table 2.2: Pairwise comparisons of average IM between epidermal zones via Wilcoxon signed rank test using the *W*-statistic

Comparison (Epidermal Tissue Zones)	Wall Category	Average IM Zone 1 +/- s.d. (MPa)	Average IM Zone 2 +/- s.d. (MPa)	<i>W</i> -value	Significance level
Early Sheath v. Early PLB	Trans	0.394 +/- 0.093	0.478 +/- 0.074	0	p<0.01
	Longi	0.340 +/- 0.082	0.470 +/- 0.077	0	p<0.01
	Peri	0.219 +/- 0.078	0.316 +/- 0.070	0	p<0.01
Early Sheath v. Early Blade	Trans	0.394 +/- 0.093	0.441 +/- 0.079	1	p<0.01
	Longi	0.340 +/- 0.082	0.384 +/- 0.084	0	p<0.01
	Peri	0.219 +/- 0.078	0.265 +/- 0.069	0	p<0.01
Early PLB v. Early Blade	Trans	0.478 +/- 0.074	0.441 +/- 0.079	6	NS
	Longi	0.470 +/- 0.077	0.384 +/- 0.084	0	p<0.01
	Peri	0.316 +/- 0.070	0.265 +/- 0.069	1	p<0.01
Late Sheath v. Late Transition	Trans	0.591 +/- 0.213	0.475 +/- 0.194	1	p<0.01
	Longi	0.518 +/- 0.196	0.443 +/- 0.180	9	p<0.05
	Peri	0.308 +/- 0.131	0.260 +/- 0.107	5	p<0.01
Late Sheath v. Late Ridge	Trans	0.591 +/- 0.213	0.332 +/- 0.167	0	p<0.01
	Longi	0.518 +/- 0.196	0.323 +/- 0.156	0	p<0.01
	Peri	0.308 +/- 0.131	0.211 +/- 0.097	7	p<0.01
Late Sheath v. Late Cleft	Trans	0.591 +/- 0.213	0.679 +/- 0.304	22	NS
	Longi	0.518 +/- 0.196	0.620 +/- 0.281	18	NS
	Peri	0.308 +/- 0.131	0.362 +/- 0.146	13	p<0.05
Late Sheath v. Late Blade	Trans	0.591 +/- 0.213	0.571 +/- 0.218	25	NS
	Longi	0.518 +/- 0.196	0.524 +/- 0.230	34	NS
	Peri	0.308 +/- 0.131	0.351 +/- 0.134	13	p<0.05
Late Transition v. Late Ridge	Trans	0.475 +/- 0.194	0.332 +/- 0.167	0	p<0.01
	Longi	0.443 +/- 0.180	0.323 +/- 0.156	0	p<0.01
	Peri	0.260 +/- 0.107	0.211 +/- 0.097	9	p<0.01

Late Transition v. Late Cleft	Trans	0.475 +/- 0.194	0.679 +/- 0.304	0	p<0.01
	Longi	0.443 +/- 0.180	0.620 +/- 0.281	0	p<0.01
	Peri	0.260 +/- 0.107	0.362 +/- 0.146	1	p<0.01
Late Transition v. Late Blade	Trans	0.475 +/- 0.194	0.571 +/- 0.218	0	p<0.01
	Longi	0.443 +/- 0.180	0.524 +/- 0.230	0	p<0.01
	Peri	0.260 +/- 0.107	0.351 +/- 0.134	0	p<0.01
Late Ridge v. Late Cleft	Trans	0.332 +/- 0.167	0.679 +/- 0.304	0	p<0.01
	Longi	0.323 +/- 0.156	0.620 +/- 0.281	11	p<0.05
	Peri	0.211 +/- 0.097	0.362 +/- 0.146	0	p<0.01
Late Ridge v. Late Blade	Trans	0.332 +/- 0.167	0.571 +/- 0.218	0	p<0.01
	Longi	0.323 +/- 0.156	0.524 +/- 0.230	0	p<0.01
	Peri	0.211 +/- 0.097	0.351 +/- 0.134	0	p<0.01
Late Cleft v. Late Blade	Trans	0.679 +/- 0.304	0.571 +/- 0.218	12	p<0.05
	Longi	0.620 +/- 0.281	0.524 +/- 0.230	7	p<0.01
	Peri	0.362 +/- 0.146	0.351 +/- 0.134	38	NS

Table 2.3: Pairwise comparisons of average IM between wall categories via Wilcoxon signed rank test using the *W*-statistic

Comparison (Wall Categories)	Tissue Zone	Average IM Category 1 +/- s.d. (MPa)	Average IM Category 2 +/- s.d. (MPa)	<i>W</i> -value	Significance level
Early Timepoint, Trans v. Longi	Sheath	0.394 +/- 0.093	0.340 +/- 0.082	0	p<0.01
	PLB	0.478 +/- 0.074	0.470 +/- 0.077	15	NS
	Blade	0.441 +/- 0.079	0.384 +/- 0.084	0	p<0.01
Early Timepoint, Trans v. Peri	Sheath	0.394 +/- 0.093	0.219 +/- 0.078	0	p<0.01
	PLB	0.478 +/- 0.074	0.316 +/- 0.070	0	p<0.01
	Blade	0.441 +/- 0.079	0.265 +/- 0.069	0	p<0.01
Early Timepoint, Longi v. Peri	Sheath	0.340 +/- 0.082	0.219 +/- 0.078	0	p<0.01
	PLB	0.470 +/- 0.077	0.316 +/- 0.070	0	p<0.01
	Blade	0.384 +/- 0.084	0.265 +/- 0.069	0	p<0.01
Late Timepoint, Trans v. Longi	Sheath	0.591 +/- 0.213	0.518 +/- 0.196	0	p<0.01
	Transition	0.475 +/- 0.194	0.443 +/- 0.180	19	NS
	Ridge	0.332 +/- 0.167	0.323 +/- 0.156	31	NS
	Cleft	0.679 +/- 0.304	0.620 +/- 0.281	7	p<0.01
	Blade	0.571 +/- 0.218	0.524 +/- 0.230	16	p<0.05
Late Timepoint, Trans v. Peri	Sheath	0.591 +/- 0.213	0.308 +/- 0.131	0	p<0.01
	Transition	0.475 +/- 0.194	0.260 +/- 0.107	0	p<0.01
	Ridge	0.332 +/- 0.167	0.211 +/- 0.097	0	p<0.01
	Cleft	0.679 +/- 0.304	0.362 +/- 0.146	0	p<0.01
	Blade	0.571 +/- 0.218	0.351 +/- 0.134	0	p<0.01
Late Timepoint, Longi v. Peri	Sheath	0.518 +/- 0.196	0.308 +/- 0.131	0	p<0.01
	Transition	0.443 +/- 0.180	0.260 +/- 0.107	0	p<0.01
	Ridge	0.323 +/- 0.156	0.211 +/- 0.097	0	p<0.01
	Cleft	0.620 +/- 0.281	0.362 +/- 0.146	0	p<0.01
	Blade	0.524 +/- 0.230	0.351 +/- 0.134	0	p<0.01

Table 2.4: Pairwise comparisons of average IM between early and late mechanical stages via Mann-Whitney U-Test

Comparison (Early v Late)	Wall Category	Average IM Early +/- S.D. (MPa)	Average IM Late +/- S.D. (MPa)	z-score	p-value
Early Sheath v. Late Sheath	Transverse	0.394 +/- 0.093	0.591 +/- 0.213	2.452	0.014 *
	Longitudinal	0.340 +/- 0.082	0.518 +/- 0.196	2.168	0.030 *
	Periclinal	0.219 +/- 0.078	0.308 +/- 0.131	1.670	0.095
Early PLB v. Late Transition	Transverse	0.478 +/- 0.074	0.475 +/- 0.194	-1.135	0.254
	Longitudinal	0.470 +/- 0.077	0.443 +/- 0.180	-1.202	0.230
	Periclinal	0.316 +/- 0.070	0.260 +/- 0.107	-2.003	0.045 *
Early PLB v. Late Ridge	Transverse	0.478 +/- 0.074	0.332 +/- 0.167	-2.671	0.008 **
	Longitudinal	0.470 +/- 0.077	0.323 +/- 0.156	-2.738	0.006 **
	Periclinal	0.316 +/- 0.070	0.211 +/- 0.097	-2.604	0.009 **
Early PLB v. Late Cleft	Transverse	0.478 +/- 0.074	0.679 +/- 0.304	1.402	0.161
	Longitudinal	0.470 +/- 0.077	0.620 +/- 0.281	0.734	0.465
	Periclinal	0.316 +/- 0.070	0.362 +/- 0.146	0.334	0.741
Early Blade v. Late Blade	Transverse	0.441 +/- 0.079	0.571 +/- 0.218	1.602	0.110
	Longitudinal	0.384 +/- 0.084	0.524 +/- 0.230	1.803	0.072
	Periclinal	0.265 +/- 0.069	0.351 +/- 0.134	1.269	0.204

Chapter 3

Ligule development is linked to differential cell mechanics and growth in adjacent zones of the leaf.

Abstract:

The maize ligule develops from the preligule band, a boundary region between the blade and the sheath that forms early in leaf development. Wild-type ligule development has previously been described in terms of division plane orientation, cell area, surface curvature, cell wall stiffness, and auxin dynamics. Prior research has focused primarily on the immediate ligular region, but some observations indicated the involvement of other zones of the leaf in early ligule morphogenesis. We measured differences in cell wall stiffness and cell geometry over a broader proximodistal span of the maize leaf epidermis around the ligular region, in both wild-type and *liguleless1;liguleless2* double mutants, which completely lack ligule and auricle development. Patterns in cell wall stiffness and cell geometry that are characteristics of wild-type ligule development were not observed in the blade-sheath boundary of the double mutant, indicating that these patterns are dependent on ligule development. We found that mechanical changes in the epidermis were not limited to the immediate ligular region, but that differences in cell wall stiffness between the blade and sheath are linked to the ligule developmental program. A broad proximodistal trend in epidermal cell depth is also dependent upon ligule development. Increased thickening of the

distal sheath zone may be important in driving the formation of the ridge within the ligular region. According to these observations, ligule development is associated with effects over a wide region of the epidermis, and the adjacent blade and sheath regions may play a more mechanistically important role in ligule outgrowth than has previously been recognized.

Introduction:

Ligule development has been well-described, both in previous studies and in the previous chapter of this thesis (Becraft and Freeling, 1991; Becraft et al., 1990; Johnston et al., 2014; Neher et al., 2023; Sharman, 1941; Sharman, 1942; Sylvester et al., 1990). However, the development of the blade-sheath boundary in the absence of ligule development has not been described in as much detail (Becraft et al., 1990; Sylvester et al., 1990). Furthermore, the development and outgrowth of the ligule could involve changes outside the preligule band, but this possibility has not been addressed in prior works.

The master regulators of ligule and auricle development are the SPL transcription factor *liguleless1* and the bZIP transcription factor *liguleless2* (Becraft et al., 1990; Harper and Freeling, 1996; Lee et al., 2007; Walsh et al., 1998; Wang et al., 2021). These transcription factors act in a partially redundant manner but mutations in each gene leads to a distinct phenotype. *liguleless1-R* mutants completely lack ligule and auricle and have an indistinct blade-sheath

boundary in the juvenile leaves but have a relatively well-defined boundary and vestigial ligule development in the later adult leaves (Becraft et al., 1990; Emerson, 1912; Sylvester et al., 1990). *lg1-R* leaves are somewhat narrower, particularly at the base of the blade, and the blades are oriented more vertically due to the lack of auricle development (Emerson, 1912). *liguleless2-R* mutants generally have normal ligule and auricle development towards the margins of the leaves, but these taper off and disappear towards the midrib (Harper and Freeling, 1996; Walsh et al., 1998). The two auricles do not extend all the way to the midrib and are not aligned with each other in their proximodistal positioning. Like *lg1-R*, the *lg2-R* mutant phenotype is more pronounced in juvenile leaves. *liguleless2* transcriptionally activates *lg1* and is thought to act upstream (Harper and Freeling, 1996; Wang et al., 2021). Mutant sectors of *lg2-R* in a wild-type heterozygous leaf develop normal ligule and auricle, suggesting that *lg2*, or one of its transcriptional targets, acts in a non-cell-autonomous way (Harper and Freeling, 1996). Conversely, *lg1-R* mutant sectors in wild-type heterozygous leaves lack ligule and auricle development, suggesting that *lg1* bestows competence to respond to the hypothetical “make ligule” signal in a cell autonomous manner (Becraft and Freeling, 1991). Additionally, the normal ligular structures on either side of the *lg1-R* mutant sectors are offset from each other proximodistally, reminiscent of the *lg2-R* mutant phenotype. Therefore, both *lg1* and *lg2* are involved in mediolaterally coordinating the proximodistal position of the blade-sheath boundary, and subsequent ligule-auricle development. The

nature and identity of the hypothetical signal involved in this process has not been determined, but the genetic evidence is consistent with *lg2* controlling the upstream or “sending” end of the signal while *lg1* controls the downstream or “receiving/responding” end of the signal (Becraft and Freeling, 1991; Harper and Freeling, 1996).

The development of the leaf in the *lg1-R* single mutant was described by Sylvester et al. (1990) using SEMs from sequentially dissected leaves. The mutant boundary region is less distinct and generally lacks PLB development. In *lg1-R* mutant leaves that form later in development, sporadic PLB formation at the boundary was sometimes observed, however, there were also patches of abnormal PLB, which lacked the longitudinal and later periclinal divisions that are characteristic of the wild-type PLB, and the ridge in the epidermal surface was shallow and uneven (Sylvester et al., 1990). This shift in division plane orientation is likely a critical part of ligule development, but it is not clear what factors are responsible.

Atomic Force Microscopy (AFM) analyses revealed differences in the elastic modulus of the cell walls in different epidermal zones, which correlated with differences in growth (Neher et al., 2023), however this is only one aspect of the overall mechanical context. The indentation modulus best reflects how the cell wall yields to pressure in an elastic manner. This pressure has both a cell-autonomous component – the cell’s own turgor, and a non-cell-autonomous component – the pressure due to the turgor of surrounding cells (Ali et al., 2023).

Turgor is generally thought to be uniform in plant tissues (Kutschera and Niklas, 2013; Nonami and Boyer, 1989; Shackel et al., 1991), although that has not been tested in this system. However, tension is not necessarily uniform throughout the organ. Non-cell-autonomous pressures usually place the outer epidermal wall in a state of high tension, particularly in the longitudinal direction, due to the anisotropy of growth and the orientation of cellulose in the cell walls throughout the organ (Ali et al., 2023; Kelly-Bellow et al., 2023; Savaldi-Goldstein et al., 2007). Local differences in growth and cell division could place certain sections of the epidermis under greater stress. Furthermore, the topography of the surface contributes to the non-cell-autonomous pressures experienced by a cell.

Experiments in the *Arabidopsis* meristem have shown that cell expansion correlates with surface curvature, suggesting cells in the boundary region are in a state of relative compression in the radial axis of the meristem, and in a state of greater tension in the tangential direction (Kierzkowski et al., 2012; Kwiatkowska and Dumais, 2003; Louveaux et al., 2016). This affects their expansion – they grow primarily in the tangential axis, in the direction of greater tension (Kwiatkowska and Dumais, 2003). This results in a geometry that should favor a radially oriented division plane according to the surface-minimization model for cell division (Besson and Dumais, 2011). However, cells in the boundary more commonly place their division plane in the tangential direction, again parallel to the direction of maximum tension (Louveaux et al., 2016). This could be explained by increased tension in the cell wall altering microtubule dynamics

(Hamant et al., 2019; Louveaux et al., 2016). Thus, cells existing in a mechanically extreme context may deviate from typical division rules. Given the emergence of a ridge in the ligular region from a relatively early stage (Neher et al., 2023; Sylvester et al., 1990), and the possible mechanical relevance of surface topography in growth and development (Kierzkowski et al., 2012; Kwiatkowska and Dumais, 2003), we need to understand more about how the preligular ridge forms.

In our previous experiments we measured epidermal cell depth in the ligular region and found that differential thickening of cells relative to the proximodistal axis must contribute to the formation of the preligule ridge (Neher et al., 2023). The differences did not occur exclusively within the PLB cells, but also the adjacent blade and sheath cells, such that the sheath surface was elevated relative to the blade surface. Our study area was not broad enough to determine over what distance this trend occurs. The differential thickening could be a highly local phenomenon, where the proximal PLB thickens and the immediately adjacent sheath expands along with it, while the distal PLB resists expanding in the depth axis. This trend could also be regional, consistent with a medium-range coordination of growth between epidermal zones. Lastly, the trend could be global, which could be accomplished either with long-distance signaling and coordination, or with a phenomenon intrinsic to the sheath and blade – something that would happen anyways with or without ligule development.

Here, we report that wild-type patterns in cell wall mechanics and cell geometry extend far beyond the ligular region and are tied to ligule development. AFM on liguleless mutants revealed that the dramatic differences in cell wall elastic properties observed in the wild-type ligular region were absent in the *lg1;lg2* double mutant. Furthermore, spatiotemporal trends between the sheath and blade epidermal zones were also altered in the mutant, suggesting the mechanical changes associated with ligule development are more far-reaching than previously recognized. Consistent with this, differential thickening of epidermal cells was found to occur over a broad region in wild-type leaves. Again the liguleless double mutant abolished not only the local trends in the ligular region, but also a more far-reaching differential thickening trend between the sheath and blade regions. These findings demonstrate that growth is coordinated between the proximodistal domains of the maize leaf, which may lead to mechanical feedback at the tissue/organ level and set the mechanical preconditions for ligule outgrowth.

Materials and Methods:

Plant growth and dissection:

Maize plants were grown in a greenhouse under standard conditions at UC Riverside. Seeds were sown in 2-gallon pots of soil and grown for about 4 weeks prior to confocal or AFM imaging. For dissection, leaves were removed

from the plant one by one, by cutting just above the disc of insertion and unwrapping each leaf from the culm. Leaf numbers were counted during dissection, and sheath length was measured using a pair of electronic calipers. Imaging and measurements were taken from the lateral and marginal domains of the primordium.

Imaging and measuring cell geometry:

Adaxial ligule regions of dissected plants were stained for ~10 minutes with 10 µg/mL propidium iodide and mounted in water. Confocal Z-stacks were collected through the adaxial epidermis using the 40X oil (1.30 NA) Olympus objective lens at a Z-step of 0.2 µm using a Hamamatsu 9100C EM-CCD camera mounted on a Nikon Ti stand with a spinning disk confocal head (CSU-W1, Yokogawa). Propidium iodide was excited at 561 nm and collected at 620/20 nm.

Scans were processed using the MorphoGraphX software package. Stacks were first processed using a Gaussian blur at a sigma value of 0.5 µm. For cell area calculations, the surface of the scan was extracted using the Edge Detect process at varying threshold values, depending on signal intensity. Surfaces were adjusted using the Fill Holes, Erode, and Opening processes as necessary to create a smooth surface. The surface was converted into a mesh using the Marching Cubes Surface process at a cube size of 1 µm. The scan signal was then projected onto the mesh surface at around 4 – 7 µm offset. Cells

segmented via the Watershed Segmentation process with manual seeding of the cells. Mis-segmented cells were corrected by comparing the segmentation to the original scan to ensure proper recognition of cell walls. The area of the segmented cells was extracted by creating a heatmap and saving the results to a .csv file.

For cell depth calculations, the blurred Z-stacks underwent ITK auto-seeded watershed segmentation, with the “level” value varying depending on signal intensity. Mis-segmented cells were manually corrected by comparing them to the original scan. Segmented 3D cells were converted into meshes using the Marching Cubes 3D process at a cube size of 1 μm . Any mis-segmented cells that could not be corrected were deleted. For comparing depth values along the proximodistal axis, cells overlying vascular bundles were also deleted so as not to be considered in the subsequent analysis. Cell depth values were obtained by creating a heatmap and saving the results to a .csv file.

For proximodistal position values, a Bezier line was used to define the longitudinal axis of the leaf. The line was created and oriented parallel to the longitudinal axis, with position 0 being the center of the ligular region, sheath as the negative direction, and blade as the positive direction. At the edge of each scan, the cells with the lowest and highest values were identified. Then in the next overlapping scan in the series, that cell was identified and set as the new position zero, and then a correction value was added to all cells from that scan

based on the “zero” cell’s position value in the previous scan. This allowed us to accurately measure the position of cells over a broad proximodistal range.

Atomic Force Microscopy

Developing ligules were dissected as described above. To eliminate turgor pressure, leaves were plasmolyzed in 0.55 M mannitol for at least 15 minutes. They were affixed to a microscope slide with double-sided tape and covered with more mannitol. AFM was performed using a JPK Nanowizard 4a AFM in force mapping mode, at the CNSI at UCLA. Indentations were performed at a constant maximum force of 500 nN, with extend and retract times of 0.1s at a Z-length of 4 μm , at a spatial resolution of 1.5625 microns per pixel. The probes used were PPP-NCL probes with a 10 nm pyramidal tip, with an average force modulus of 45 N/m. Each tip was calibrated separately to find the exact force modulus.

Data were processed using the JPKSPM software. The raw indentation data were converted into IM using a Hertzian contact model. Multiple overlapping scans were measured, processed, and reassembled by identifying common features in the overlapping areas. Data were processed using both a sliding window approach and a manual resampling approach using MATLAB, as described previously (Neher et al., 2023).

Results:

Wild-type patterns of cell wall rigidity are not observed in liguleless mutants

We previously performed atomic force microscopy (AFM) across the epidermis in the ligular region of wild-type maize inbreds B73 and Mo17. We reported differences in the rigidity (indentation modulus/IM) of the cell walls within the ligular region that were associated with the PLB and early ligule outgrowth. The PLB was the most rigid epidermal zone in the earlier stages of development. Later in development, the sheathward proximal PLB was the softest zone, while the bladeward distal PLB was the most rigid. Notably, there were also significant differences between the rigidity of cells in the sheath and blade.

In order to determine which wild-type mechanical trends were genetically linked to ligule development, we used AFM to examine cell wall mechanics in *lg1;lg2* double mutants. Despite the lack of a PLB and a less well-defined blade/sheath boundary, the blade-sheath junction is still distinguishable. There is a bend in the epidermal cell files near the blade-sheath junction, sheath cells are larger, the sheath appears more opaque when viewed with transmitted light through a stereoscope, the blade has a greater density of veins, and the blade epidermal surface has greater curvature over lateral veins. These features were similar between wild-type and the double mutant and were useful in identifying the mutant blade-sheath junction.

Wild-type leaves had a peak in rigidity in the ligular region, however no local maximum in IM was observed in the liguleless double mutant across the blade-sheath junction (Fig. 3.1A,B). This was confirmed via both the sliding window processing method and by manual resampling to separately evaluate transverse anticlinal, longitudinal anticlinal, and periclinal walls (Figs. 3.1A,B, 3.2A). Therefore, in the absence of ligule development there is no cell wall rigidification at the blade-sheath boundary. The late-stage trends in IM observed in wild-type leaves were also not observed in the double mutant (Fig. 3.1C,D). In contrast to the wild-type pattern of a local minimum in IM in the proximal ligular region and a local maximum in IM in the distal ligular region, the mutant blade-sheath transition was intermediate between blade and sheath IM values (Fig. 3.1C,D). No consistent trends in IM were observed in the liguleless double mutant (Figs. 3.1, 3.2). The regional mechanical patterns observed in the wild-type epidermis are therefore linked to PLB and ligule development, rather than an independent phenomenon.

Manual resampling in the wild-type samples had also revealed elastic asymmetry in the blade and sheath with transverse walls having significantly higher IM than longitudinal walls (Neher et al., 2023, Fig. 2.9, Table 2.3). Cells in the wild-type ligular region had reduced elastic asymmetry – their transverse and longitudinal walls had similar IM values. This difference was not observed in the liguleless double mutant (Fig. 3.2C,D). The cells in the blade-sheath transitional region showed elastic asymmetry similar to the blade and sheath (Fig. 3.2C,D).

Therefore, PLB development is connected to both regional and subcellular changes in cell wall mechanics.

In addition to changes in the immediate ligular region, *lg1 lg2* double mutants also showed differences in mechanical patterns in the blade and sheath compared to wild-type plants. In early wild-type development (samples with a sheath length less than 1.5 mm), sheath rigidity tended to be less than or equal to the blade, for all cell wall categories (Fig. 3.3A). This trend reversed for the anticlinal walls in the later stages of development, in leaves with sheath lengths greater than 1.5 mm (Fig. 3.3A). The rigidity ratio between blade and sheath transverse and longitudinal walls correlated significantly with sheath length. In the double mutant, this trend was still present. Samples with higher sheath length had lower blade/sheath rigidity ratios (Fig 3.3B). While the blade-sheath rigidity ratio was lower in developmentally older samples, the sheath was not consistently softer during the early stages of development, and overall the rigidity ratios were more variable. This is consistent with a non-cell-autonomous effect associated with ligule development – the PLB could communicate with adjacent leaf zones to mechanically coordinate ligule outgrowth.

Differential thickening of epidermal cells extends beyond the immediate ligular region

We previously found that differential thickening of epidermal cells relative to the proximodistal axis of the ligular region contributed to the formation of a ridge, from which the ligule grows out. Cells in the proximal portion of the ligular region, and adjacent sheath cells thickened more than cells in the distal ligular region, which were the thinnest cells in the epidermis by the late PLB stage. Cells in the blade thickened an intermediate amount. However, it was not clear to what extent this was a local, regional, or global trend. Sheath cells are also larger in area than blade cells, but we had not measured blade and sheath cells further than 100 μm away from the PLB, so it was not clear if this was also a local or global trend.

We sought to determine whether differences in the geometry of epidermal cells were restricted to the ligular region or broader trends, and furthermore whether these trends were linked to ligule development or not. We collected confocal Z-stacks through the epidermis using overlapping tiles in long epidermal strips spanning the ligular region and at least 400 microns in both sheathward and bladeward directions, in wild-type and liguleless leaves. Scans were processed using MorphoGraphX to segment the cells in both 2.5D and 3D. Cell geometry

data was extracted from the cell mesh outlines and plotted relative to proximodistal position (Figs. 3.4, 3.5).

In wild-type leaves, epidermal cells showed a consistent trend in the proximodistal direction. Sheath cells were generally larger than preligule or blade cells. A gradual proximodistal gradient was observed in the sheath – more distally located cells were larger in area than those more proximally located (Fig. 3.4A,B). Cells in the ligular region were the smallest, particularly those located in the nascent ligule-auricle cleft. Blade cells were larger than PLB cells, but smaller than sheath cells (Fig. 3.4A,B). These trends were generally conserved in the liguleless double mutant (Fig. 3.4C,D), however the mutant does not form a PLB and cells in the region between blade and sheath were not particularly small, but intermediate in area between the sheath and blade. The other trends were consistent with those observed in wild-type samples. Sheath cells were large, with distal sheath cells being the largest, and blade cells were smaller (Fig. 3.4C,D). These observations indicate that the increased size of sheath cells, and proximodistal gradient in cell area within the sheath zone, is intrinsic to the sheath and is not dependent on ligule development.

Wild-type samples showed proximodistal trends in epidermal cell depth (Fig. 3.5). Cells overlying lateral veins were excluded from the analysis due to large mediolateral oscillations in cell depth, which is particularly pronounced in the blade. Early in development, the wild-type sheath cells were either thinner or equally thick as blade cells (Fig. 3.5A). There was little to no proximodistal

gradient within the sheath and ligular zones. Later in development, a shallow ridge became visible within the ligular region. Cell depth increased most in the distal sheath region. In samples with a sheath length of >1.0 mm, we consistently found the distal sheath cells to be the largest in the Z-dimension (Fig. 3.5B). The proximal region of the blade epidermis was thinner in these samples, but thickened gradually moving in the distal direction. To determine if there were statistical differences across the leaf, we pooled together all cell depth values for inter-vein epidermal cells falling between -350 and -250 microns for the sheath, and 250 and 350 microns for the blade, thus comparing cells more distant from the PLB than we had imaged previously (Fig. 3.5B). Trends in early samples varied, with the earliest samples showing that the blade was significantly thicker (Fig. 3.5A). Slightly later, a trend of greater thickening in the sheath began to emerge but was not statistically significant in every sample (Fig. 3.5A). In samples with sheath lengths longer than 1.0 mm, the trend was consistent, with sheath cells being significantly thicker than blade cells (Fig. 3.5B). Therefore, differential thickening in the wild-type leaves was not localized exclusively to the ligular region. Rather, there was a broad trend in cell thickness that extended several hundred microns away from the small cells of the preligule band, but did not encompass the entire leaf.

While the wild-type trend in cell area was only locally altered at the blade-sheath junction in the liguleless double mutant, the trends in cell depth were affected more broadly. Early-stage mutant samples had no consistent

proximodistal trend in cell depth (Fig. 3.5C). Later-stage mutant samples often had a gradient in cell depth, with distal cells being somewhat thicker in the Z-dimension than more proximal cells (Fig. 3.5D). Whereas the distal sheath had the thickest cells in later wild-type leaves, this was never the case in the liguleless double mutant (Fig. 3.5D). Therefore, the wild-type patterns of cell thickness appear to be correlated with ligule development. This further implies that the preligule band, once initiated, restricts growth locally and signals to adjacent regions in a way that alters their growth behavior, particularly in the depth dimension. This results in a consistent pattern of differential cell thickening over a wide area, elevating the distal portion of the sheath surface relative to the proximal portion of the blade surface and forming a ridge within the ligular region.

Discussion:

We compared the proximodistal patterns in epidermal cell wall mechanics and cell geometry between wild-type and liguleless maize. The liguleless double mutant was affected not only at the blade-sheath junction, but also more broadly between the adjacent sheath and blade zones. This confirms the patterns observed in the wild-type boundary region are indeed linked to ligule development. Furthermore, it implies that ligule development causes subtle but mechanically relevant changes in the behavior of cells in adjacent leaf zones.

AFM analyses in wild-type leaves had revealed a peak in cell wall stiffness in the ligular region early in development, followed by a partitioning of the ligular region into a proximal soft zone and distal rigid zone. In the *lg1;lg2* double mutant, this pattern was abolished. This is consistent with a boundary-specific cell wall rigidification program that occurs downstream of the liguleless transcription factors. Previous transcript-levels experiments showed that boundary-defining genes including the maize ortholog of *CUC2* are expressed in the PLB, but become restricted to the more distal portion of the ligular region at later stages (Johnston et al., 2014). Similarly, the wild-type boundary region is more rigid, but the rigid zone becomes restricted distally as the ligule begins to grow out (Neher et al., 2023). The pattern of cell wall rigidity correlates with the expression pattern of *CUC2*, and this is dependent on ligule development. This parallels findings in the Arabidopsis leaf margin, where *CUC2* and other genes regulate a cell wall modifying program that is associated with increased cell wall stiffness (Bouré et al., 2022).

Subtle changes in the proximodistal rigidity pattern occurred outside the ligular region. Notably, wild-type samples early in development typically had a high blade:sheath rigidity ratio. Later in development, the blade:sheath rigidity ratio decreased. The sheath was significantly softer earlier in development, and the blade:sheath rigidity ratio correlated significantly with sheath length, a proxy for developmental stage. In the liguleless double mutant, this trend was altered. There was still a tendency for the blade:sheath IM ratio to decrease over the

course of development, but the correlation was weaker and variation was higher throughout development. There was no significant change in sheath IM between the early and late stages of development. Early-stage sheath cells were not significantly softer than early blade cells, nor late-stage sheath cells. Overall, this is consistent with a dysregulation of cell wall mechanical properties compared to the wild-type. The soft-sheath early phase in the wild-type may be connected to the formation of the preligule ridge, which begins to form around the same time. The altered mechanical pattern between sheath and blade provides circumstantial evidence that ligule development may involve changes in cell growth and mechanical properties outside the immediate ligular region, which nevertheless contribute to ligule outgrowth.

Some complications should be noted when interpreting the liguleless AFM data. In addition to the reported proximodistal pattern, there are also mediolateral changes in IM that correlate with the presence of underlying vascular bundles. The effect is more pronounced over the larger lateral veins, which are more well-developed at this stage. This mediolateral pattern was essentially negligible in wild-type because the proximodistal pattern was strong and consistent. However, because the liguleless double mutant lacks the proximodistal pattern, mediolateral variation is not masked. The AFM scans were not always aligned perfectly with the longitudinal axis, so fluctuations in IM along the length of the scan may result from passing over a large vein. This could partially account for the greater variance of blade:sheath IM ratios in the double mutant.

Whereas in wild type the preligule band was well-defined and provided a convenient landmark that aided in the analysis of the samples, the liguleless blade-sheath transition is much more indistinct, making it somewhat more difficult to identify the “zero” position for the sliding window analysis, as well as delimiting the blade, sheath, and “transitional” zones during manual resampling. However, several features of the wild-type leaf are still observed in the double mutant and enabled us to identify the mutant boundary area. The proximal blade is wider than the sheath, so the cell files flare outward near the blade-sheath boundary. Cell area is smaller in the blade than in the sheath. There is a greater density of vascular bundles in the blade, and the underlying bundles cause a greater deflection in the blade surface, resulting in a more dramatic, oscillating mediolateral curvature in the blade than in the sheath. Lastly, a stereoscope was used to facilitate positioning of the AFM probe, and the sheath generally appears more opaque than the blade when viewed using transmitted light. Therefore, while the exact threshold between the blade and sheath was more ambiguous in the double mutant, we are still able to make reasonable comparisons to the wild-type.

Confocal scans processed using MorphoGraphX revealed proximodistal patterns in cell depth that were tied to ligule development. In the wild-type, a pattern emerged during development, such that by the late PLB stage, the distal zone of the sheath and proximal extremity of the ligular region always have deeper cells than other epidermal regions. The proximal sheath is relatively thin

in the depth axis, but the distal portion of the sheath is thicker than the proximal portion of the blade. Within the ligular region there is always a distinct “trough” that emerges in the cell depth curve. Initially the trough is located somewhat more distally due to decreased thickening of cells in the distal ligular region, consistent with pattern of boundary gene expression and the high IM zone. By the beginning of ligule fringe outgrowth, the trough is somewhat more proximally located due to the periclinal divisions in the proximal PLB, which have thickened considerably but then repeatedly bisected themselves in the depth axis. All these trends are lost in the *lg1;lg2* double mutant. Not only is there no differential thickening at the blade-sheath junction, there is no portion of the sheath that is distinctly thicker than the blade. The ligule development program does not only inform differential growth locally, it affects growth over an approximately 1 mm span of the leaf.

Cell area measurements relative to the proximodistal axis showed similar trends between wild-type and *lg1;lg2*, except within the immediate ligular region. The distinct band of small cells that constitutes the PLB was not observed in the double mutant, consistent with previous reports. There was usually a proximodistal gradient in cell area within the wild-type sheath zone, with distal cells being larger, and this was also observed in the double mutant. Additionally, blade epidermal cells were smaller than sheath epidermal cells in both wild-type and mutant leaves. While there could be other subtle cell geometry differences in the double mutant, the overall trends in area were consistent. Therefore, the

ligule development program specifically influences differential cell thickening over a broad proximodistal range.

These findings imply that the formation of the preligule ridge does not solely involve differential cell growth within the ligular region. Rather, growth may be coordinated over a wider area, particularly in the depth dimension. A large ~500 μm zone of the distal sheath surface elevates relative to the blade surface, consistent with previously-published images of the developing ligule. We show that this differential thickening is not an intrinsic, default behavior of the sheath, but rather is connected to the ligule development program. We do not have enough evidence to determine whether the soft-sheath IM pattern is connected to the cell depth pattern, but it could conceivably indicate a differential growth mechanism, which is lost in the double mutant, abolishing both the cell wall mechanical pattern and the cell depth pattern. This implies that once the ligule developmental program initiates, some signal is sent to adjacent leaf zones to adjust their growth patterns. The identity of this signal is unknown – it could be chemical or possibly mechanical in nature. While the role of auxin in ligule development is still mysterious, it would be an ideal candidate for this signal, as it can affect cell wall pH, cytoskeletal organization, and growth via TMK1 signaling, which could occur independently of canonical auxin transcriptional responses (Lin et al., 2021; Xu et al., 2014).

We hypothesize that the formation of the ridge in the ligular region is more directly driven by increased thickening of the sheath, rather than the ligular

region itself. We have not yet assessed the contribution of the underlying cell layers due to difficulty in obtaining readily segmentable images from deeper tissue. However, the relatively minor difference in epidermal cell depth (~2 – 5 μm) does not account for the total vertical offset between the sheath surface and the blade surface (~10 – 20 μm), so the underlying sheath tissue layers are likely also involved in driving the formation of the ridge. In summary, the PLB restricts growth locally while signaling to the nearby sheath to thicken more. This is a surprising example of coordination between different organ zones, and may be critical to proper ligule organogenesis.

Our data suggest that differential cell wall mechanical properties may cause regional differences in growth, contributing to changes in the topography of the developing organ. However, we have not thoroughly considered effects acting in the opposite direction – once topographical features emerge in the leaf surface, the resulting curvature could affect the mechanical forces experienced by cells in different positions (Kierzkowski et al., 2012; Kwiatkowska and Dumais, 2003; Louveaux et al., 2016). Consistent with this, as the curvature of the surface increases, so too do the geometric differences between the proximal and distal ligular regions. Cells in the distal ligular region occupy a concave region of the surface and are likely to be relatively compressed in the proximodistal direction, but remain under tension in the mediolateral direction. These cells are distinctly smaller and tend to be wider than they are long. Cells in the proximal ligular region occupy the convex portion of the surface, which could place them under

increased tension in the proximodistal direction. These cells are somewhat larger and are more often longer than they are wide. These observations are consistent with findings in meristems (Kierzkowski et al., 2012; Kwiatkowska and Dumais, 2003; Louveaux et al., 2016). This mechanism could act as a form of positive feedback – first differential thickening of the sheath and blade create a contour in the epidermal surface, and resulting mechanical patterns sharpen the initially shallow ridge to form a sharp cleft. We do not have enough information to determine whether curvature also affects cell division orientation. Presumably, division plane placement is determined via some combination of the default surface minimization rules, topology-based rules and maximum tension rules, with the tension rules only overriding the other rules in mechanically extreme circumstances (Besson and Dumais, 2011; Hamant et al., 2019; Jackson et al., 2019; Louveaux et al., 2016; Robinson, 2021). We also note that cells on the nascent ridge are often columnar in shape and may also experience shear forces. Periclinal divisions are rarely ever observed in the epidermal layer, but in this case there may be both geometric and mechanical factors that favor periclinal divisions (Martinez et al., 2018). More research will be necessary to understand the mechanical factors involved in early ligule outgrowth.

References:

- Ali, O., Cheddadi, I., Landrein, B. and Long, Y.** (2023). Revisiting the relationship between turgor pressure and plant cell growth. *New Phytologist* **238**, 62–69.
- Becraft, P. W. and Freeling, M.** (1991). Sectors of liguleless-1 tissue interrupt an inductive signal during maize leaf development. *Plant Cell* **3**, 801–807.
- Becraft, P. W., Bongard-Pierce, D. K., Sylvester, A. W., Poethig, R. S. and Freeling, M.** (1990). The liguleless-1 gene acts tissue specifically in maize leaf development. *Dev. Biol.* **141**, 220–232.
- Besson, S. and Dumais, J.** (2011). Universal rule for the symmetric division of plant cells. *Proceedings of the National Academy of Sciences* **108**, 6294–6299.
- Bouré, N., Peaucelle, A., Goussot, M., Adroher, B., Soubigou-Taconnat, L., Borrega, N., Biot, E., Tariq, Z., Martin-Magniette, M.-L., Pautot, V., et al.** (2022). A cell wall-associated gene network shapes leaf boundary domains. *Development* **149**, dev200359.
- Emerson, R. A.** (1912). The inheritance of the ligule and auricles of corn leaves. *Nebr. Agri. Exp. Stn. Ann. Rep.* **25**, 81–88.
- Hamant, O., Inoue, D., Bouchez, D., Dumais, J. and Mjolsness, E.** (2019). Are microtubules tension sensors? *Nat Commun* **10**, 2360.
- Harper, L. and Freeling, M.** (1996). Interactions of liguleless1 and liguleless2 function during ligule induction in maize. *Genetics* **144**, 1871–1882.
- Jackson, M. D. B., Duran-Nebreda, S., Kierzkowski, D., Strauss, S., Xu, H., Landrein, B., Hamant, O., Smith, R. S., Johnston, I. G. and Bassel, G. W.** (2019). Global Topological Order Emerges through Local Mechanical Control of Cell Divisions in the Arabidopsis Shoot Apical Meristem. *Cell Systems* **8**, 53-65.e3.
- Johnston, R., Wang, M., Sun, Q., Sylvester, A. W., Hake, S. and Scanlon, M. J.** (2014). Transcriptomic analyses indicate that maize ligule development recapitulates gene expression patterns that occur during lateral organ initiation. *Plant Cell* **26**, 4718–4732.
- Kelly-Bellow, R., Lee, K., Kennaway, R., Barclay, J. E., Whibley, A., Bushell, C., Spooner, J., Yu, M., Brett, P., Kular, B., et al.** (2023). Brassinosteroid coordinates cell layer interactions in plants via cell wall and tissue mechanics. *Science* **380**, 1275–1281.

- Kierzkowski, D., Nakayama, N., Routier-Kierzkowska, A.-L., Weber, A., Bayer, E., Schorderet, M., Reinhardt, D., Kuhlemeier, C. and Smith, R. S.** (2012). Elastic domains regulate growth and organogenesis in the plant shoot apical meristem. *Science* **335**, 1096–1099.
- Kutschera, U. and Niklas, K. J.** (2013). Cell division and turgor-driven stem elongation in juvenile plants: A synthesis. *Plant Science* **207**, 45–56.
- Kwiatkowska, D. and Dumais, J.** (2003). Growth and morphogenesis at the vegetative shoot apex of *Anagallis arvensis* L. *J. Exp. Bot.* **54**, 1585–1595.
- Lee, J., Park, J.-J., Kim, S. L., Yim, J. and An, G.** (2007). Mutations in the rice liguleless gene result in a complete loss of the auricle, ligule, and laminar joint. *Plant Mol. Biol.* **65**, 487–499.
- Lin, W., Zhou, X., Tang, W., Takahashi, K., Pan, X., Dai, J., Ren, H., Zhu, X., Pan, S., Zheng, H., et al.** (2021). TMK-based cell-surface auxin signalling activates cell-wall acidification. *Nature* **599**, 278–282.
- Louveaux, M., Julien, J.-D., Mirabet, V., Boudaoud, A. and Hamant, O.** (2016). Cell division plane orientation based on tensile stress in *Arabidopsis thaliana*. *Proceedings of the National Academy of Sciences* **113**, E4294–E4303.
- Martinez, P., Allsman, L. A., Brakke, K. A., Hoyt, C., Hayes, J., Liang, H., Neher, W., Rui, Y., Roberts, A. M., Moradifam, A., et al.** (2018). Predicting division planes of three-dimensional cells by soap-film minimization. *Plant Cell* **30**, 2255–2266.
- Neher, W. R., Rasmussen, C. G., Braybrook, S. A., Lažetić, V., Stowers, C. E., Mooney, P. T., Sylvester, A. W. and Springer, P. S.** (2023). The maize preligule band is subdivided into distinct domains with contrasting cellular properties prior to ligule outgrowth. *Development* **150**, dev201608.
- Nonami, H. and Boyer, J. S.** (1989). Turgor and Growth at Low Water Potentials 1. *Plant Physiol* **89**, 798–804.
- Robinson, S.** (2021). Mechanobiology of cell division in plant growth. *New Phytologist* **231**, 559–564.
- Savaldi-Goldstein, S., Peto, C. and Chory, J.** (2007). The epidermis both drives and restricts plant shoot growth. *Nature* **446**, 199–202.
- Shackel, K. A., Greve, C., Labavitch, J. M. and Ahmadi, H.** (1991). Cell Turgor Changes Associated with Ripening in Tomato Pericarp Tissue. *Plant Physiol* **97**, 814–816.
- Sharman, B. C.** (1941). Development of the ligule in *Zea mays* L. *Nature* **147**, 641–641.

- Sharman, B. C.** (1942). Developmental anatomy of the shoot of *Zea mays* L. *Ann. Bot.* **6**, 245–282.
- Sylvester, A. W., Cande, W. Z. and Freeling, M.** (1990). Division and differentiation during normal and *liguleless-1* maize leaf development. *Development* **110**, 985–1000.
- Walsh, J., Waters, C. A. and Freeling, M.** (1998). The maize gene *liguleless2* encodes a basic leucine zipper protein involved in the establishment of the leaf blade–sheath boundary. *Genes Dev.* **12**, 208–218.
- Wang, R., Liu, C., Chen, Z., Sun, S. and Wang, X.** (2021). *Oryza sativa* *LIGULELESS 2s* determine lamina joint positioning and differentiation by inhibiting auxin signaling. *New Phytol.* **229**, 1832–1839.
- Xu, T., Dai, N., Chen, J., Nagawa, S., Cao, M., Li, H., Zhou, Z., Chen, X., De Rycke, R., Rakusová, H., et al.** (2014). Cell surface ABP1-TMK auxin-sensing complex activates ROP GTPase signaling. *Science* **343**, 1025–1028.

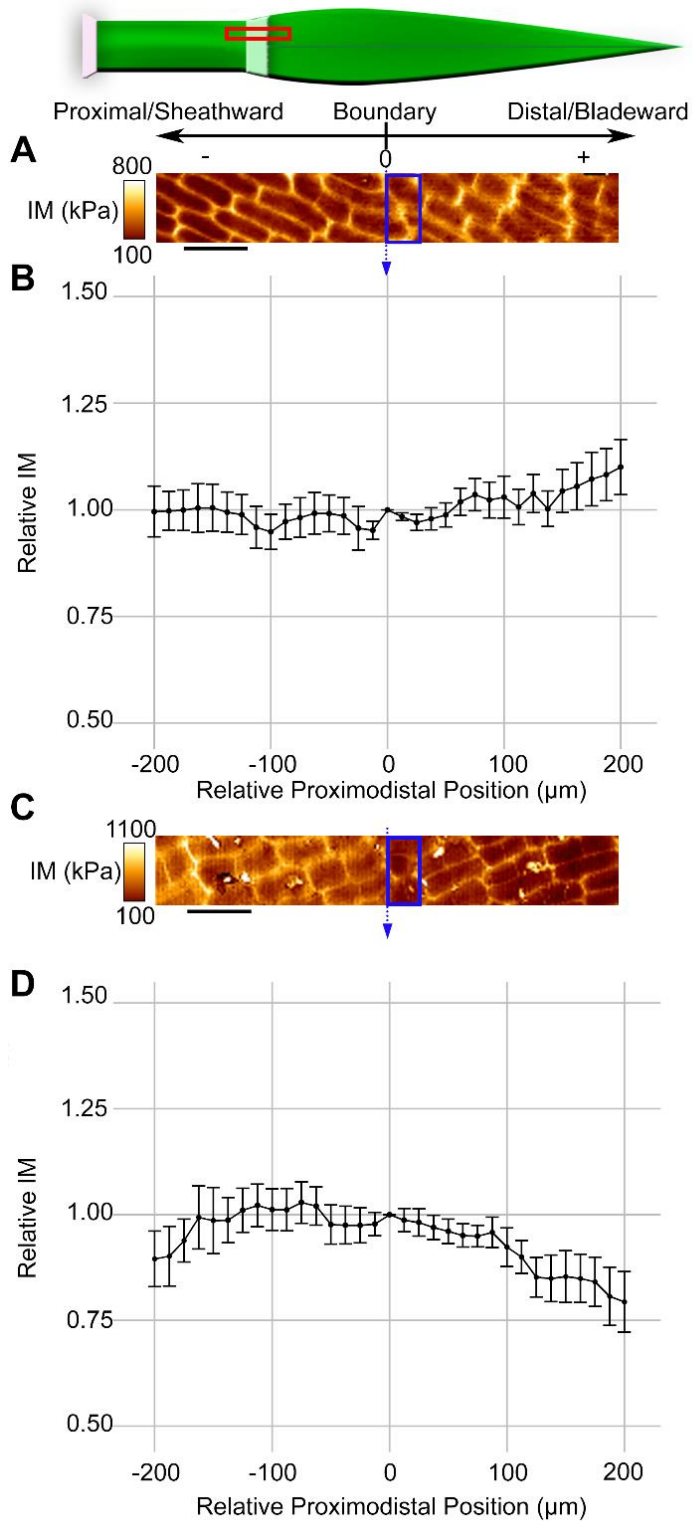
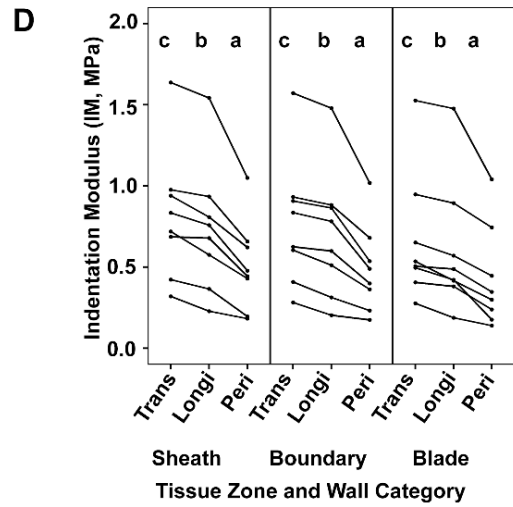
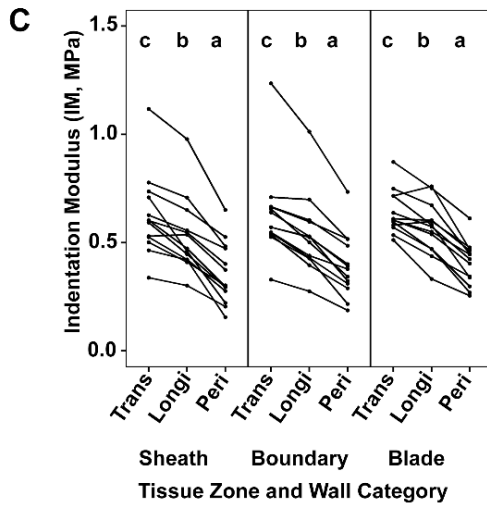
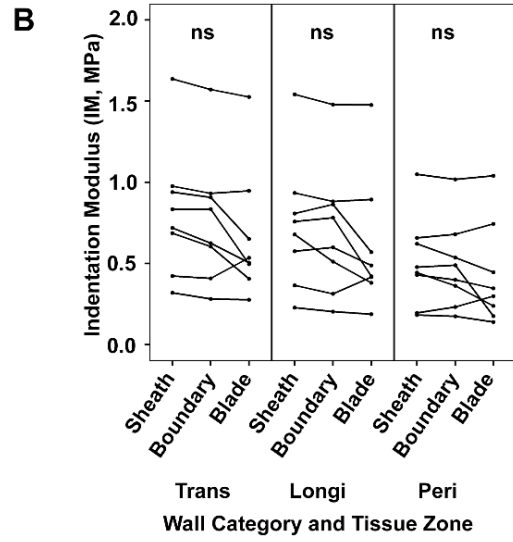
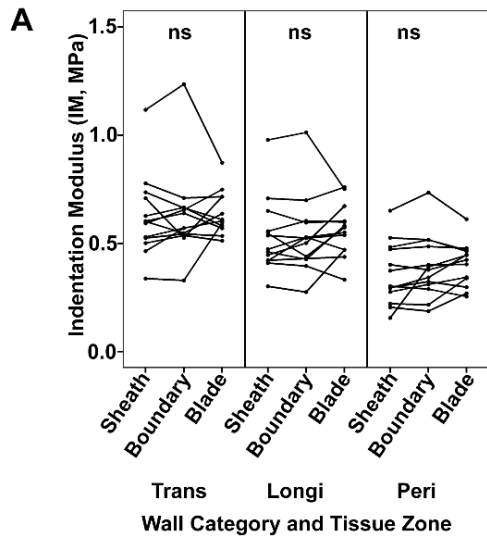


Figure 3.1: *liguleless1-R; liguleless2-R* double mutants lack boundary-specific cell wall rigidification.

Cartoon at top shows orientation of leaf and region of interest for AFM scans and sliding window analysis, with the local maximum in IM for each leaf set as position 0. (A) Representative scans of leaf in the early stage (<1.5 mm sheath length) reveals no significant local maximum in IM within the ligular region. Two overlapping 50 x 200 μm scans are shown. Blue box indicates the position of the window for the measurement at relative position 0. Red lines indicate limits of the mutant ligular region. (B) Sliding window analysis averaging all *lg1;lg2* samples exhibiting the early pattern (Sheath length <1.5 mm; n=14). (C) Representative scans of leaf in the later stage of development (D) Sliding window analysis averaging all B73 samples exhibiting the late pattern (Sheath length > 1.5 mm, n=9). (A,C) are to scale relative to (B,D) Scale bars = 50 μm . Error bars = S.E.



**Figure 3.2: Manual resampling reveals a lack of a consistent trend in IM
across the blade-sheath boundary of *lg1;lg2* leaf epidermis**

IM was resampled for each wall category in each epidermal region of each sample. Samplings from different wall categories or tissue zones in the same leaf are connected with lines. Each dot indicates the average IM of at least 50 indentations from a particular wall category in a particular epidermal zone in one leaf. (A) All early-stage (Sheath length <1.5 mm) *lg1;lg2* samples, grouped by epidermal zone. (B) All late-stage (Sheath length > 1.5 mm) *lg1;lg2* samples, grouped by epidermal zone. (C,D) Same data but instead grouped by wall category. Statistical analysis was performed independently for each panel and subpanel. Statistical significance was determined via Kruskal-Wallis test followed by pairwise Wilcoxon signed rank tests using the *W*-value at an alpha of $p < 0.05$.

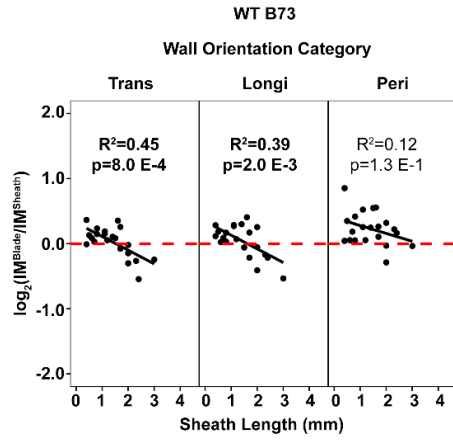
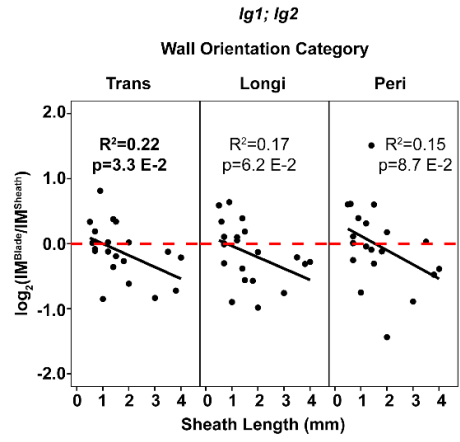
A**B**

Figure 3.3: The rigidity ratio between blade and sheath epidermal cells differs between wild-type and liguleless development

(A) In wild-type, the IM of the blade is consistently greater than the IM of the sheath early in development (< 1.5 mm sheath length). Later in development (>1.5 mm sheath length), the sheath IM becomes greater than the blade IM. The blade-sheath IM ratio correlates significantly with sheath length. (B) In *lg1;lg2* double mutants, the blade-sheath IM ratio is generally lower than in wild-type. Particularly, there is no distinct phase early in development when the sheath cells are softer.

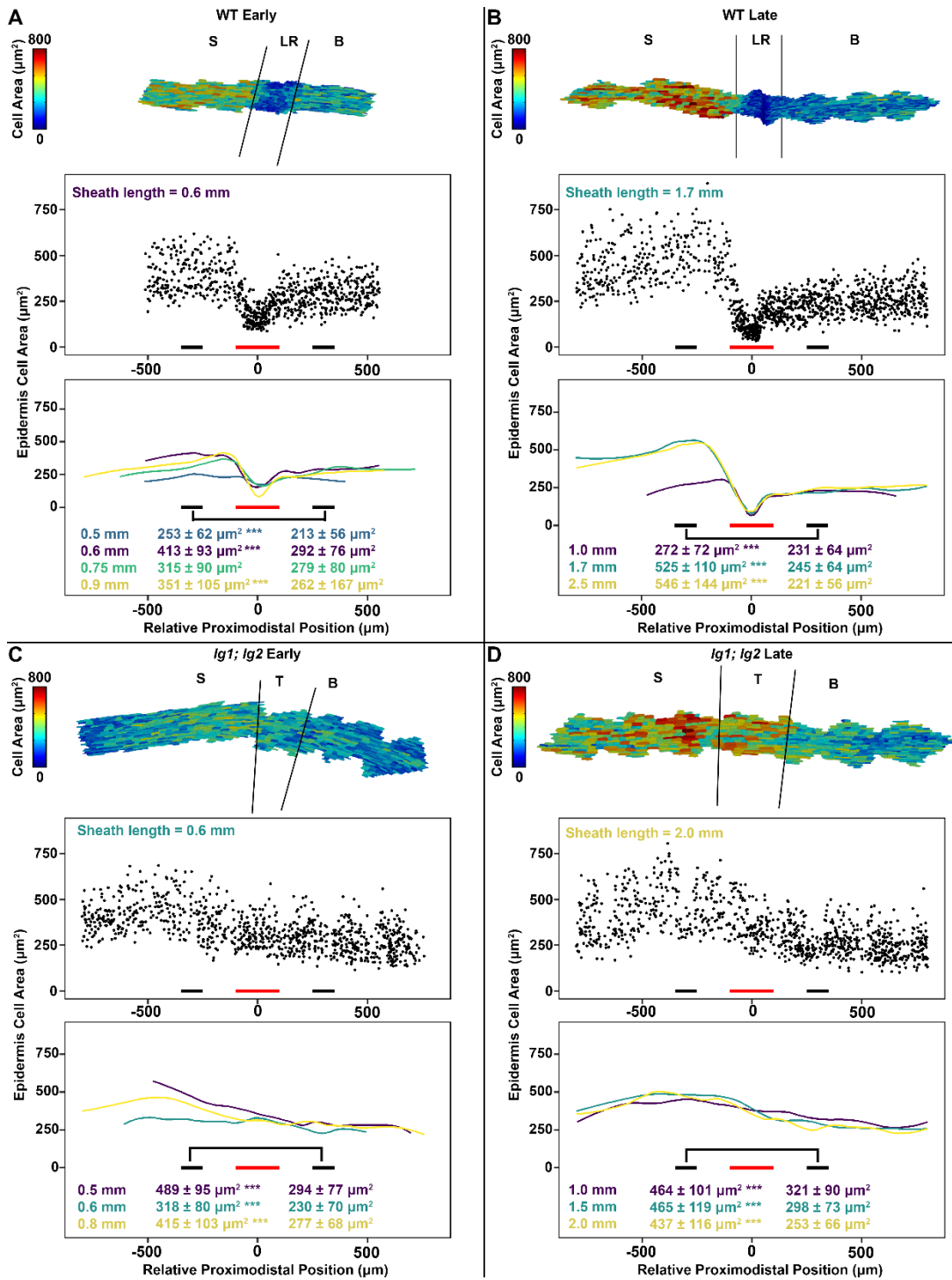


Figure 3.4: Differences in cell area between the blade and sheath are consistent between wild-type and *lg1;lg2* leaves

Cell area data were extracted from overlapping confocal micrographs in long epidermal strips of wild-type and liguleless maize. Heatmaps are cell area projected onto 2.5D mesh of the epidermal surface with segmented cell outlines generated using MorphoGraphX in a representative leaf. Dotplots are the extracted cell area values from that leaf. Line plots are smoothed averages created via local regression fitting in R. In each sample, the average cell area value was calculated for the ranges -350 – -250 (Distal sheath epidermis) and 250 – 350 (Proximal blade epidermis). Statistical significance was calculated via Mann-Whitney U-Test. * $p < 0.05$, *** $p < 0.001$. (A) Early in wild-type development, the leaf surface is relatively flat and sheath cells are usually larger than blade cells, and the PLB is visible as a band of very small cells. (B) Later in wild-type development, a ridge forms and epidermal cell area is consistently greater in the distal sheath compared to the proximal blade. (C-D) In *lg1;lg2*, there is no preligule band at the blade-sheath boundary, but there is still a consistent difference in cell area between the distal sheath and proximal blade. Therefore, the differential in cell area between the sheath and blade is not dependent on ligule development.

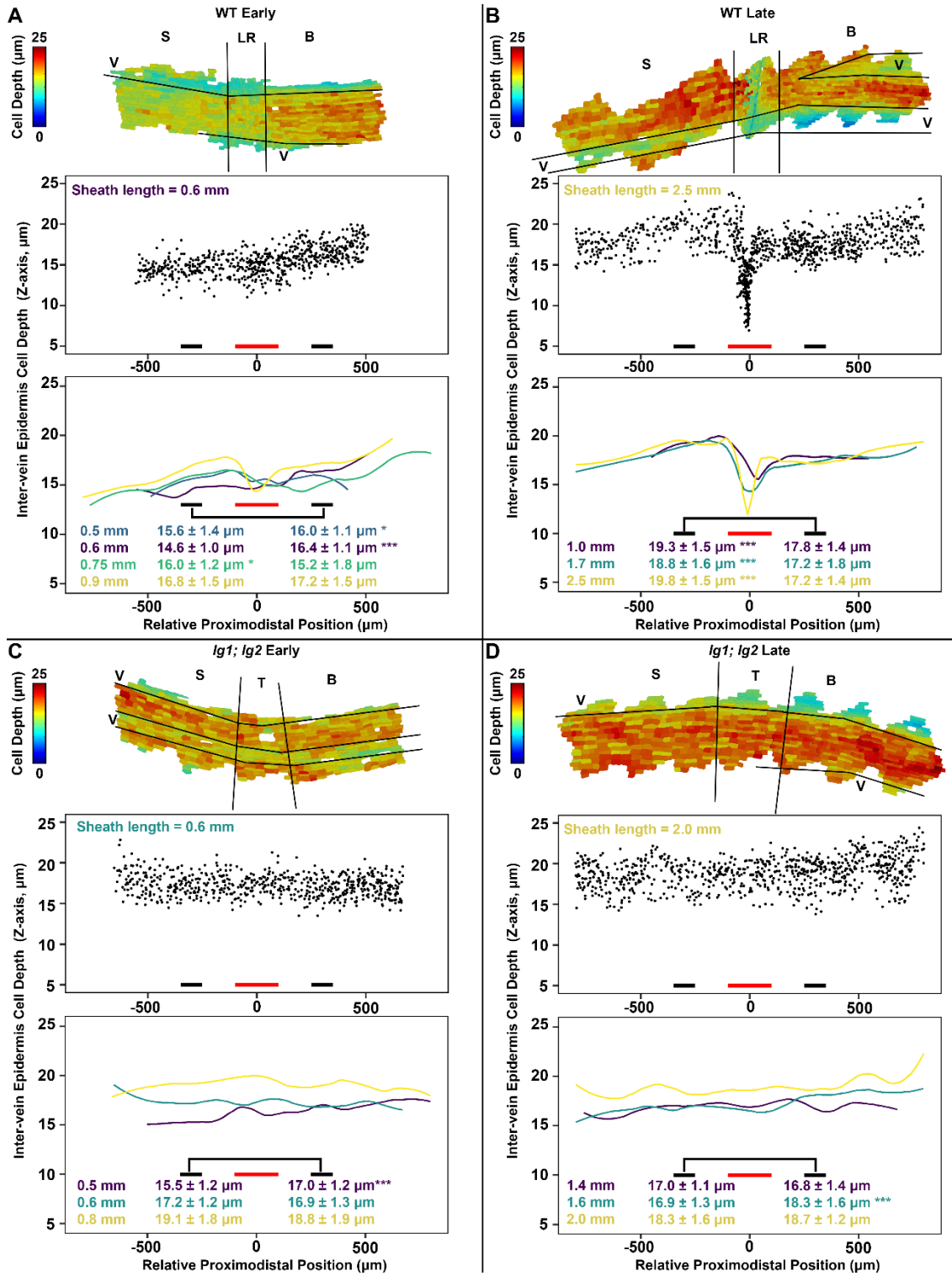


Figure 3.5: Ligule development is linked to broad proximodistal trends in cell depth

Cell depth data were extracted from overlapping confocal micrographs in long epidermal strips of wild-type and liguleless maize. Heatmaps are cell depth projected onto 3D mesh outlines of epidermal cells generated using MorphoGraphX in a representative leaf. Dotplots are the extracted cell depth values from that leaf. Line plots are smoothed averages created via local regression fitting in R. Cells overlying vascular bundles were excluded from the analysis. In each sample, the average cell depth value was calculated for the ranges -350 – -250 (Distal sheath epidermis) and 250 – 350 (Proximal blade epidermis). Statistical significance was calculated via Mann-Whitney U-Test. * $p < 0.05$, *** $p < 0.001$. (A) Early in wild-type development, the leaf surface is relatively flat and trends in cell depth are inconsistent. (B) Later in wild-type development, a ridge forms and epidermal cell depth is consistently greater in the distal sheath compared to the proximal blade. (C-D) In *lg1;lg2*, there is no consistent difference in cell depth between the distal sheath and proximal blade. Therefore, ligule development is linked to differential thickening of epidermal cells over a broad area, not just the immediate ligular region.

Table 3.1: Pairwise comparisons of average IM between *Ig1*; *Ig2* epidermal zones via Wilcoxon signed rank test using the *W*-statistic

Comparison (Epidermal Tissue Zones)	Wall Category	Average IM Zone 1 +/- s.d. (MPa)	Average IM Zone 2 +/- s.d. (MPa)	<i>W</i> -value	Significance level
Early Sheath v. Early Boundary	Trans	6.5 ± 2.3	6.6 ± 2.2	32	NS
	Longi	5.7 ± 2.4	5.7 ± 2.1	32.5	NS
	Peri	3.7 ± 1.6	4.0 ± 1.6	18	NS
Early Sheath v. Early Blade	Trans	6.5 ± 2.3	6.4 ± 1.0	37	NS
	Longi	5.7 ± 2.4	5.6 ± 1.3	31	NS
	Peri	3.7 ± 1.6	4.0 ± 1.0	25	NS
Early Boundary v. Early Blade	Trans	6.6 ± 2.2	6.4 ± 1.0	37	NS
	Longi	5.7 ± 2.1	5.6 ± 1.3	36	NS
	Peri	4.0 ± 1.6	4.0 ± 1.0	38.5	NS
Late Sheath v. Late Boundary	Trans	6.6 ± 2.3	6.3 ± 2.3	8	NS
	Longi	6.0 ± 2.5	5.8 ± 2.7	18	NS
	Peri	4.1 ± 1.8	4.0 ± 1.7	21	NS
Late Sheath v. Late Blade	Trans	6.6 ± 2.3	5.3 ± 2.0	6	NS
	Longi	6.0 ± 2.5	4.6 ± 2.1	6	NS
	Peri	4.1 ± 1.8	3.4 ± 1.9	12	NS
Late Boundary v. Late Blade	Trans	6.3 ± 2.3	5.3 ± 2.0	8	NS
	Longi	5.8 ± 2.7	4.6 ± 2.1	8	NS
	Peri	4.0 ± 1.7	3.4 ± 1.9	11	NS

Table 3.2: Pairwise comparisons of average IM between *Ig1*; *Ig2* wall categories via Wilcoxon signed rank test using the *W*-statistic

Comparison (Wall Categories)	Tissue Zone	Average IM Category 1 +/- s.d. (MPa)	Average IM Category 2 +/- s.d. (MPa)	<i>W</i> -value	Significance level
Early Timepoint, Trans v. Longi	Sheath	6.5 ± 2.3	5.7 ± 2.4	5	p<0.01
	Boundary	6.6 ± 2.2	5.7 ± 2.1	0	p<0.01
	Blade	6.4 ± 1.0	5.6 ± 1.3	6	p<0.01
Early Timepoint, Trans v. Peri	Sheath	6.5 ± 2.3	3.7 ± 1.6	0	p<0.01
	Boundary	6.6 ± 2.2	4.0 ± 1.6	0	p<0.01
	Blade	6.4 ± 1.0	4.0 ± 1.0	0	p<0.01
Early Timepoint, Longi v. Peri	Sheath	5.7 ± 2.4	3.7 ± 1.6	0	p<0.01
	Boundary	5.7 ± 2.1	4.0 ± 1.6	0	p<0.01
	Blade	5.6 ± 1.3	4.0 ± 1.0	0	p<0.01
Late Timepoint, Trans v. Longi	Sheath	6.6 ± 2.3	6.0 ± 2.5	3	p<0.05
	Boundary	6.3 ± 2.3	5.8 ± 2.7	4	p<0.05
	Blade	5.3 ± 2.0	4.6 ± 2.1	0	p<0.01
Late Timepoint, Trans v. Peri	Sheath	6.6 ± 2.3	4.1 ± 1.8	0	p<0.01
	Boundary	6.3 ± 2.3	4.0 ± 1.7	0	p<0.01
	Blade	5.3 ± 2.0	3.4 ± 1.9	0	p<0.01
Late Timepoint, Longi v. Peri	Sheath	6.0 ± 2.5	4.1 ± 1.8	0	p<0.01
	Boundary	5.8 ± 2.7	4.0 ± 1.7	0	p<0.01
	Blade	4.6 ± 2.1	3.4 ± 1.9	0	p<0.01

Table 3.3: Pairwise comparisons of average IM between *Ig1*; *Ig2* early and late mechanical stages via Mann-Whitney U-Test

Comparison (Early v Late)	Wall Category	Average IM Early +/- S.D. (MPa)	Average IM Late +/- S.D. (MPa)	z-score	p-value
Early Sheath v. Late Sheath	Transverse	6.5 ± 2.3	6.6 ± 2.3	-0.25	0.80
	Longitudinal	5.7 ± 2.4	6.0 ± 2.5	-0.32	0.75
	Periclinal	3.7 ± 1.6	4.1 ± 1.8	-0.25	0.80
Early Boundary v. Late Boundary	Transverse	6.6 ± 2.2	6.3 ± 2.3	-0.03	0.97
	Longitudinal	5.7 ± 2.1	5.8 ± 2.7	-0.11	0.91
	Periclinal	4.0 ± 1.6	4.0 ± 1.7	-0.11	0.91
Early Blade v. Late Blade	Transverse	6.4 ± 1.0	5.3 ± 2.0	1.7	0.09
	Longitudinal	5.6 ± 1.3	4.6 ± 2.1	1.4	0.16
	Periclinal	4.0 ± 1.0	3.4 ± 1.9	1.1	0.27

Conclusion:

In the first chapter of this dissertation, I showed that the transcription factor LOB downregulates phototropism genes in the leaf-meristem boundary of *Arabidopsis* seedlings. The three phototropism genes repressed by LOB, *PHOT1*, *PKS2* and *NPH3*, have been previously identified as working together to control leaf positioning in response to low-intensity blue light (de Carbonnel et al., 2010). Whereas LOB reduces leaf inclination responses to blue light, it more generally promotes a more vertical leaf orientation. After growth in white light, plants that were exposed to pure red light, *lob* loss-of-function mutants exhibited significant differences in leaf angle compared to wild-type. It is not clear whether this difference is connected to phototropic signaling. On one hand, the presence of blue light in the standard white light growth condition could continue to affect seedling architecture even after 24h of red light. Alternatively, the more horizontal leaf angle of *lob* seedlings after the red treatment could be independent of phototropism, perhaps connected to the numerous cell wall genes regulated by LOB (Bell et al., 2012). Unlike the previously reported organ separation phenotype in the inflorescence, these phenotypes were not rescued by *pLOB:BAS1*, suggesting that LOB can affect plant architecture by multiple mechanisms (Bell et al., 2012).

We have not yet identified a cellular defect responsible for the leaf angle phenotype in *lob* mutants. For example, if cells in the *lob* mutant boundary are larger than those in the wild-type boundary, it would provide an intuitive

explanation for the horizontal leaf attachment angle seen in *lob*, with the overexpansion of the boundary cells affecting the leaf “hinge” angle. Because phototropic bending is intrinsically non-cell autonomous, a local change in phototropic signaling could subtly affect other aspects of leaf morphology, such as petiole length and petiole curvature, which were not thoroughly analyzed in this dissertation. It is also conceivable that a local difference in phototropic sensitivity could affect PIN localization and auxin flow through the leaf and boundary at a more global level. Further experiments will be needed to understand how LOB affects leaf angle at a mechanical/growth level.

In the second and third chapters of this dissertation, I showed that local, boundary-specific cell wall rigidification is a component of the ligule development program. The ligular region is a zone where cell area becomes smaller than the adjacent sheath and blade zones creating a distinct preligule band structure. Within this zone there is a slightly narrower band of highly rigid cells, which correlates with the expression pattern of the maize *CUC2* ortholog (Johnston et al., 2014). This adds to a growing body of data that suggests that cell wall-related gene networks in the boundary may alter the biophysical properties of the wall (Bouré et al., 2022; Sampathkumar et al., 2019). The proximal PLB then softens dramatically preceding the outgrowth of the ligule. This is consistent with other AFM experiments which show cell wall loosening preceding organ growth (Bou Daher et al., 2018; Peaucelle et al., 2011).

My data also strongly support a previously-proposed model for ligule development (Johnston et al., 2014; Sylvester et al., 1990). Transcript and SEM data had indicated that an initially homogenous preligule band was later split into multiple small cell populations with distinct gene expression patterns. My data are consistent with this hypothesis, showing significant differences in cell geometry, division orientation, and cell wall mechanics between proximal and distal PLB subdomains. It remains unclear exactly how many PLB-derived domains exist. There could be up to six: the blade-sheath transition zone, the adaxial/sheathward ligule precursors, the internal daughter cells of periclinal divisions which may be ligule cortex precursors, the abaxial/bladeward ligule precursors, the ligule/auricle cleft, and the preauricle. It remains unclear how and when the transverse axis of the ligule is patterned, the preauricle is specified, and the auricle/blade threshold is determined.

The mechanical and growth patterns in wild-type leaves were not restricted to the ligular region, but extended over a greater proximodistal span that included adjacent blade and sheath cells. These differences were less pronounced in the liguleless double mutant, demonstrating that they are linked to ligule development. Particularly, the wild-type had a distinct soft-sheath phase early in development, and by later developmental stages the distal sheath was significantly thicker than other epidermal regions. This must contribute to the formation of the ridge at the blade-sheath boundary, which precedes widespread periclinal divisions in the PLB. Thus, coordinated growth between adjacent leaf

zones may be important in establishing the early preligule ridge. The resulting proximodistal curvature may contribute to differences in non-cell autonomous forces experienced by cells in different positions (Kierzkowski et al., 2012; Kwiatkowska and Dumais, 2003; Louveaux et al., 2016). Indeed, the geometry of cells appears to correlate with the predicted direction of maximum tension based on the curvature of the epidermal surface, although this has not yet been explicitly tested.

The onset of periclinal divisions was known to be important in early ligule outgrowth, but it is not clear if these divisions are formative. Periclinal divisions are often developmentally relevant because they produce new cell layers. The periclinal divisions in the preligule band produce internal epidermally derived cell layers, which may contribute to the mesophyll-like tissue of membranous ligules (Chaffey, 1994). However, our data suggest the periclinal divisions may be attributed to normal cell division rules. The cells that divide periclinally tend to be columnar in shape, such that depth is their longest axis, and a surface area minimization model usually predicted periclinal divisions in these cells (Martinez et al., 2018). Furthermore, we might also consider that the periclinally dividing cells are located in the convex-curved portion of the epidermal surface, and may even experience shear forces. The predominance of longitudinal divisions early in ligule development, and periclinal divisions in the middle stages, could be partially due to non-cell autonomous forces (Louveaux et al., 2016). Further

experiments are necessary to determine the mechanisms controlling cell division orientation during ligule development.

In conclusion, the ligule is a promising system for studying biomechanics during plant development and morphogenesis. On one hand, local differences in cell wall stiffness correlate with growth. On the other hand, resulting changes in non-cell autonomous forces may feed back to alter the growth and division patterns of cells. The ligule therefore provides an exciting opportunity to explore the interplay between cell fate patterning, cell wall-related gene expression, biochemical and biophysical cell wall properties, and growth.

References:

- Bell, E. M., Lin, W., Husbands, A. Y., Yu, L., Jaganatha, V., Jablonska, B., Mangeon, A., Neff, M. M., Girke, T. and Springer, P. S.** (2012). *Arabidopsis* LATERAL ORGAN BOUNDARIES negatively regulates brassinosteroid accumulation to limit growth in organ boundaries. *Proc. Natl. Acad. Sci. U.S.A.* **109**, 21146–21151.
- Bou Daher, F., Chen, Y., Bozorg, B., Clough, J., Jönsson, H. and Braybrook, S. A.** (2018). Anisotropic growth is achieved through the additive mechanical effect of material anisotropy and elastic asymmetry. *eLife* **7**, e38161.
- Bouré, N., Peaucelle, A., Goussot, M., Adroher, B., Soubigou-Taconnat, L., Borrega, N., Biot, E., Tariq, Z., Martin-Magniette, M.-L., Pautot, V., et al.** (2022). A cell wall-associated gene network shapes leaf boundary domains. *Development* **149**, dev200359.
- Chaffey, N. J.** (1994). Structure and function of the membranous grass ligule: a comparative study. *Botanical Journal of the Linnean Society* **116**, 53–69.
- de Carbonnel, M., Davis, P., Roelfsema, M. R. G., Inoue, S., Schepens, I., Lariguet, P., Geisler, M., Shimazaki, K., Hangarter, R. and Fankhauser, C.** (2010). The *Arabidopsis* PHYTOCHROME KINASE SUBSTRATE2 Protein Is a Phototropin Signaling Element That Regulates Leaf Flattening and Leaf Positioning. *Plant Physiol.* **152**, 1391–1405.
- Johnston, R., Wang, M., Sun, Q., Sylvester, A. W., Hake, S. and Scanlon, M. J.** (2014). Transcriptomic analyses indicate that maize ligule development recapitulates gene expression patterns that occur during lateral organ initiation. *Plant Cell* **26**, 4718–4732.
- Kierzkowski, D., Nakayama, N., Routier-Kierzkowska, A.-L., Weber, A., Bayer, E., Schorderet, M., Reinhardt, D., Kuhlemeier, C. and Smith, R. S.** (2012). Elastic domains regulate growth and organogenesis in the plant shoot apical meristem. *Science* **335**, 1096–1099.
- Kwiatkowska, D. and Dumais, J.** (2003). Growth and morphogenesis at the vegetative shoot apex of *Anagallis arvensis* L. *J. Exp. Bot.* **54**, 1585–1595.
- Louveaux, M., Julien, J.-D., Mirabet, V., Boudaoud, A. and Hamant, O.** (2016). Cell division plane orientation based on tensile stress in *Arabidopsis thaliana*. *Proceedings of the National Academy of Sciences* **113**, E4294–E4303.

- Martinez, P., Allsman, L. A., Brakke, K. A., Hoyt, C., Hayes, J., Liang, H., Neher, W., Rui, Y., Roberts, A. M., Moradifam, A., et al. (2018).** Predicting division planes of three-dimensional cells by soap-film minimization. *Plant Cell* **30**, 2255–2266.
- Peaucelle, A., Braybrook, S. A., Le Guillou, L., Bron, E., Kuhlemeier, C. and Höfte, H. (2011).** Pectin-induced changes in cell wall mechanics underlie organ initiation in Arabidopsis. *Curr. Biol.* **21**, 1720–1726.
- Sampathkumar, A., Peaucelle, A., Fujita, M., Schuster, C., Persson, S., Wasteneys, G. O. and Meyerowitz, E. M. (2019).** Primary wall cellulose synthase regulates shoot apical meristem mechanics and growth. *Development* **146**, dev179036.
- Sylvester, A. W., Cande, W. Z. and Freeling, M. (1990).** Division and differentiation during normal and liguleless-1 maize leaf development. *Development* **110**, 985–1000.